Air pollution sources in inner west Melbourne

Publication 2060 | March 2024

ISBN: 978-0-6457569-2-0

Authorised and published by the Victorian Government, 1 Treasury Place, Melbourne

epa.vic.gov.au

Environment Protection Authority Victoria

GPO BOX 4395 Melbourne VIC 3001

1300 372 842

Authors

Rosemary Fedele[1], Perry Davy[2], Melita Keywood[3], Max Mclennan-Gillings[1], Jennifer Powell[3], Jacinda Shen[1], Sally Taylor[3] and Paul Torre[1].

1 – Environment Protection Authority Victoria, EPA Science, Macleod, 3085, Australia
2 – GNS Science, Atmospheric Chemistry, Lower Hutt Wellington, 5040, New Zealand
3 – CSIRO Oceans and Atmosphere, Aspendale, 3195, Australia

Acknowledgements

The authors acknowledge EPA Victoria's Air, Odour and Noise Sciences Unit and our project partner, the Port of Melbourne, for facilitating this work. As well as CPBJH Joint Venture, Transurban and Spotswood-Kingsville RSL for supporting this work.

EPA acknowledges Aboriginal people as the first peoples and Traditional custodians of the land and water on which we live, work and depend. We pay respect to Aboriginal Elders past and present and recognise the continuing connection to, and aspirations for Country.

Give feedback about this publication online: epa.vic.gov.au/publication-feedback

Contents

Executive summary **6**

Introduction **9**

Objectives/purpose 9

Methods and approach **9**

Ambient air monitoring sites 9

Site 1: Barbara Beyer Reserve, Yarraville 10

Site 2: Spotswood-Kingsville RSL 10

Source-specific air monitoring sites 10

Sample collection and analysis of chemical composition 12

Source apportionment and receptor modelling 14

Data analysis and reporting 14

Supplementary air monitoring data 14

Results and Discussion **15**

Overview of $PM_{2.5}$ concentrations at site 1 and site 2 15

Seasonal changes 16

Wind direction and $PM_{2.5}$ 16

Key chemical species in $PM_{2.5}$ 16

Black Carbon 17

Organic Carbon 18

Sources of $PM_{2.5}$ 19

Seasonal variations of sources 21

Highest concentrations 24

Biomass burning 25

Motor vehicle emissions 27

Crustal matter 29

Shipping 30

Industry 31

Marine aerosol 32

Secondary sulphate 33

Secondary nitrate 34

Ammonium nitrate on 10 July 2021 34
Summary **37**
Reducing air pollution 40
References **42**
Appendix 1. Conceptual model for inner west Melbourne **47**
Appendix 2. Source specific sampling **53**
Appendix 3. Chemical analysis and data quality assurance **56**
Appendix 4. $PM_{2.5}$ annual average concentrations using different sampling regimes **63**
Appendix 5. Particle chemistry results for sites 1 and 2 **65**
Appendix 6. Source apportionment and receptor modelling using Positive Matrix Factorisation (PMF) **78**
Appendix 7. Exceptional events **89**
Ammonium nitrate on 10 July 2021 at sites 1 and 2 89
Fireworks overnight on 31 January – 1 February 2022 at site 3 90
Elevated iron concentrations from 4 to 25 November 2021 at site 1 90
Elevated summertime methanesulfonate (MSA^-) concentrations at sites 1 and 2 91

List of figures

Figure 1. Locations of: ambient air monitoring sites, source-specific sampling sites, 11
Figure 2. Time series and CPF polar plots for $PM_{2.5}$ daily average concentrations ($\mu g\ m^{-3}$) at site 1 16
Figure 3. Box and whisker plot of $PM_{2.5}$ chemical species daily average concentrations at site 1 17
Figure 4. Box and whisker plot of $PM_{2.5}$ chemical species daily average concentrations at site 2 17
Figure 5. Timeseries and CPF polar plots for black carbon (BC) and organic carbon (OC) 18
Figure 6. $PM_{2.5}$ average source contributions at sites 1 and 2 from 5 May 2021 to 12 May 2022. 19
Figure 7. $PM_{2.5}$ average source contributions at sites 1 and 2 from 5 May 2021 to 12 May 2022. 20
Figure 8. Comparison of the 8 similar source types identified at both sites 1 and 2 20
Figure 9. Timeseries of $PM_{2.5}$ daily source contributions at sites 1 and 2. 22
Figure 10. Average seasonal $PM_{2.5}$ source contributions at sites 1 and 2. 23
Figure 11. $PM_{2.5}$ source contributions on 10 July 2021 24
Figure 12. $PM_{2.5}$ source contributions on 29 April 2021 25
Figure 13. Timeseries and CPF polar plots for $PM_{2.5}$ fresh biomass burning source contributions 26
Figure 14. Timeseries and CPF polar plots for $PM_{2.5}$ aged biomass burning source contributions 26
Figure 15. Active fires and 96-hour air back trajectories on 2 April 2021. 27

Figure 16. Active fires and 48-hour air back trajectories on 8 April 2021. 27
Figure 17. Timeseries and CPF polar plots for $PM_{2.5}$ diesel vehicle emission source contributions 28
Figure 18. Timeseries and CPF polar plots for $PM_{2.5}$ petrol vehicle emission source contributions 29
Figure 19. Timeseries and CPF polar plots for $PM_{2.5}$ crustal source contributions 30
Figure 20. Timeseries and CPF polar plots for $PM_{2.5}$ shipping source contributions 30
Figure 21. Timeseries and CPF polar plots for $PM_{2.5}$ industry (Ca) source contributions 31
Figure 22. Timeseries and CPF polar plots for $PM_{2.5}$ industry (PO_4^{3-}) source contributions 32
Figure 23. Industry sites located approximately 550 m south of site 1 32
Figure 24. Timeseries and CPF polar plots for $PM_{2.5}$ marine aerosol source contributions 33
Figure 25. Timeseries and CPF polar plots for $PM_{2.5}$ secondary sulphate source contributions 34
Figure 26. Timeseries and CPF polar plots for $PM_{2.5}$ secondary nitrate source contributions 34
Figure 27. NO_2 hourly average concentrations at Footscray and $PM_{2.5}$ hourly average concentrations at sites 1, 2 and Footscray during 3 to 19 July 2021. 35
Figure 28. 96-hour air back-trajectories arriving at site 1 every three hours during 9 and 10 July 2021 36
Figure 29. Industries with ammonia emissions in Victoria in 2020 37

List of tables

Table 1. Summary of project sites 12
Table 2. Summary of chemical species and analytical methods used for sample analysis. 13
Table 3. Supplementary air monitoring data 15
Table 4. Ten sources of $PM_{2.5}$ observed at both sites 1 and 2. 39

Note: Figures and tables in Appendices are not shown here.

Executive summary

Background

Understanding the sources of air pollution is key to improving air quality and protecting human health. EPA have completed a study to identify sources of air pollution in Melbourne's inner west, the findings from this study are presented in this report.

This study focused on sources of airborne particles smaller than 2.5 micrometers in diameter ($PM_{2.5}$). These tiny particles are so small that when breathed deep into the lungs they can enter the blood stream. They can cause adverse health effects over time, such as respiratory and cardiovascular disease.

By understanding the major sources of pollution, we can better target interventions to prevent pollution and protect human health.

EPA works with industry, business and communities to reduce air pollution. A focus of this work in recent years has been in Melbourne's inner west. This area is known for pollution from multiple sources of fine particles such as trucks, major roads, industry and shipping. Its proximity to Port Phillip Bay also means natural sources like sea salt are present.

EPA has monitored $PM_{2.5}$ in the air for decades. While that monitoring tells us *how much* $PM_{2.5}$ is present, it doesn't tell us *what* those tiny particles are made of, or *where* they come from.

To find out, this study examined $PM_{2.5}$ samples in the inner west to determine their sources.

This study answers the following research questions:

- What are the key chemical species in $PM_{2.5}$ in inner west Melbourne?
- What are the sources contributing to $PM_{2.5}$ in inner west Melbourne?
- What are the major human activities contributing to $PM_{2.5}$ that we should focus our interventions on?

Study methods

The study examined $PM_{2.5}$ samples collected from 11 sites across inner west Melbourne between 28 February 2021 and 25 June 2022.

Two of the 11 sites were generally representative of ambient air conditions. These were Site 1: Yarraville and Site 2: Spotswood. Samples were collected at these sites every third day between May 2021 and May 2022. Additional samples were collected at Site 2 outside of the main sampling period, from 28 February 2021, and were also included part of the dataset.

The remaining 9 sites were located close to known pollution sources, such as shipping docks or roads with heavy vehicle traffic/general traffic. Samples were collected at different time periods at these sites for the express purpose of characterising the chemical composition of the targeted $PM_{2.5}$ pollution sources.

To achieve the aims of the study, EPA worked with CSIRO and GNS Science to:

- sample $PM_{2.5}$ particles across inner west Melbourne
- analyse the particle samples for 62 different chemical species, including trace elements
- determine the likely sources of the particles using a chemical element mass balance (receptor) model.

Results

The main **chemical species** identified were black carbon (BC) and organic carbon (OC), comprising ~ 60% of the average $PM_{2.5}$ concentrations at the ambient air quality sites. Some BC and OC particles are harmful to human health, and some have a warming effect on the atmosphere.

The **major sources** of $PM_{2.5}$ in the inner west Melbourne during the study period between May 2021 and May 2022 were:

- residential wood heaters (in winter)
- bushfire hazard reduction burns (in autumn)
- diesel vehicle emissions
- undetermined sources of 'secondary sulphate'. There are multiple sources of sulphur such as natural sources, burning of fossil fuels or wood burning
- sea salt from Port Philip Bay – known as 'marine aerosol'
- motor vehicle emissions reacting with sea salt to form nitrous oxides – known as 'secondary nitrate'.

A single **major pollution event** comprising of elevated $PM_{2.5}$ concentrations occurred during the study period on 10 July 2021. During this event, 3 main sources contributed to around 90% of the $PM_{2.5}$ levels recorded:

- residential wood headers
- secondary sulphate
- ammonium nitrate particles, which likely formed when motor vehicle exhausts from Melbourne reacted with ammonia possibly from agricultural sources.

Minor sources identified during the study period between May 2021 and May 2022 were:

- petrol vehicle emissions
- road dust – known as 'crustal matter'
- ship exhausts
- industry.

Some of these sources are local, such as vehicle emissions, wood heaters, industry and shipping. And other sources were regional or from afar such as hazard reduction burns and sea salt.

Sources related to human activities (labelled blue in Figure S1) can be managed to reduce pollution. Targeting our interventions on human activities linked to major $PM_{2.5}$ sources will have the greatest impact on reducing $PM_{2.5}$ pollution and improving human health in inner west Melbourne.

Other sources were natural, such as sea salts, and cannot be managed. Sea salts are not harmful to human health.

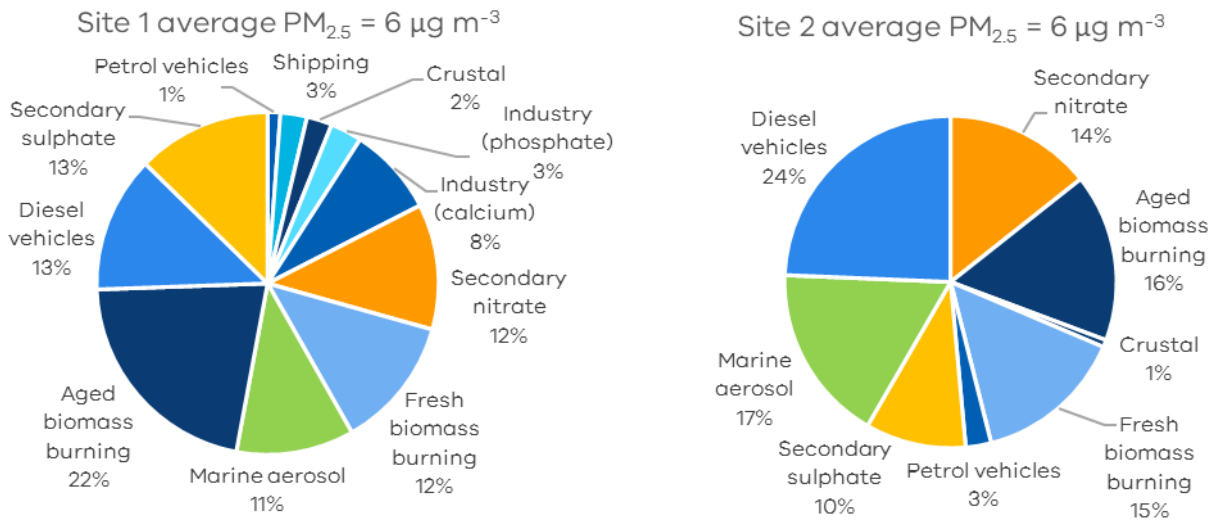

Figure S1. $PM_{2.5}$ average source contributions at sites 1 and 2 from 5 May 2021 to 12 May 2022. The average concentration of $PM_{2.5}$ over the study period at both sites was 6 µg m^{-3}

Bushfires and dust storms are also natural sources that can impact Melbourne. However, no bushfires or dust storms impacted metropolitan Melbourne during the study period for the project.

What this means – controlling $PM_{2.5}$ pollution at the source

Results show that more work needs to be done to control sources of air pollution that originate from human activity. For example, results from our study show that diesel vehicle emissions are lower during the weekends when industrial and commercial traffic is reduced, and truck curfews in inner west Melbourne are in place.

Targeting our interventions on human activities linked to major $PM_{2.5}$ sources will have the greatest impact on reducing $PM_{2.5}$ pollution and improving human health in inner west Melbourne.

The study has identified a range of human-related sources of $PM_{2.5}$ in the inner west. Polluters, community, EPA and other decision-makers can use this information to help target pollution-reduction efforts. These efforts may involve:

- conducting cost-benefit analyses of activities that create air pollution to better understand the health impacts and the costs of air pollution
- assessing mitigation measures and policy options for specific sources of air pollution
- informing programs for improving public health outcomes for people impacted by air pollution
- identifying key contributors to climate warming
- understanding the air pollution issues that may arise around new developments, such as the Fisherman's Bend urban renewal project.

This study supports the objectives of the Victorian Air Quality Strategy, which is working to reduce air pollution and tackle major pollution sources.

Introduction

EPA works to protect the health of Victorians and their environment. An important part of our work is leading research into air pollution sources. This research helps us better understand and address current and potential impacts on the health of Victorians.

Air pollution health studies have shown that long term exposure to airborne particles smaller than 2.5 µm in diameter ($PM_{2.5}$) contribute to respiratory and cardiovascular disease (USEPA, 2009; WHO Regional Office for Europe, 2013; WHO, 2021).

The World Health Organization's (WHO) most recent Air Quality Guidelines include an annual average limit for $PM_{2.5}$ of 5 µg m^{-3} (WHO, 2021). This is more stringent that the current Victorian Environment Reference Standard (ERS) (Victorian Government, 2021) which adopts the Australian National Environment Protection (Ambient Air Quality) Measure (NEPM) (Australian Government, 2021) annual limit for $PM_{2.5}$ of 8 µg m^{-3}. It is anticipated that the ERS and NEPM $PM_{2.5}$ guidelines will be reviewed in future to be in line with WHO guidelines. Annual median $PM_{2.5}$ concentrations in metropolitan Melbourne over the last 5 years were all below 8 µg m^{-3}, but most were above 5 µg m^{-3} (EPA Victoria, 2022). Therefore, if we are to meet WHO limits in future, work is needed to reduce $PM_{2.5}$ pollution in metropolitan Melbourne.

Inner west Melbourne has multiple sources of airborne particles including:

- residential wood heaters
- vehicle traffic
- industrial and commercial sources
- shipping emissions from the Port of Melbourne.

There is also community concern over air pollution from large community infrastructure projects (such as the Western Distributer) and smoke from fires and hazard reduction burns.

With the growing population, urban residential areas are also encroaching on industrial areas and transport corridors (see Appendix 1 for more information).

This study was initiated in response to concerns about health impacts of air pollution. There is a need to identify major sources of air pollution to better target programs that reduce air pollution emissions.

Objectives/purpose

This study addresses the following research questions:

- What are the key chemical species in airborne $PM_{2.5}$ in inner west Melbourne? (i.e. what are the particles made of?)
- What are the sources contributing to airborne $PM_{2.5}$ in inner west Melbourne? (i.e. where do the particles come from?)
- What are the major human activities contributing to $PM_{2.5}$ (i.e. what activities should interventions focus on first?)

Methods and approach

Ambient air monitoring sites

The study sampled air quality at 3 ambient air monitoring locations in inner west Melbourne: Yarraville, Spotswood and Brooklyn (Figure 1 and Table 1).

This report presents 12 months of monitoring from the ambient sites in Yarraville and Spotswood (Sites 1 and 2), which are located approximately 2.4 km apart.

Results from the third ambient site, Brooklyn (Site 9), will be discussed in a separate supplementary report that is yet to be released. Brooklyn is an area with localised and complex particle pollution issues. Data at Brooklyn was collected over 3 months in 2022 and will be compared with historical data collected in Brooklyn in 2010 and 2011, to investigate how air pollution at this site has changed over time.

Site 1: Barbara Beyer Reserve, Yarraville

This site is considered generally representative of air quality in inner west Melbourne. The monitoring station itself is approximately 50 m from the nearest vehicle traffic source (Whitehall Street), so air sampled at this location should represent a well-mixed blend of neighbourhood $PM_{2.5}$ sources, as well as any emissions from truck routes, the Port and West Gate Tunnel construction activities.

Approximately 8,000 vehicles per day (including 900 trucks) were counted in 2020 at various locations within a 1 km radius of this site (Department of Transport Victoria, 2021). The nearest residential homes are located approximately 220 m to the west, on Hyde and Nicholson Streets.

Site 2: Spotswood-Kingsville RSL

The site is considered typical of a residential inner west Melbourne location. It is set about 30 m from the nearest houses and located on the residential street, the Avenue, approximately 65 m from Williamstown Road and Melbourne Road. The West Gate Freeway and West Gate Tunnel construction activities are 150 m to the north of the monitoring station.

Approximately 31,000 vehicles per day (including 4,000 trucks) were counted in 2020 at various locations within a 1 km radius of this site (Department of Transport Victoria, 2021). There was almost 4 times more vehicle traffic around this site than at site 1.

Source-specific air monitoring sites

Samples of $PM_{2.5}$ emission-sources were collected at 9 sites. These sites were located around shipping docks, transport truck depots and near heavy-trafficked roads (see Figure 1 and Table 1 for more information).

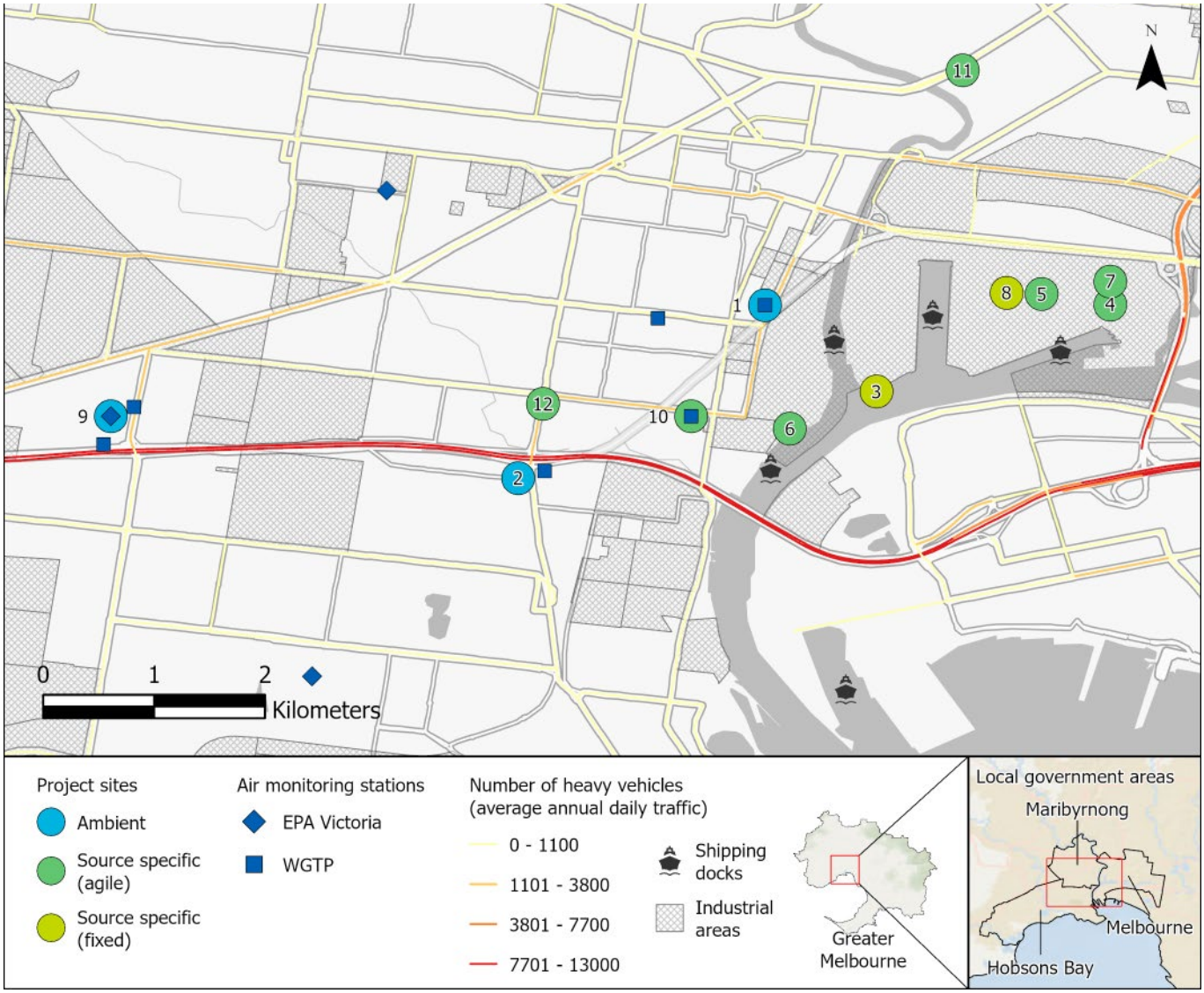

Figure 1. Locations of: ambient air monitoring sites, source-specific sampling sites, and other air monitoring stations operated by EPA Victoria and West Gate Tunnel Project (WGTP) in inner west Melbourne (for more information about EPA and WGTP air monitoring stations see section: 'Supplementary air monitoring data' below). Information on heavy-vehicle traffic volume (Department of Transport Victoria, 2021), and the location of industrial areas and shipping docks are provided as they are potential sources of air pollution surrounding each site.

Table 1. Summary of project sites

Site	Site location	Latitude	Longitude	Site type	Site context	Target source	Samples	Start date	End date
1	Barbara Beyer Reserve	-37.813	144.900	Ambient	Residential	Mixed	124	5/05/2021	13/05/2022
2	Spotswood-Kingsville RSL	-37.827	144.880	Ambient	Residential	Mixed	140	28/02/2021	13/05/2022
3	Tip of Coode Island	-37.820	144.909	Source specific	Industrial port	Shipping	20	29/09/2021	4/04/2022
4	Coode Road near ACFS	-37.812	144.928	Source specific	Industrial port	Stevedoring	3	30/11/2021	22/02/2022
5	Anderson Road	-37.812	144.922	Source specific	Industrial port	Heavy vehicles	3	24/01/2022	28/03/2022
6	Holden Dock	-37.823	144.902	Source specific	Industrial port	Shipping	1	22/03/2022	23/03/2022
7	Coode Rd X Appleton Dock Rd	-37.811	144.928	Source specific	Industrial port	Heavy vehicles	4	5/04/2022	24/05/2022
8	End of Phillips Road	-37.812	144.920	Source specific	Industrial port	Stevedoring	10	6/04/2022	20/06/2022
9	Brooklyn Reserve	-37.822	144.847	Ambient	Residential	Industry	20	29/05/2022	31/08/2022
10	Francis Street	-37.822	144.894	Source specific	Residential	Heavy vehicles	3	18/06/2022	20/06/2022
11	Smithfield Road	-37.794	144.916	Source specific	Arterial road	Light vehicles	3	18/06/2022	22/06/2022
12	Francis St X Williamstown Rd	-37.821	144.882	Source specific	Arterial road	Heavy vehicles	3	22/06/2022	25/06/2022

Sample collection and analysis of chemical composition

Ambient monitoring at sites 1 and 2 included collection of 24-hour samples of $PM_{2.5}$ every three days over one year (5 May 2021 to 12 May 2022) to account for seasonal variability.

Sample collection commenced on 28 February 2021 at site 2, due to gaining early access to the site. This resulted in 16 additional samples being collected at this site between 28 Feb 2021 and 5 May 2021. These extra samples were included in the source apportionment and receptor modelling analysis.

Source-specific monitoring used several approaches including agile (movable) and fixed monitoring locations (non-movable). More detail about source-specific monitoring can be found in Appendix 2.

All sampling and equipment maintenance at sampling sites was carried out by EPA Victoria. $PM_{2.5}$ samples at each sampling site were collected with two ARA (16.7 LPM) N-FRM $PM_{2.5}$ samplers (ARA Instruments, 2023). Two samplers were used at each site to collect $PM_{2.5}$ samples on two different filters for chemical and mass analysis:

- Whatman Teflon PTFE membrane filters, 46.2 mm diameter with PMP (polymethylpropylene) support ring, 2 µm pore size (Teflon filters).

- Pallfex Tissuquartz 2500QAT-UP fiber filters, 47 mm diameter (quartz filters).

Pre-weighed Teflon filters were supplied by GNS Science to EPA Victoria. Teflon filters were stored for preservation at 4°C after sample collection.

Sampled Teflon filters were sent fortnightly to GNS Science for gravimetric analysis, followed by determination of black carbon (light reflectance).

Elemental composition of the samples were determined by X-ray fluorescence (XRF) spectroscopy techniques at the New Zealand National Isotope Centre at Gracefield, Lower Hutt, New Zealand.

Sampled and analysed Teflon filters were then sent to the CSIRO Climate Science Centre, Aspendale, Victoria, for determination of soluble ion and anhydrous sugar composition of the samples by liquid chromatography techniques.

Pre-treated quartz filters were supplied by CSIRO to EPA Victoria. Quartz filters were stored for preservation at -20°C after sample collection.

Elemental carbon and organic carbon composition the samples were determined by a thermal desorption and optical detection analyser at the CSIRO Climate Science Centre, Aspendale, Victoria.

Table 2 lists the chemical species and analytical method used on each filter. More detail on laboratory analytical methods and data quality assurance can be found in Appendix 3.

Table 2. Summary of chemical species and analytical methods used for sample analysis.

Filter type	Chemical species	Analytical methods
Teflon	$PM_{2.5}$ gravimetric mass	Gravimetric mass (AS 3580.9.10, 2017)
	Black carbon (BC or light absorbing carbon)	Black carbon (BC): light absorption using a M43D Digital Smoke Stain Reflectometer (Ancelet, et al., 2011)
	Elements: sodium (Na), magnesium (Mg), aluminium (Al), silicon (Si), phosphorus (P), sulphur (S), chlorine (Cl), potassium (K), calcium (Ca), titanium (Ti), vanadium (V), chromium (Cr), manganese (Mn), iron (Fe), cobalt (Co), nickel (Ni), copper (Cu), zinc (Zn), gallium (Ga), arsenic (As), selenium (Se), bromine (Br), strontium (Sr), molybdenum (Mo), cadmium (Cd), tin (Sn), antimony (Sb), tellurium (Te), caesium (Cs), barium (Ba), lanthanum (La), cerium (Ce), samarium (Sm), lead (Pb), mercury (Hg), indium (In), tungsten (W)	Elements: X-ray fluorescence (XRF) using a PANalytical Epsilon 5 EDXRF spectrometer (USEPA IO-3.3, 1999)
	Soluble Ions: sodium (Na^+), ammonium (NH_4^+), potassium (K^+), magnesium (Mg^{2+}), calcium (Ca^{2+}), hydrogen (H^+), chloride (Cl^-), bromide (Br^-), nitrate (NO_3^-), sulphate (SO_4^{2-}), oxalate ($C_2O_4^{2-}$), phosphate (PO_4^{3-}), fluoride (F^-), acetate (CH_3COO^-), formate ($HCOO^-$), methanesulfonate (MSA^-)	Soluble ions: suppressed ion chromatography (IC) using a Dionex ICS-3000 reagent free IC system (Keywood, et al., 2019) Anhydrous Sugars: high performance anion exchange chromatography with pulsed amperometric detection (HPAECPAD) using a Dionex ICS-3000 chromatograph with electrochemical detection (Keywood, et al., 2019)

	Anhydrous Sugars: levoglucosan, mannosan, mannitol, sorbitol, glactosan, glucose and arabitol	
Quartz	Carbon: organic carbon (OC), elemental carbon (EC)	Carbon: thermal desorption and optical detection using a DRI Model 2015 Multiwavelength Thermal/Optical Carbon Analyzer (Keywood, et al., 2019)

Source apportionment and receptor modelling

The chemical composition results of $PM_{2.5}$ samples were input into a receptor model to determine source chemical profiles and source mass contributions to $PM_{2.5}$ by positive matrix factorisation (PMF). PMF was performed using EPAPMF software version 5.0.14 in accordance with the user guide. Data screening and source apportionment analysis was performed in accordance with the protocols and recommendations set out by Paatero, et al. (2014) and Brown, et al. (2015).

Data analysis and reporting

The results of receptor modelling have been provided with as much information as possible about the source-contributions to $PM_{2.5}$ concentrations. The methods used to illustrate the significance of various sources of air pollution are described below:

- Comparison of average concentrations with days of significance; for example, days of elevated $PM_{2.5}$ concentrations or 'high-pollution days'.
- Seasonal variations (using monthly averages) and weekend/weekday split of source contributions to examine variations in source activity. Time variation plots were produced using R statistical software and the openair package (R Core Team, 2011; Carslaw & Ropkins, 2012; Wickham, 2016). In time variation plots (for example, see Figure 2 month and weekday plots), lines represent the average concentration and shaded bars are 95% confidence intervals.
- The relationship between the source contributions to $PM_{2.5}$ concentrations and wind direction. Bivariate polar plots using CPF (Conditional Probability Function) analysis were produced using R statistical software and the openair package (R Core Team, 2011; Carslaw & Ropkins, 2012). CPF analysis provides a method to find wind directions related to high values of specific chemical species or sources. The probability that a source contribution originates from a given wind direction is estimated by comparing the wind direction distribution for the upper 25 % of source contributions relative to the total wind direction distribution. Sources are likely to be located in the directions that have high CPF values.
- Back trajectories of air parcels for sample days of interest were used to examine long-range atmospheric transport processes and determine potential particulate matter source locations. Air mass back trajectories were calculated using the HYSPLIT (HYbrid Single-Particle Lagrangian Integrated Trajectory) model (Stein, et al., 2015; Rolph, et al., 2017).

Supplementary air monitoring data

Ambient air monitoring was also supplemented with data from EPA Victoria and West Gate Tunnel Project (WGTP) air monitoring stations. Refer to Figure 1 for air monitoring station locations and Table 3 for their association with project sites. WGTP station 1 is the same air monitoring station as the project site 1. WGTP station 5 is approximately 220 m from project site 2.

$PM_{2.5}$ 24-hour average samples are routinely collected at an interval of one in every three days for gravimetric mass analysis at EPA's Footscray and Alphington air monitoring sites. The Alphington site is not located in the inner west Melbourne, and is not pictured in Figure 1. For this project, Footscray and Alphington monitoring data was used for investigating regional pollution events and to compare 2 methods used for measuring $PM_{2.5}$ concentrations (Appendix 4). Project samples were collected on the same days at both Footscray and Alphington stations for the duration of this project.

Table 3. Supplementary air monitoring data, method, locations, and their association with project sites.

Parameter (unit)	Method	Location of air monitoring station	Co-located project site
$PM_{2.5}$ (µg/m^3)#	Gravimetric mass (AS 3580.9.10, 2017) Beta attenuation monitor (AS 3580.9.12, 2013)	EPA stations: Footscray, Alphington	
	Beta attenuation monitor (AS 3580.9.12, 2013)	WGTP station 1*	Site 1
		WGTP station 5^	Site 2
NO_2 (ppb)	Gas phase chemiluminescence (AS 3580.5.1, 2011)	EPA station: Footscray	
Wind speed (m/s) and direction (°TN)	Ultrasound anemometer (AS 3580.14, 2014)	WGTP station 1*	Site 1
		WGTP station 5	Site 2

All $PM_{2.5}$ concentrations reported at Australian standard conditions of 0°C and 1013 hPa

* Data missing for most of January 2022, wind data missing for April 2022

^ Data missing for August 2021 and February 2022 (due to issues with data supply)

Results and Discussion

Overview of $PM_{2.5}$ concentrations at site 1 and site 2

Annual average $PM_{2.5}$ concentrations were 6 µg m^{-3} at both sites 1 and 2 (ambient sites). These concentrations were based on samples collected every three days from 5 May 2021 to 12 May 2022.

Other measurements of $PM_{2.5}$ concentrations were made daily either at the same location (at site 1) or nearby (approximately 200 m from site 2). $PM_{2.5}$ annual average concentrations calculated based on daily measurements were about the same at both ambient sites for the project period (7 µg m^{-3} for both sites 1 and 2) than $PM_{2.5}$ concentrations calculated based on samples collected every three days. See Appendix 4 for more information.

$PM_{2.5}$ daily average concentrations were correlated (r^2 = 0.73) between sites 1 and 2 (Appendix 5, Figure A7), this indicates that $PM_{2.5}$ daily average concentrations are similar at both sites.

There were no significant differences in $PM_{2.5}$ concentrations during different days of the week at both sites 1 and 2.

Seasonal changes

The $PM_{2.5}$ seasonal cycle (Figure 2) shows that $PM_{2.5}$ particle levels at sites 1 and 2 were higher in the first 6 months of 2022 (summer, autumn and winter), than in the last 6 months of 2021 (winter, spring and summer), at both sites 1 and 2. This pattern is typical in metropolitan Melbourne and occurs due to seasonal differences in particle sources (such as wood heater use in colder months) and different weather conditions throughout the seasons, which either build-up or disperse air pollution.

Wind direction and $PM_{2.5}$

At site 1, the highest $PM_{2.5}$ concentrations occurred during easterly winds and when winds were less than approximately 2 m s^{-1} (Figure 2). A slightly different pattern was seen for site 2, where the highest $PM_{2.5}$ concentrations occured during calm winds less than approximately 1 m s^{-1}.

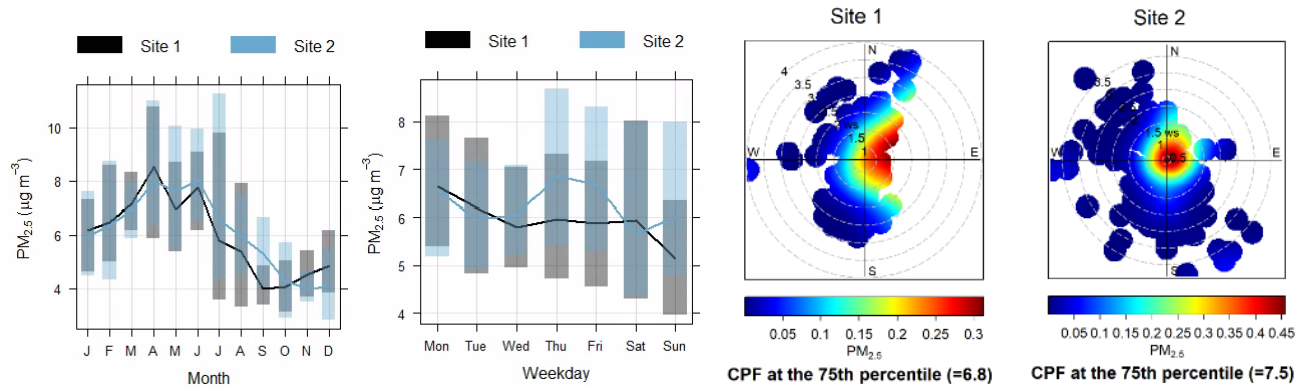

Figure 2. Time series and CPF polar plots for $PM_{2.5}$ daily average concentrations (µg m^{-3}) at site 1 from May 2021 to May 2022, and at site 2 from March 2021 to May 2022. Wind speeds are meters per second (m s^{-1}).

Key chemical species in $PM_{2.5}$

Summary statistics of all chemical species measured at sites 1 and 2 can be seen in Figure 3 and Figure 4 (and these data are presented in table format in Appendix 5).

Black carbon (BC) and organic carbon (OC) were the most abundant chemical species and made up roughly 60% of the average $PM_{2.5}$ concentrations at both sites 1 and 2.

Average BC concentrations were 1.6 µg m^{-3} and 2 µg m^{-3} at sites 1 and 2 respectively, or approximately 30% of the average $PM_{2.5}$ concentrations.

Average OC concentrations were 2 µg m^{-3} at both sites 1 and 2, or approximately 30% of the average $PM_{2.5}$ concentrations.

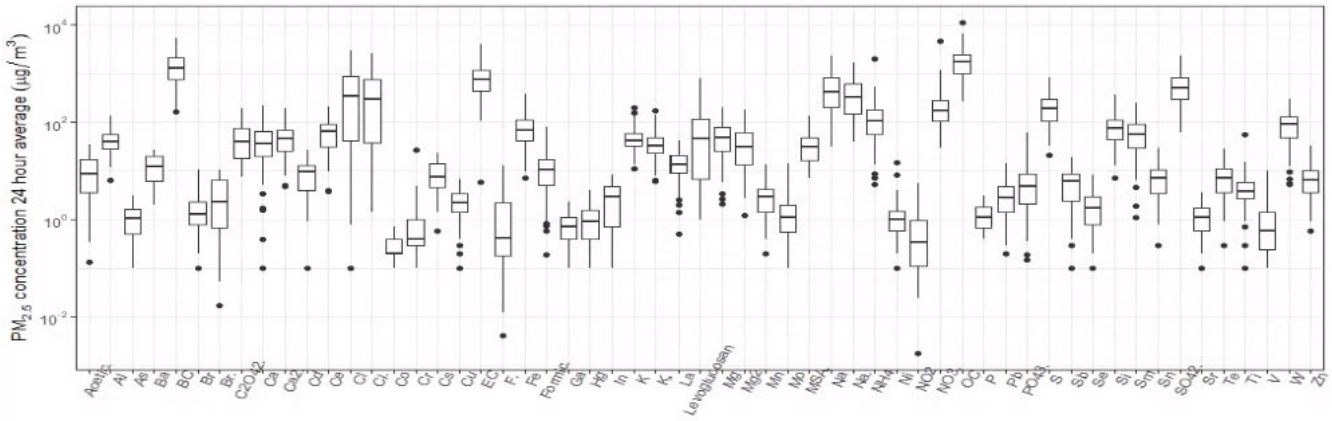

Figure 3. Box and whisker plot of $PM_{2.5}$ chemical species daily average concentrations at site 1 from May 2021 to May 2022. Boxes represent median, 25th and 75th percentiles, lines represent the smallest and largest values, no further than 1.5 times the inter-quartile ranges from the box edge. Dots are outliers.

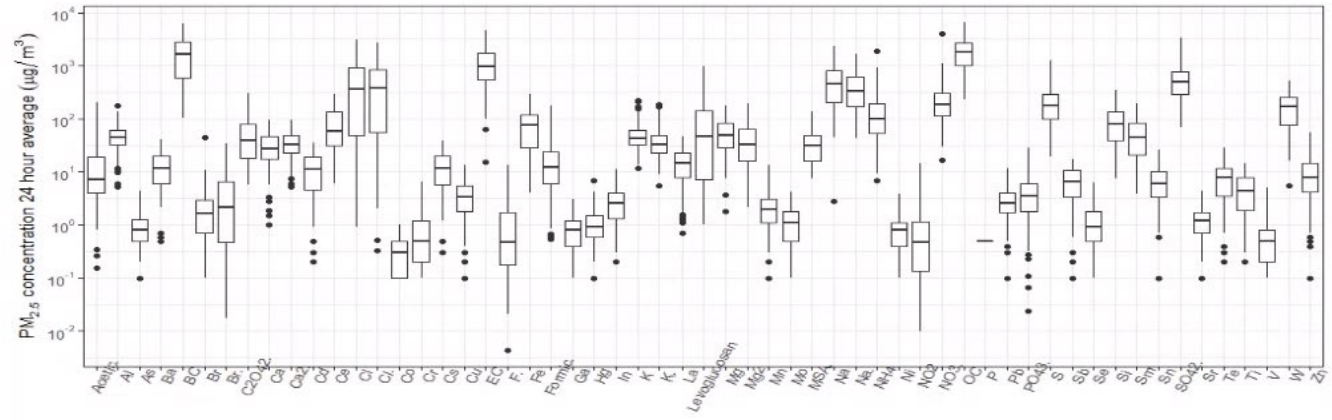

Figure 4. Box and whisker plot of $PM_{2.5}$ chemical species daily average concentrations at site 2 from March 2021 to May 2022. Boxes represent median, 25th and 75th percentiles, lines represent the smallest and largest values, no further than 1.5 times the inter-quartile ranges from the box edge. Dots are outliers.

Black Carbon

BC is a product of incomplete combustion, typically emitted by engines, biomass burning or industrial processes (Cohen, et al., 2000). BC is considered inert in the atmosphere, it is relatively small in particle size (nanometre scale), and may cause negative health effects by itself. But when BC particles (soot) are combined with other chemical components of BC sources, like polycyclic aromatic hydrocarbons (PAH), and inhaled, these sources may also be harmful or carcinogenic (Luben, et al., 2017 and references therein). BC particles are also regarded as the most effective light-absorbing particles in the atmosphere and have a warming effect on the atmosphere (Pani, et al., 2020). Therefore, reducing BC particles will help protect human health and manage climate impacts, and reduce air pollution.

The BC seasonal cycle (Figure 5) at site 1 shows a similar pattern to the broader $PM_{2.5}$ seasonal cycle. A slightly different seasonal cycle was seen at site 2, with a BC peak in July. These differences are likely due to the differing proportions of BC sources at each site. Concentrations of BC were lower on the weekends than weekdays at both sites 1 and 2. The weekend difference commonly occurs when sources of particles are from human activities (for example, motor vehicle emissions). BC daily average

concentrations at sites 1 and 2 were weakly correlated (r^2 = 0.6) (Appendix 5, Figure A8), which indicates that BC daily average concentrations were similar at both sites.

Organic Carbon

OC is composed of different organic species, including harmful polycyclic aromatic hydrocarbons (PAHs) and humic-like substances (HULIS). OC is associated with sources such as industrial emissions and the combustion/evaporation of fuels. They can also form via chemical reactions in the atmosphere when they come into contact with gases such as volatile organic compounds (VOCs) (Mohr, et al., 2013; Satish & Rastogi, 2019; Yuan, et al., 2020).

OC particles can scatter light or become light-absorbing over time. The light-absorbing component of OC is typically called brown carbon. Therefore, reducing OC particles will help protect human health and manage climate impacts, and reduce air pollution.

The OC seasonal cycle (Figure 5) is different to the $PM_{2.5}$ and BC seasonal cycles. These differences are likely due to the different sources of OC particles. The highest OC concentrations occur in the autumn months (March to May), and there are two peaks in the OC seasonal cycle, in April and September. Unlike BC, OC does not show a decrease on weekends compared to weekdays. OC daily average concentrations at sites 1 and 2 were not well correlated (r^2 = 0.4) (Appendix 5, Figure A8), however this was due to one outlier where OC concentrations were much higher at site 1 compared to site 2 on this day.

For all other key chemical species in the study, see Appendix 5 for seasonal cycles, weekly trends, and CPF polar plots (like those in Figure 5, which are for BC and OC only).

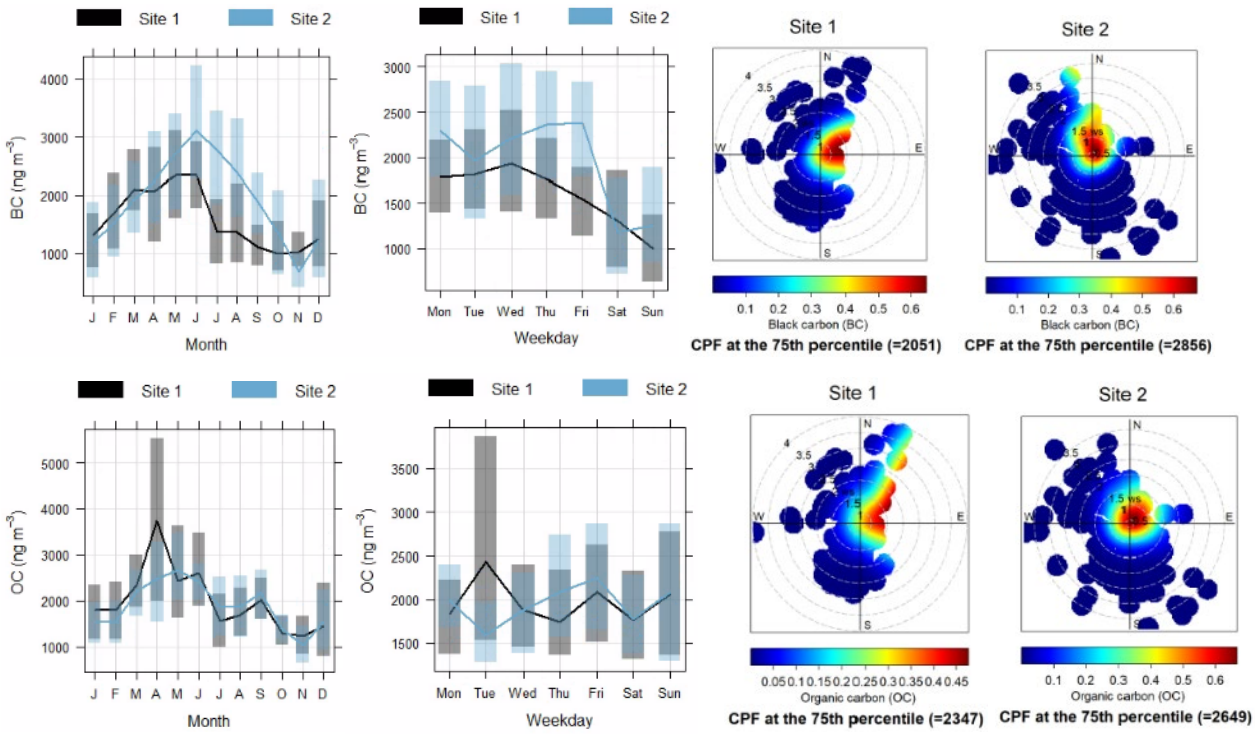

Figure 5. Timeseries and CPF polar plots for black carbon (BC) and organic carbon (OC) daily average concentrations (ng m^{-3}) at site 1 from May 2021 to May 2022 and at site 2 from March 2021 to May 2022. Wind speeds are meters per second (m s^{-1}).

Sources of $PM_{2.5}$

Source apportionment and receptor modelling analysis was conducted to identify the sources of $PM_{2.5}$ (for more information see Appendix 6). The analysis identified 8 common sources of $PM_{2.5}$ collected at sites 1 and 2. These were:

- aged-biomass burning (e.g. hazard reduction burns or residential wood heating)
- fresh-biomass burning (e.g. residential wood heating)
- secondary sulphate (e.g. natural sources, burning of fossil fuels or biomass burning)
- marine aerosol (e.g. sea salt)
- secondary nitrate (e.g. a mixture of sea salt and motor vehicle exhaust emissions)
- diesel motor vehicle exhaust
- petrol motor vehicle exhaust
- crustal material (e.g. soil/dust).

At site 1, three additional local sources were identified, these were from shipping and two industries nearby. Each of these sources are described in separate sections below.

The average $PM_{2.5}$ concentrations and source mass contributions are shown in Figure 6 and Figure 7. These sources, on average, explained 96 % and 93 % of the $PM_{2.5}$ gravimetric mass at sites 1 and 2 respectively. While some natural sources were present (for example, marine aerosol shown in green in Figure 6), most of the sources of $PM_{2.5}$ identified in inner west Melbourne came from human activities and some were a combination of natural and human activities (for example, secondary sulphate and secondary nitrate shown in orange hues in Figure 6).

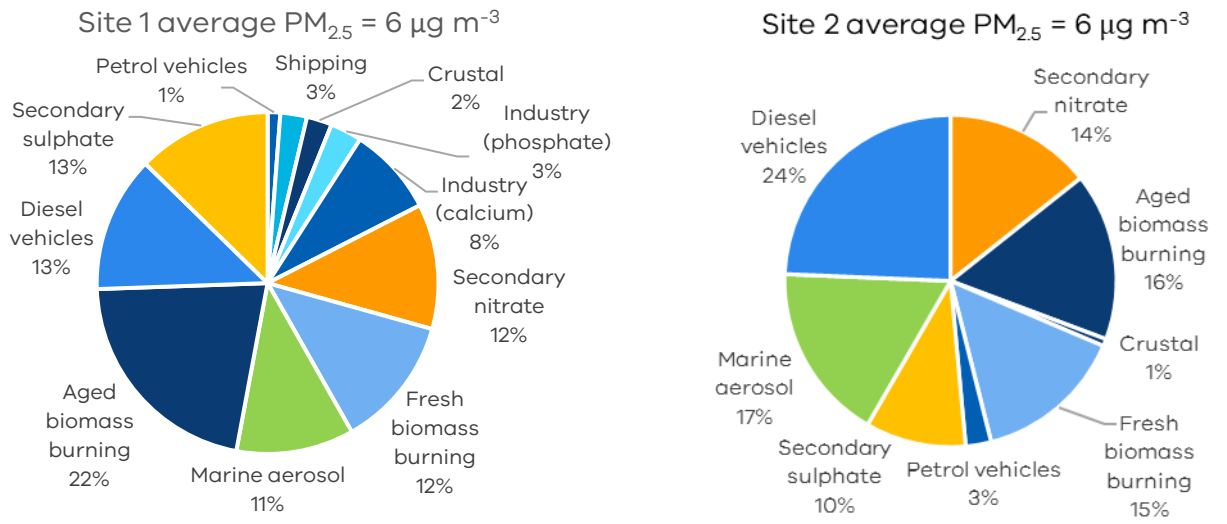

Figure 6. $PM_{2.5}$ average source contributions at sites 1 and 2 from 5 May 2021 to 12 May 2022.

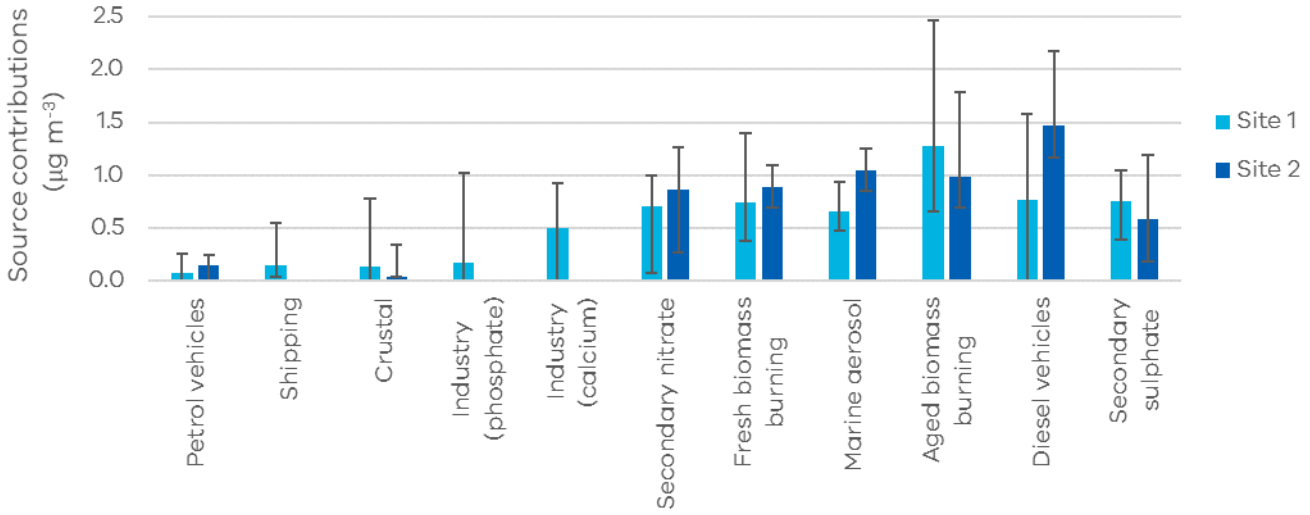

Figure 7. $PM_{2.5}$ average source contributions at sites 1 and 2 from 5 May 2021 to 12 May 2022. Error bars are the 5th and 95th percentiles.

Concentrations of the 8 common source types can be compared between sites to give an indication of whether they are of regional or local influence. Where source types are highly correlated between the two sites, this may indicate they are regional $PM_{2.5}$ sources.

From Figure 8 we can see that there is a mixture of local and regional sources in inner west Melbourne. Strong correlations are seen for marine aerosol and secondary sources (nitrate and sulphate). Whereas the weaker correlations observed for motor vehicle sources suggests that these sources are more localised at sites 1 and 2 - such as motor vehicle emissions from roads nearby the sites.

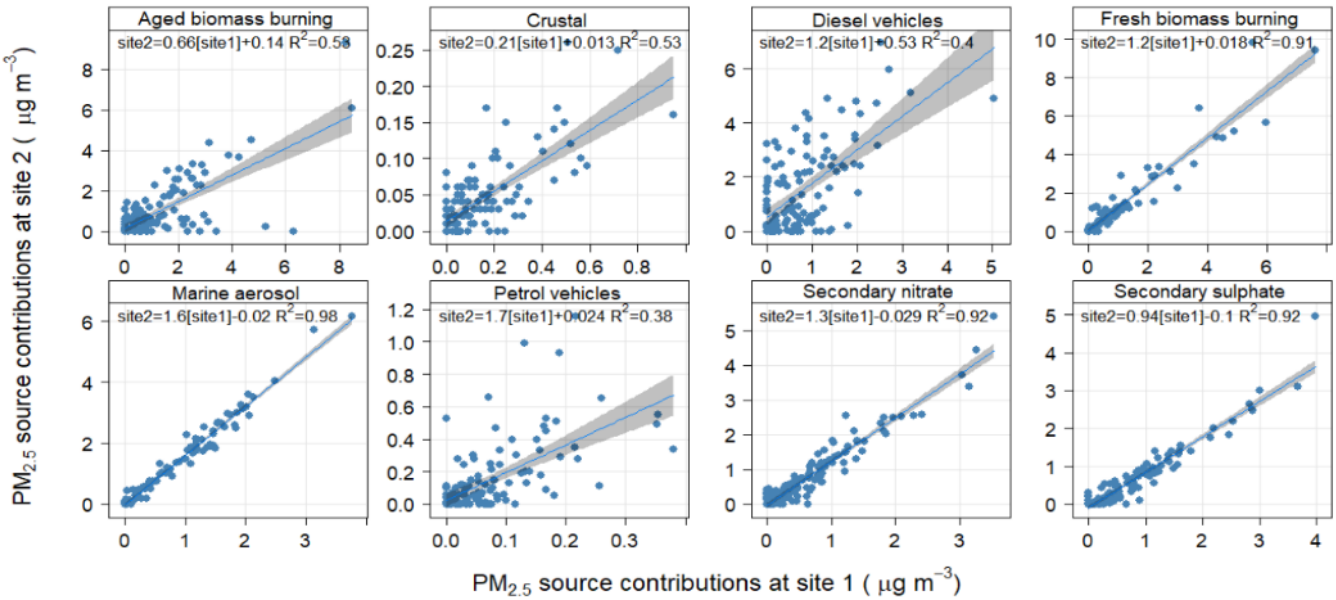

Figure 8. Comparison of the 8 similar source types identified at both sites 1 and 2 from 5 May 2021 to 12 May 2022.

Seasonal variations of sources

Total $PM_{2.5}$ concentrations were highest from summer through to winter (Figure 2). This study examined how each source varied throughout the seasons (Figure 9 and Figure 10).

Aged biomass burning emissions (due to hazard reduction burns) and diesel vehicle emissions were the main contributing sources of $PM_{2.5}$ in autumn at both sites. At site 2 marine aerosol was also a main contributing source in **autumn**.

Aged and fresh biomass burning emissions (from residential wood heaters) and diesel vehicle emissions were the main contributing sources of $PM_{2.5}$ in **winter** at both sites.

Diesel vehicle emissions, aged biomass burning (likely due to hazard reduction burns), secondary sulphate and marine aerosol were the main contributing sources of $PM_{2.5}$ in **spring** at both sites.

Marine aerosol, diesel vehicle emissions and secondary aerosol sources were the main contributing sources of $PM_{2.5}$ in **summer** at both sites. At site 1, industry emissions were also a contributing source in summer.

Crustal matter, shipping and petrol vehicle emissions were present as minor contributors to $PM_{2.5}$ at both sites. However, shipping concentrations were so low at site 2 that the receptor modelling results could not accurately attribute shipping as a factor at site 2 (for more information see Appendix 6).

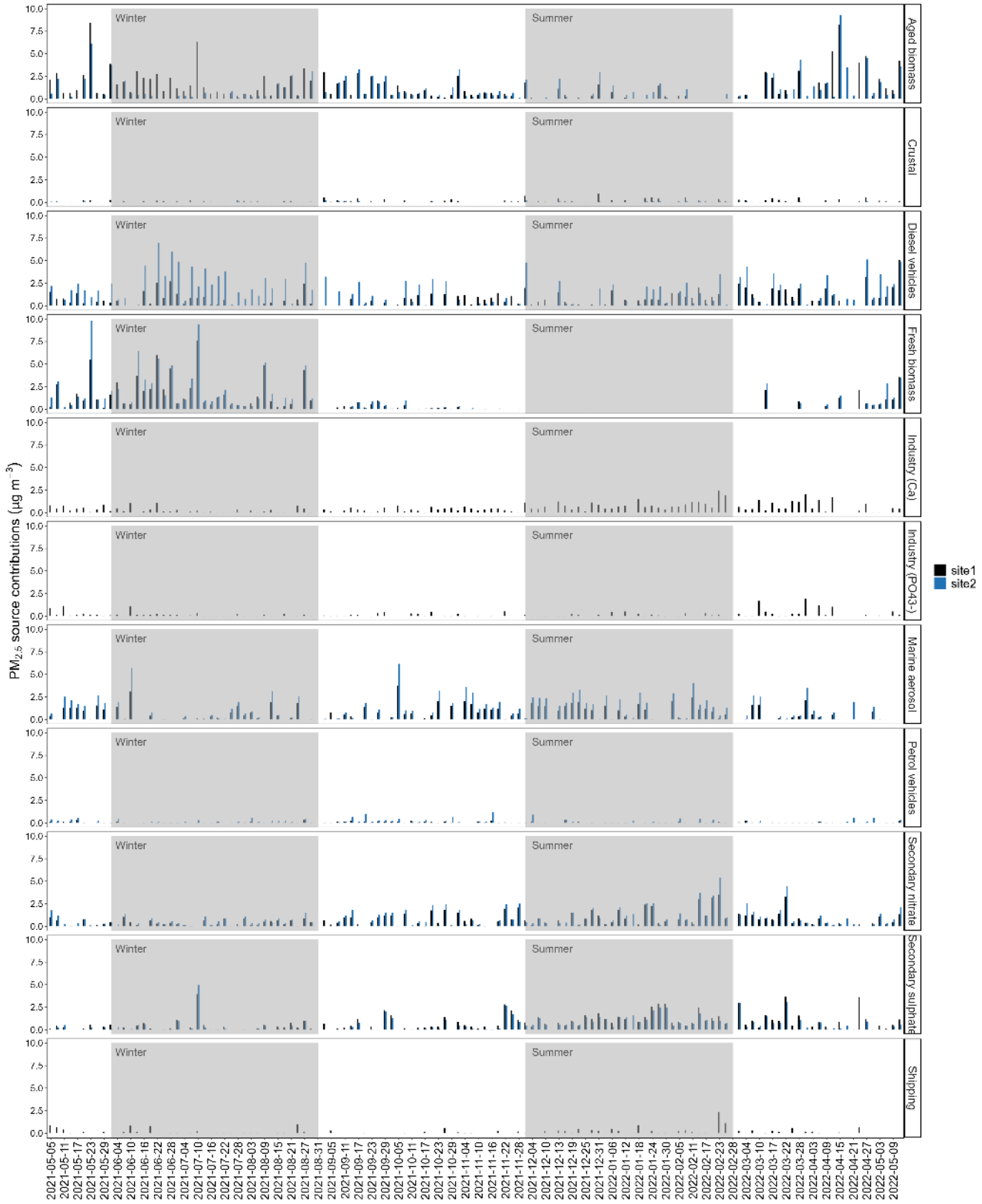

Figure 9. Timeseries of $PM_{2.5}$ daily source contributions at sites 1 and 2. Industry and shipping only have data for site 1.

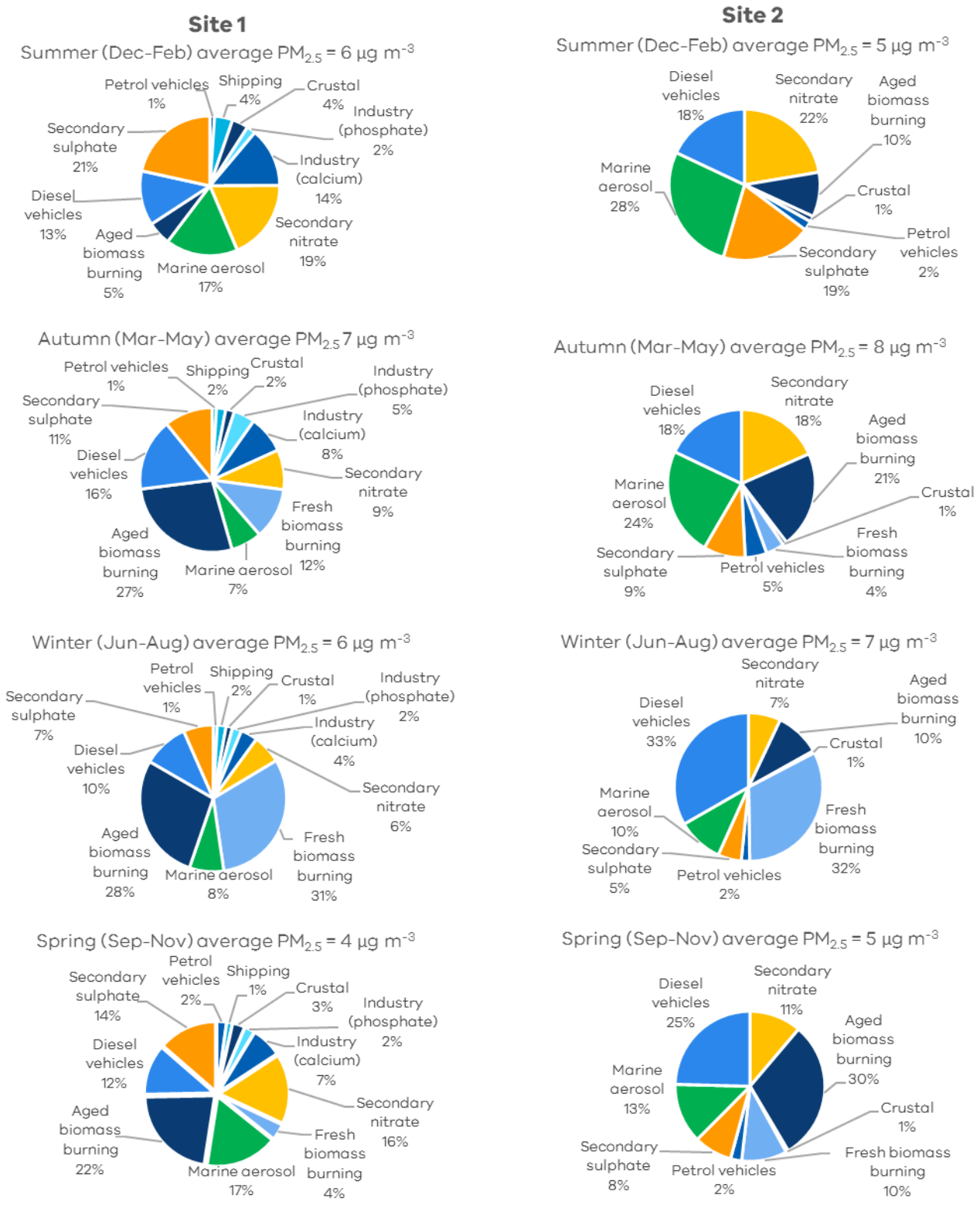

Figure 10. Average seasonal $PM_{2.5}$ source contributions at sites 1 and 2.

Highest concentrations

The highest $PM_{2.5}$ daily average concentrations were recorded on 10 July 2021 at sites 1 and 2. The $PM_{2.5}$ source contributions on this day are presented in Figure 11. The chemical composition and sources were different to the annual average chemical composition and sources shown in Figure 6 and Figure 7.

Three main sources contributed up to 93% and 90% of elevated levels of $PM_{2.5}$ on this day at sites 1 and 2 respectively. These sources were:

- fresh biomass burning
- secondary sulphate
- a third source that was not identified by the receptor modelling analysis.

Further investigation into this third source, described below under the section titled 'Ammonium nitrate on 10 July 2021', resulted in this source being attributed to an ammonium nitrate exceptional pollution event. The similar sources observed at both sites on 10 July 2021 indicate that this was a regional scale pollution event. In fact, $PM_{2.5}$ concentrations were elevated at all EPA air monitoring stations in metropolitan Melbourne on 10 July 2021.

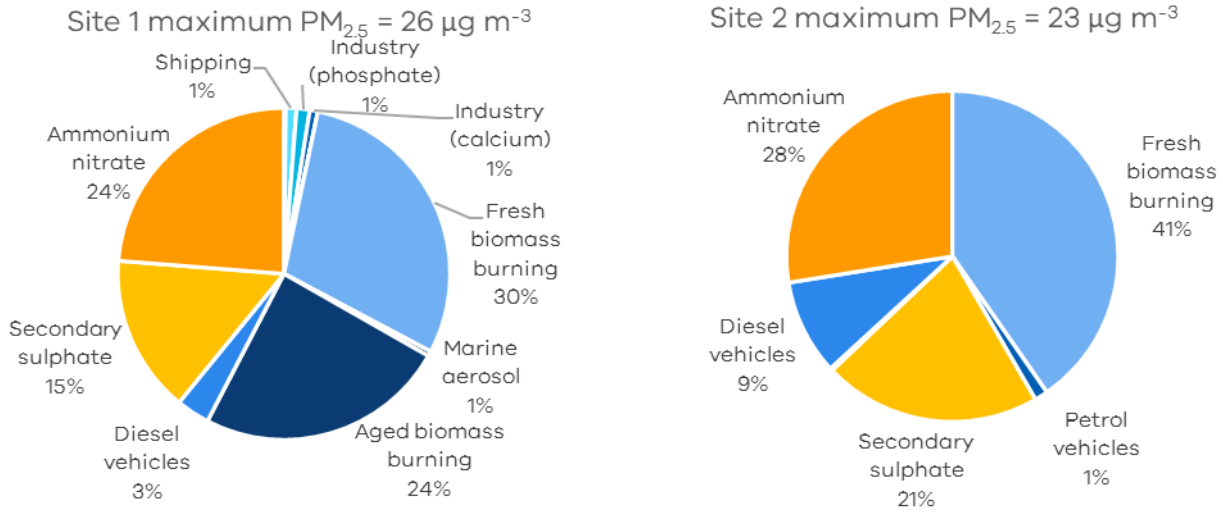

Figure 11. $PM_{2.5}$ source contributions on 10 July 2021 when the highest $PM_{2.5}$ daily average concentrations were recorded at sites 1 and 2.

The second highest $PM_{2.5}$ daily average concentration was recorded on 29 April 2021, at site 2. No sample was collected at site 1 on this day as sampling had not yet begun at this site. The $PM_{2.5}$ source contributions on this day are presented in Figure 12. The chemical composition and sources on this day were different to the 10 July 2021 and annual average chemical composition and sources.

Two main sources contributed up to 75% of elevated levels of $PM_{2.5}$ on this day:

- diesel vehicle emissions
- aged biomass burning.

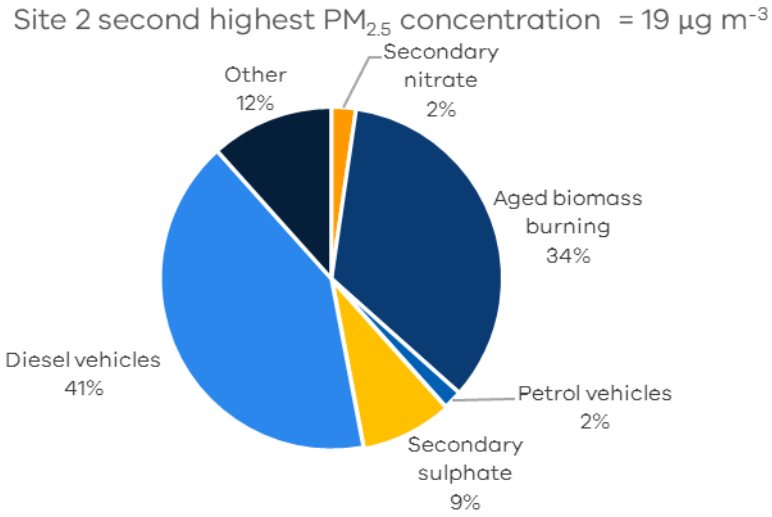

Figure 12. $PM_{2.5}$ source contributions on 29 April 2021 when the second highest $PM_{2.5}$ daily average concentrations were recorded at site 2. No sample was collected at site 1 on this day.

In summary, the most predominant sources of $PM_{2.5}$ in inner west Melbourne are from human activities and include biomass burning (from residential wood heaters and hazard reduction burning), diesel vehicle exhaust emissions and secondary aerosols.

Focusing policy on human activities associated with these sources will be most effective in reducing $PM_{2.5}$ pollution.

While natural sources (marine aerosols) also contribute to $PM_{2.5}$, we cannot control these sources. We also note that $PM_{2.5}$ concentrations can be very high during bushfire events; however, no bushfires impacted metropolitan Melbourne during the project.

Each $PM_{2.5}$ source is discussed in more detail in the following sections.

Biomass burning

Biomass burning aerosols in urban areas are primarily due to residential wood heater use during winter.

Biomass burning, such as bushfires and hazard reduction burns can affect air quality, climate, human health and visibility.

Carbonaceous aerosols (BC, EC (elemental carbon) and OC) are the dominant chemical species in biomass burning, with potassium (K) and levoglucosan – a unique tracer for the combustion of cellulose found in trees and plants (Iinuma, et al., 2007) – also present. Two source profiles were associated with these chemical species. Each source profile can be seen in Figure A16 and Figure A17.

In the first source profile, BC, EC and OC were the primary chemical species with levoglucosan and K also present. As such, this was assigned as a fresh biomass burning source (Figure A16 and Figure A17).

Studies have shown levoglucosan concentrations drop as the air mass moves away from the biomass burning source. This happens because levoglucosan is chemically reactive, and levoglucosan is removed quicker than K or OC from a biomass burning source (Li, et al., 2021 and references therein). This fresh biomass burning source likely originated from local wood smoke emissions, most likely from domestic solid fuel fires during winter.

Seasonal source contributions of fresh biomass burning emissions were highest during winter (accounting for 32 % of $PM_{2.5}$), when wood heaters are used (Figure 10 and Figure 13).

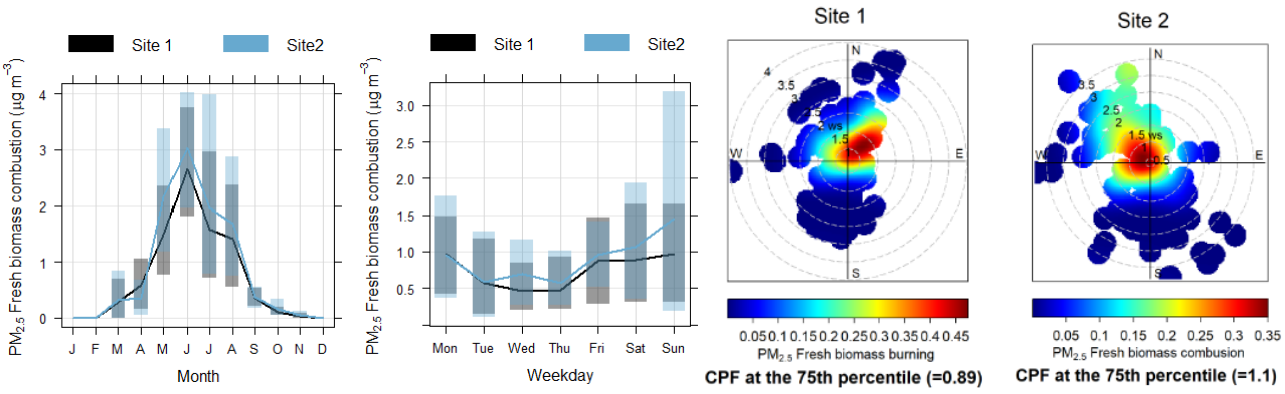

Figure 13. Timeseries and CPF polar plots for $PM_{2.5}$ fresh biomass burning source contributions (µg m^{-3}) at sites 1 and 2 from 5 May 2021 to 12 May 2022. Wind speeds are meters per second (m s^{-1}).

In the second source profile BC, EC and OC were the primary chemical species, with K and oxalate ($C_2O_4^{2-}$) present, but no levoglucosan.

In addition to K and levoglucosan, the gases from biomass burning may also produce secondary OC during transport (Zhang, et al., 2007). The absence of levoglucosan and presence of OC in this profile suggests it is an aged biomass burning source, most likely from outside of metropolitan Melbourne. The source is most likely from agricultural or hazard reduction burns, as there were no bushfires during the sample collection period.

The highest concentrations of aged biomass burning occurred in autumn during northerly winds (Figure 14), which means the air mass came from inland. Autumn is also the peak time for hazard reduction burns in Victoria.

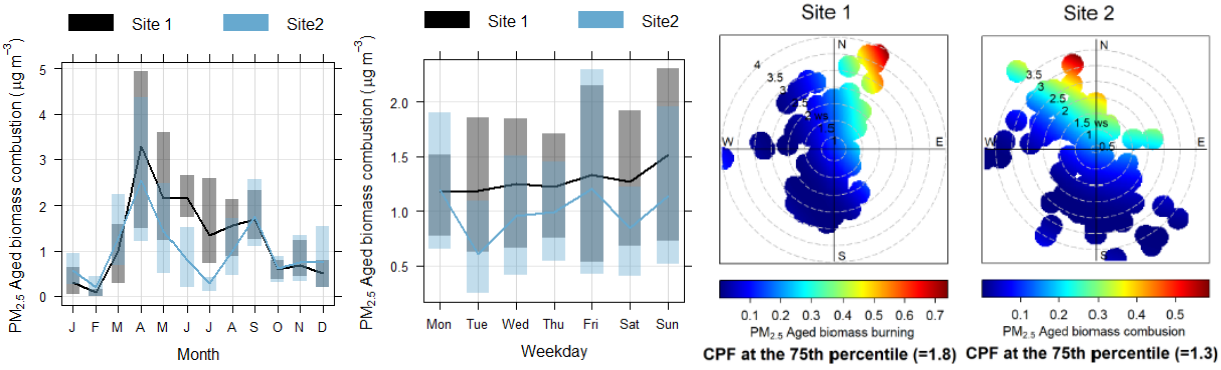

Figure 14. Timeseries and CPF polar plots for $PM_{2.5}$ aged biomass burning source contributions (µg m^{-3}) at sites 1 and 2 from 5 May 2021 to 12 May 2022. Wind speeds are meters per second (m s^{-1}).

Satellite images confirmed that hazard reduction burning occurred on the two days with the highest contribution to aged biomass burning – 2 and 8 April 2021 at site 2. Note that no samples were collected at site 1 during April 2021. as sampling had not yet begun at this site (Figure 15 and Figure 16).

Several fires were burning on:

- 2 April 2021 in central northern Victoria. Air mass back trajectories arrived at site 2 on 2 April 2021 having travelled over central northern Victoria.
- 8 April 2021 across Victoria. Air mass back trajectories arrived at site 2 on 8 April 2021 having travelled across Victoria.

Samples collected on these two days capture two biomass burning pollution events that lasted over 24-hours at site 2 and, based on the nature of this source and good correlations seen for this source at sites 1 and 2 over the entire sampling period (Figure 8), are likely to have impacted a broader area across metropolitan Melbourne.

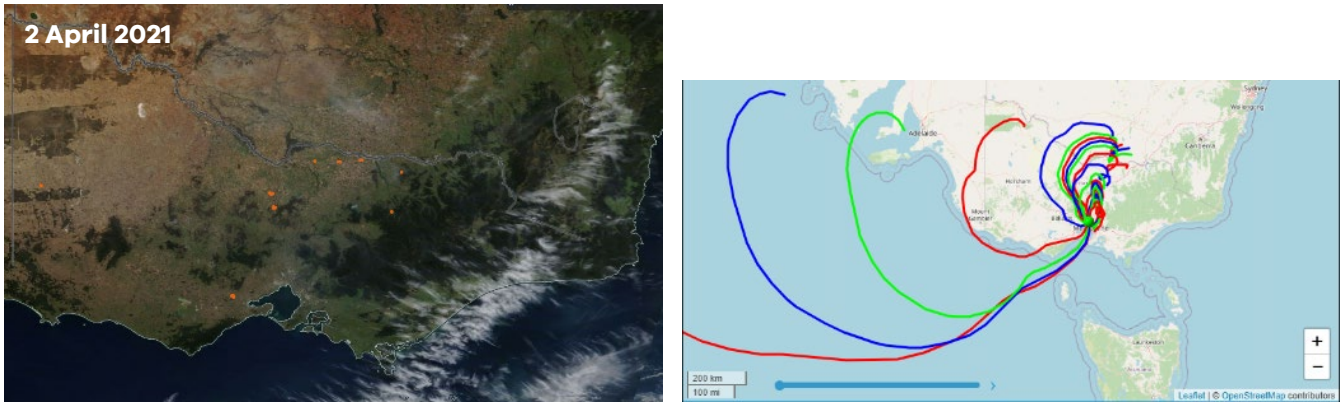

Figure 15. Active fires and 96-hour air back trajectories on 2 April 2021. Left plot: Satellite image of Victoria with location of active fires on 2 April 2021 shown by orange-coloured areas (thermal anomalies). Satellite image source: https://worldview.earthdata.nasa.gov. Right plot: 96-hour air back trajectories (Stein, et al., 2015; Rolph, et al., 2017) at 10 m height arriving at site 2 every three hours during 2 and 3 April 2021.

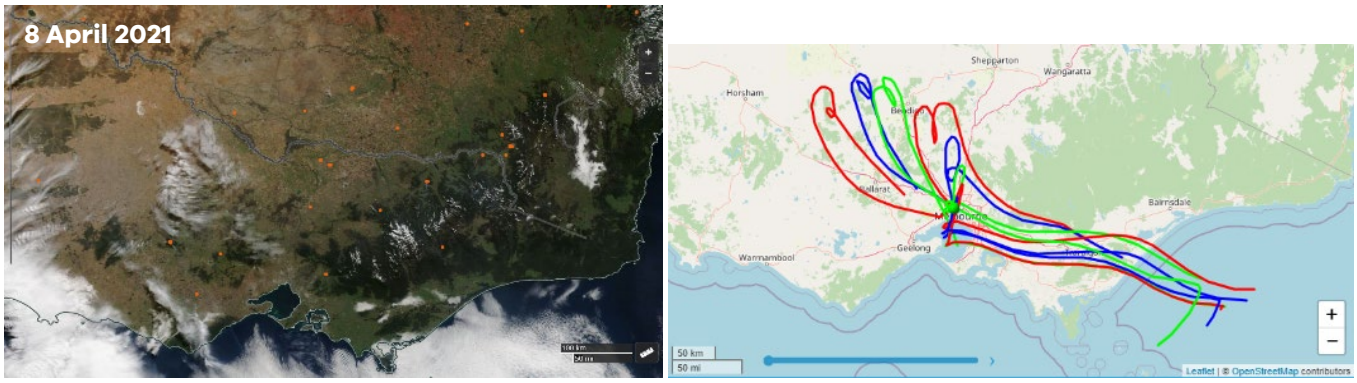

Figure 16. Active fires and 48-hour air back trajectories on 8 April 2021. Left plot: Satellite image of Victoria with location of active fires on 8 April 2021 shown by orange-coloured areas (thermal anomalies). Satellite image source: https://worldview.earthdata.nasa.gov. Right plot: 48-hour air back trajectories (Stein, et al., 2015; Rolph, et al., 2017) at 10 m height arriving at site 2 every three hours between 12:00 7 April 2021 and 00:00 9 April 2021.

Motor vehicle emissions

Motor vehicle emissions can affect air quality, human health and climate. Carbonaceous aerosols (BC, EC and OC) have been shown to be the key chemical species in $PM_{2.5}$ associated with motor vehicle emissions (Wang, et al., 2022). Harmful trace elements (e.g., Fe, Cu, Zn, Mn) are also associated with vehicle exhaust emissions, motor oils, and vehicle or road surface wear and tear (Whitacre, et al., 2002; De Silva, et al., 2021 and references therein).

Two source profiles were attributed to motor vehicle emissions, with one source contributing significantly more to the $PM_{2.5}$ mass than the other:

In the first source profile, black carbon (BC), iron (Fe) and copper (Cu) were the key chemical species, with titanium (Ti) and organic carbon (OC) also present. BC is a product of incomplete combustion (soot), typically emitted by diesel engines. Fe has been associated with road surface wear (Whitacre, et al., 2002), Cu with break wear, tyre wear and engine oil, and Ti is also associated with break wear (De Silva, et al., 2021 and references therein).

OC is composed of different organic species, including hydrocarbons (PAHs), which are commonly associated with vehicle exhaust emissions. The presence of these chemical species suggest that this is a diesel / heavy vehicle source. These emissions are also lower during weekends (Figure 17) when industrial and commercial traffic is reduced and truck curfews in inner west Melbourne are in place (no trucks are allowed on Francis Street, Moore Street and Sommerville Road between 8 pm and 6 am weekdays and from 1 pm Saturday to 6 am Monday).

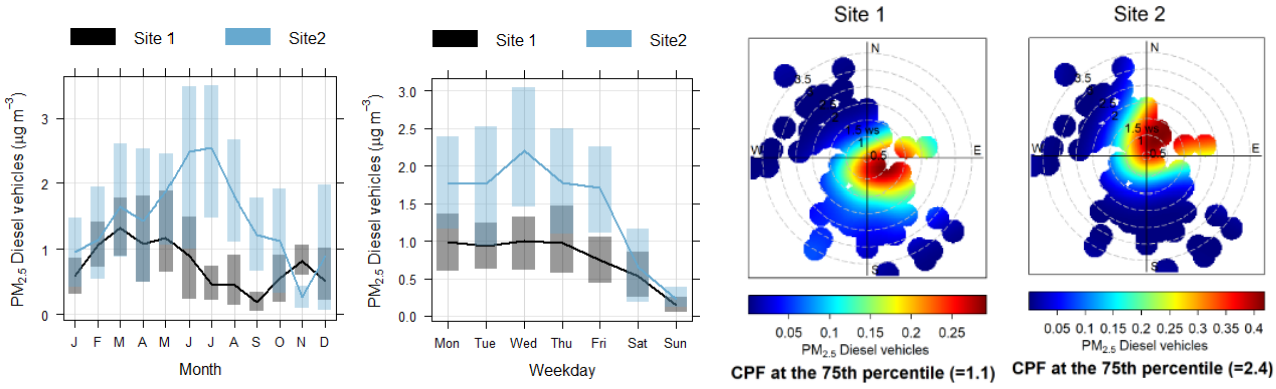

Figure 17. Timeseries and CPF polar plots for $PM_{2.5}$ diesel vehicle emission source contributions (µg m^{-3}) at sites 1 and 2 from 5 May 2021 to 12 May 2022. Wind speeds are meters per second (m s^{-1}).

In the second source profile, zinc (Zn) was the primary constituent. Sources of Zn include lubrication oil additives, fuel, and tyre and brake wear and tear (Whitacre, et al., 2002; Pant & Harrison, 2013; Deniver van der Gon, et al., 2013; De Silva, et al., 2021 and references therein). The lack of BC in this profile suggests a vehicle source that does not include diesel vehicles.

Studies have shown that $PM_{2.5}$ particles derived from vehicle fleet emissions are primarily composed of diesel vehicle emissions, and the second highest contributor is from petrol/gasoline vehicle emissions (Wang, et al., 2022). Therefore, it is likely that this is a petrol vehicle emission source. This source profile did not show a reduction of emissions on Saturdays, but emissions were lower on Sundays compared to the rest of the week (Figure 18). This is likely representative of the movements of passenger petrol vehicles.

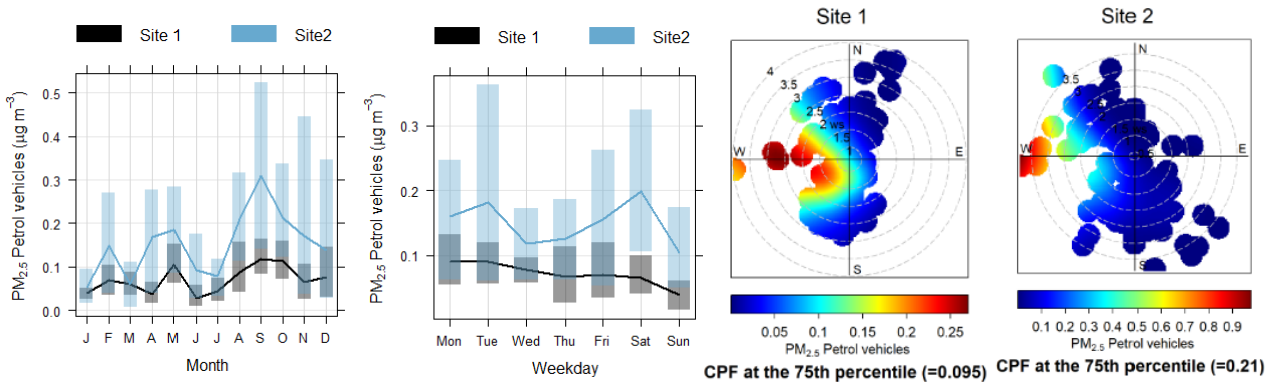

Figure 18. Timeseries and CPF polar plots for $PM_{2.5}$ petrol vehicle emission source contributions (µg m^{-3}) at sites 1 and 2 from 5 May 2021 to 12 May 2022. Wind speeds are meters per second (m s^{-1}).

Interestingly, the reduction in the **petrol vehicle** source in June and July 2021 corresponds with two COVID lockdown periods (29 May to 10 June 2021 and 16 to 25 July 2021), Victorians' movements were restricted to 5-10 km from their homes, and with only 5 reasons to leave their homes (shopping for necessary food and supplies, authorised work, exercise, caregiving or to get vaccinated).

A reduction of **diesel vehicle** exhaust emissions was not observed in June and July 2021, possibly because business involving truck movements (e.g. delivery and resupply of goods) were considered authorised work and not restricted during these COVID lockdown periods.

Motor vehicle emission sources were significantly higher at site 2 than site 1 (Figure 17 and Figure 18). Our analysis showed that vehicle volumes were almost 4 times higher at site 2 compared with site 1. With truck volumes approximately 4.4 times higher at site 2 than site 1 (Table A3 and Figure A3).

Crustal matter

Crustal matter is commonly referred to as windblown dust. It is primarily composed of aluminosilicate minerals. The source profiles reflect this, with aluminium (Al) and silicon (Si) being the primary constituents, and calcium (Ca), titanium (Ti) and iron (Fe) are also present (Figure A16 and Figure A17). These trace metals have been associated with wear and tear of vehicle brakes and road surface (De Silva, et al., 2021 and references therein; Whitacre, et al., 2002).

In urban locations, the passage of motor vehicles over roads can be the primary source of emissions. Crustal matter emissions were lower on weekends compared to weekdays (Figure 19) similar to diesel vehicle emissions (see Figure 17). This supports that the crustal matter source was primarily road dust.

The variation in wind direction between diesel vehicle emissions and crustal road matter can be explained by the different processes that drive the two sources. Crustal airborne particles are generated – and therefore have higher concentrations – on warm, dry, windy days. On wet, calm days, crustal particle generation is supressed. However, diesel vehicle emissions are independent of the weather, and appear when a diesel vehicle is idling or driving by.

The minor contributions of crustal matter to $PM_{2.5}$ identified in this study are only a component of the total dust sources expected around the sites. Most dust particles are larger particle sizes, typically measured as PM_{10}.

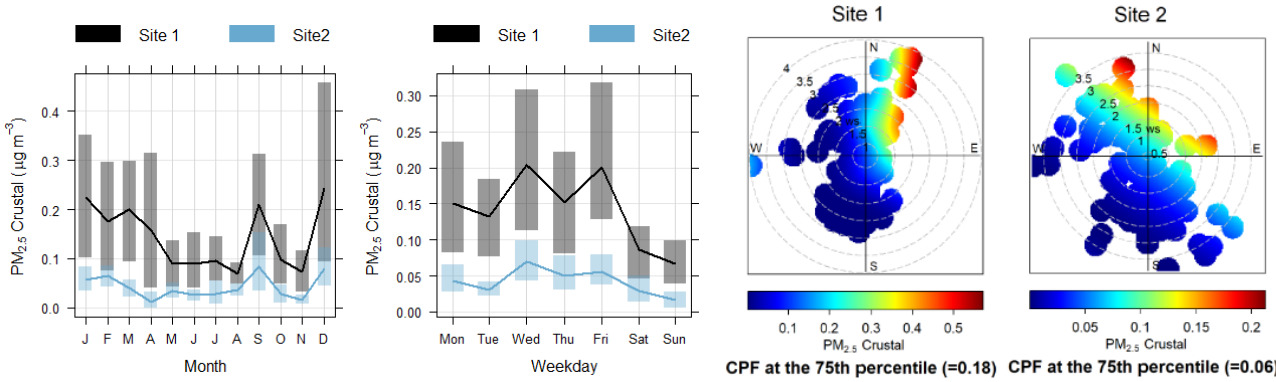

Figure 19. Timeseries and CPF polar plots for $PM_{2.5}$ crustal source contributions (μg m^{-3}) at sites 1 and 2 from 5 May 2021 to 12 May 2022. Wind speeds are meters per second (m s^{-1}).

Shipping

Vanadium (V) and nickel (Ni) are associated with combustion products from ship engines. The source profiles reflected this, with V and Ni being the primary constituents (Figure A16). The main source of these particles are the ships' use of residual or bunker oil as fuel, which is generally of poor quality. High levels of sulphur, PAHs and heavy metals in the oil result in particulate matter emissions that are high in sulphate and contaminated with metals (V, Ni, Ca, Fe) (Fridell, et al., 2008; Moldanova, et al., 2009).Concentrations of V and Ni were so low at site 2 that the PMF model was unable to attribute a shipping factor to site 2 (for more information see Appendix 6).

Elevated concentrations of $PM_{2.5}$ from shipping were found to be highest at site 1 when the wind came from the south, which is the direction of Melbourne's shipping channels and the Port of Melbourne (Figure 20).

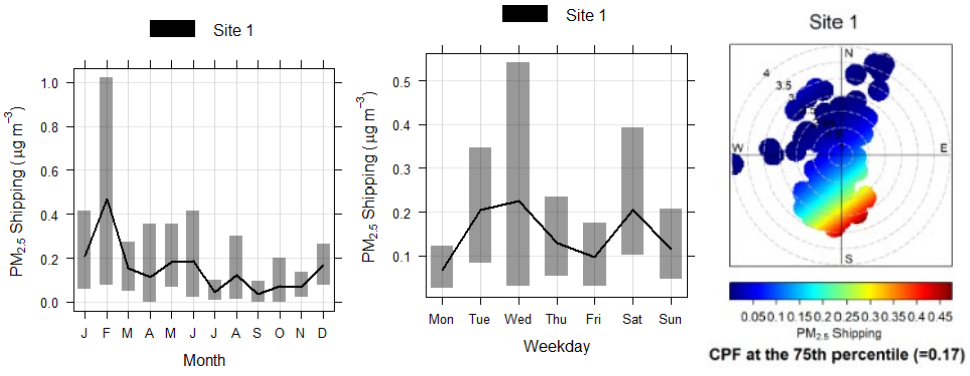

Figure 20. Timeseries and CPF polar plots for $PM_{2.5}$ shipping source contributions (μg m^{-3}) at site 1 from 5 May 2021 to 12 May 2022. Wind speeds are meters per second (m s^{-1}).

The minor contributions of shipping to $PM_{2.5}$ detected in this study are only a small component of the broader array of combustion products known to come from ship engines and impact air quality. Species emitted to the atmosphere from ships engines include:

- combustion products (COx, NOx)
- gaseous sulphur oxides (SOx) that relate to fuel composition
- volatile organic compounds (VOCs) from incomplete fuel combustion
- particulate matter which includes trace heavy metals (e.g. vanadium and nickel) included in this study (Agrawal, et al., 2008; Fridell, et al., 2008; Agrawal, et al., 2008; Healy, et al., 2009).

Researchers at the Australian Maritime College/University of Tasmania estimated total shipping emissions for Melbourne at 440,000 kg per year, for the year 2010/2011 (Goldsworthy & Goldsworthy, 2015). The results of our study confirm that these shipping combustion emissions are present and contributing to air pollution in inner west Melbourne.

Industry

Two industry sources were identified at site 1.

The primary chemical species associated with the first industry source profile was calcium (Ca) (Figure A16). Analysis of the wind direction and highest concentrations of calcium at site 1 confirmed the direction of the calcium source was from the south (Figure A18 and Figure 21). We identified an industry located approximately 550 m south of site 1 that uses large quantities of gyprock outdoors (Figure 23). Gyprock contains calcium, so it is very likely that this is the industry site impacting site 1.

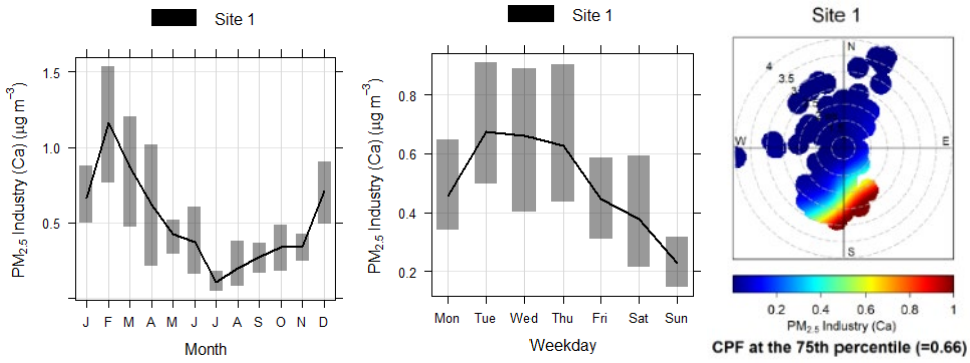

Figure 21. Timeseries and CPF polar plots for $PM_{2.5}$ industry (Ca) source contributions (µg m^{-3}) at site 1 from 5 May 2021 to 12 May 2022. Wind speeds are meters per second (m s^{-1}).

The primary chemical species associated with the second industry source profile was phosphate (PO_4^{3-}) (Figure A16). Analysis of the wind direction and highest concentrations of phosphate at site 1 confirmed the direction of the phosphate source was from the south (Figure A15 and Figure 22). Immediately south of the calcium industry site is a decommissioned phosphoric acid and food-grade phosphate manufacturing plant (Figure 23). Clean-up of the phosphate industrial site was occurring during this study. The waste on site consisted of residual white phosphorus that had adhered to surfaces of bricks, rocks and mud.

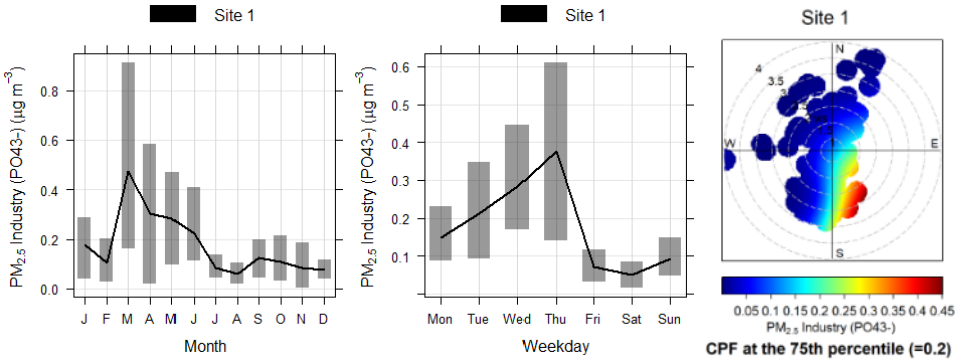

Figure 22. Timeseries and CPF polar plots for $PM_{2.5}$ industry (PO_4^{3-}) source contributions ($\mu g\ m^{-3}$) at site 1 from 5 May 2021 to 12 May 2022. Wind speeds are meters per second ($m\ s^{-1}$).

Figure 23. Industry sites located approximately 550 m south of site 1 (blue diamond). Industry associated with calcium (Ca) outlined in blue and industry associated with phosphate (PO_4^{3-}) outlined in orange (image: Nearmap, accessed on 10 November 2022).

Marine aerosol

Marine aerosol in $PM_{2.5}$ is composed of mostly the chemical species sodium (Na) and chloride (Cl). The source profiles in this study reflect this, with Na and Cl being the primary constituents (Figure A16 and Figure A17). These elements were strongly correlated (see Figures A5 and A6) and present in the same ratio as found in sea salt ([Na] = 0.65-0.75[Cl]) (Lide, 1992). Sea salt is a natural source of $PM_{2.5}$ found in

the air near the sea. Other sources of Na and Cl include biomass burning, motor vehicle emissions, crustal matter, fireworks and industrial emissions.

Concentrations of $PM_{2.5}$ from marine aerosol were found to be highest at both sites during high-speed winds from the south, which is the direction of the ocean and Port Phillip Bay (Figure 24). Research has shown that the concentration of marine aerosol shows a strong dependence of wind speed across the ocean surface, with aerosols ranging in size from about 2 µg m^{-3} to as much as 50 µg m^{-3} or more, being dispersed with wind speeds of more than 15 m s^{-1} (Fitzgerald, 1991).

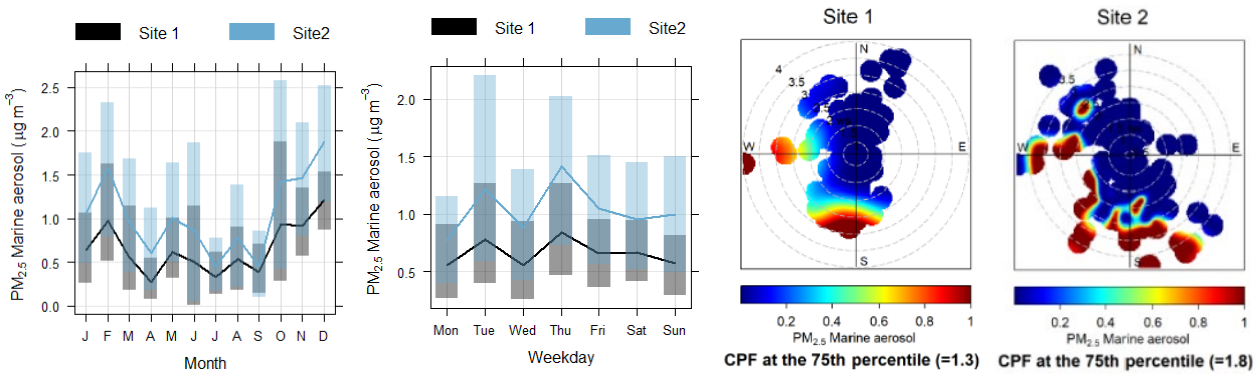

Figure 24. Timeseries and CPF polar plots for $PM_{2.5}$ marine aerosol source contributions (µg m^{-3}) at sites 1 and 2 from 5 May 2021 to 12 May 2022. Wind speeds are meters per second (m s^{-1}).

Secondary sulphate

The primary chemical species in this source profile are ammonium (NH_4^+) and sulphate (SO_4^{2-}) (Figure A16 and Figure A17). The sulphate detected as $PM_{2.5}$ may be generated from a variety of sources, including:

- sulphur in mineral structures of crustal matter
- cell structure of trees (biomass burning)
- volcanic emissions
- marine aerosol
- vehicle fuels (petrol, diesel and fuel oils used by ships)
- other fossil fuels such as coal.

Sulphate particles are also formed from gas-to-particle reactions in the atmosphere, where precursor gases such as sulphur dioxide, hydrogen sulphide or dimethyl sulphide transform to sulphate particles. These reactions can take hours to days depending on the reaction pathway, the availability of catalytic metals (e.g. Fe, Mn), relative humidity and the strength of solar radiation (Seinfeld & Pandis, 2006). Therefore, concentrations of secondary sulphate sources are likely to be highest some distance downwind of an emission source (Polissar, et al., 2001). In this case, CPF polar plots may not be the best way to identify nearby secondary sulphate sources, as wind direction may shift as particles travel over distance, nevertheless these plots show the wind direction during the highest secondary sulphate concentrations at both sites (Figure 25).

It is assumed that sulphate is present in a fully neutralised form – as ammonium sulphate (Cahill, et al., 1989; Cohen, 1999; Malm, et al., 1994).

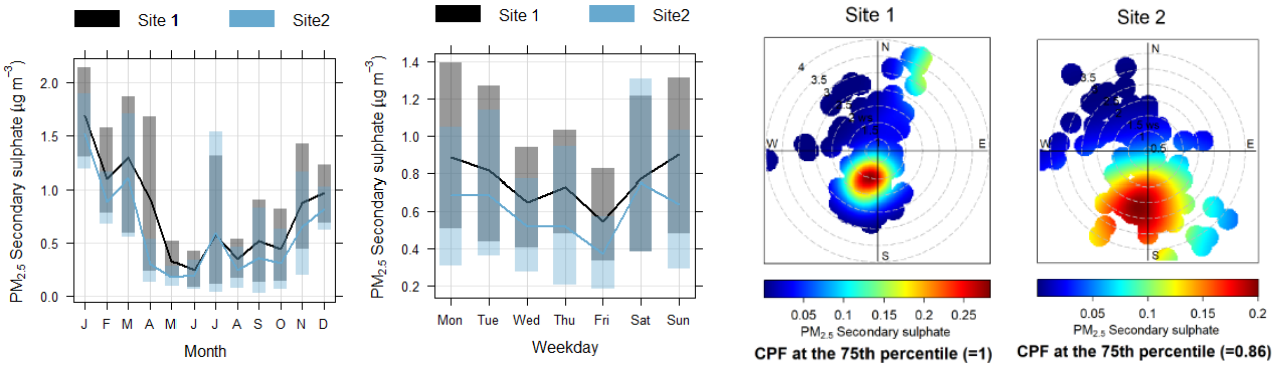

Figure 25. Timeseries and CPF polar plots for $PM_{2.5}$ secondary sulphate source contributions (µg m^{-3}) at sites 1 and 2 from 5 May 2021 to 12 May 2022. Wind speeds are meters per second (m s^{-1}).

Secondary nitrate

The primary chemical species in this source profile is nitrate (NO_3^-) (Figure A16 and Figure A17). The formation of nitrate aerosol is typically attributed to atmospheric reactions of ammonia, sea salt and mineral dust with nitric acid or nitrogen oxides such as NO_2, NO_3 and N_2O_5 (Zhang, et al., 2015). Studies have indicated that the mineral dust ($CaCO_3$) and sea salt (NaCl) emitted from natural sources could undergo atmospheric aging through reactions with nitric acid or nitrogen oxides, resulting in the formation of $Ca(NO_3)_2$ and $NaNO_3$ (Zhang, et al., 2015).

The presence of sodium (Na) in the source profile (Na:NO_3 = 0.8 at both sites 1 and 2) suggests that this source is primarily aged sea salt. The seasonal cycle of this source also shows elevated concentrations in warmer months, which also supports that this is an aged sea salt or marine source (Figure 26).

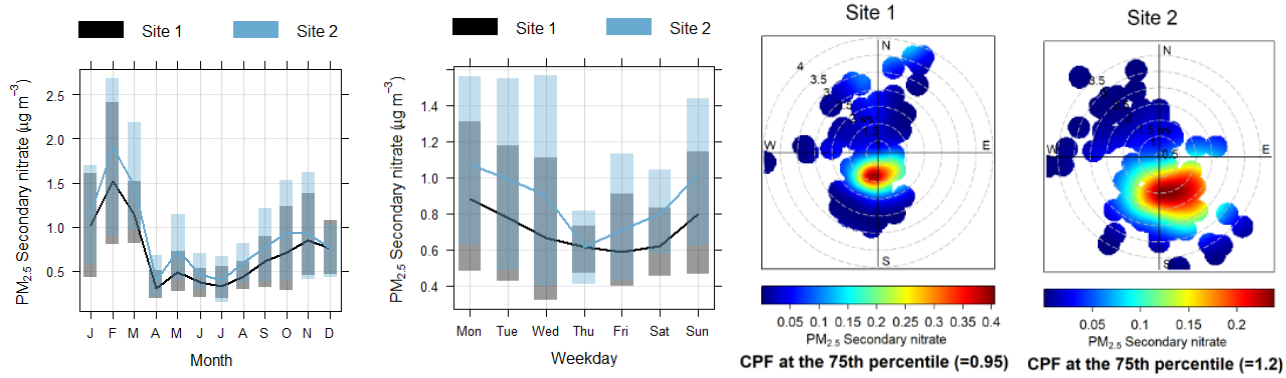

Figure 26. Timeseries and CPF polar plots for $PM_{2.5}$ secondary nitrate source contributions (µg m^{-3}) at sites 1 and 2 from 5 May 2021 to 12 May 2022. Wind speeds are meters per second (m s^{-1}).

Ammonium nitrate on 10 July 2021

On 10 July 2021, when the maximum $PM_{2.5}$ concentration was recorded at both sites 1 and 2, approximately a quarter of the $PM_{2.5}$ mass (6.2 µg m^{-3} and 6.4 µg m^{-3} at sites 1 and 2 respectively) was not predicted by the PMF model or represented by the sources described above. This can happen when exceptional pollution events occur that don't follow typical pollution patterns. While PMF is very good at identifying typical pollution patterns, it can also go some way to help identify exceptional pollution events. However, these events are typically not very well represented by the PMF model, so we need to use other means to understand exceptional pollution events.

On 10 July 2021, PMF analysis underpredicted elevated ammonium (NH_4^+) and nitrate (NO_3^-) concentrations at both sites 1 and 2 (see Appendix 7). The differences between the observed versus predicted concentrations of NH_4^+ and NO_3^- was approximately 90% and 80% of the missing $PM_{2.5}$ mass concentration (6.2 µg m^{-3} and 6.4 µg m^{-3}). Taking into consideration the PMF modelling uncertainty of at least 10%, it is reasonable to assume that the unpredicted $PM_{2.5}$ mass can be attributed to an ammonium nitrate aerosol.

In urban areas, at temperatures below about 5 °C, ammonium nitrate particles can form – via condensation of nitric acid and ammonia vapours – onto particles as small as a few nanometers in diameter (Wang, et al., 2020). Because of the strong temperature dependence of this reaction, it is expected to occur in winter, driven by vertical mixing and in an urban setting such as inner west Melbourne, strongly impacted by human activities such as motor vehicles. The ambient temperature on 10 July 2021 ranged from 0 to 15 °C across metropolitan Melbourne. NO_2 concentrations were also elevated on 10 July 2021, which is likely from build-up of vehicle traffic pollution (Figure 27). However, it is unclear where the source of ammonia came from.

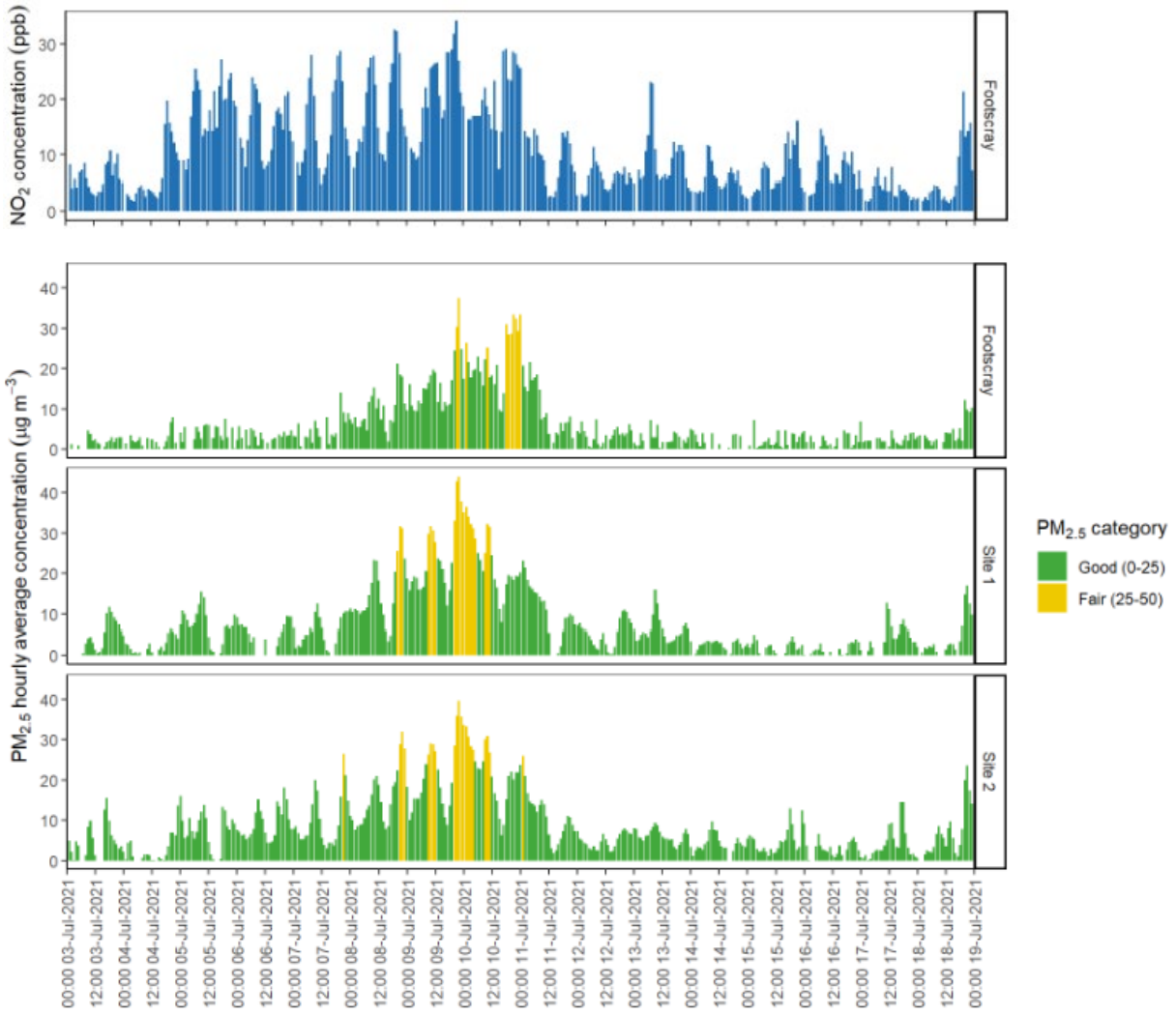

Figure 27. NO_2 hourly average concentrations at Footscray and $PM_{2.5}$ hourly average concentrations at sites 1, 2 and Footscray during 3 to 19 July 2021.

Wind conditions in metropolitan Melbourne were calm on the 10 July 2021 and for a couple of days before, with a high-pressure system over Victoria and wind speeds of less than 2 m s^{-1}. These conditions enabled air pollution to recirculate and build up over several days. In stable wind conditions like this, and because this event occurred for one day only, CPF polar plots are not suitable for identifying the source of pollution. Instead, air back-trajectories were used to show the movement of air parcels over time.

Figure 28 shows 96-hour air back trajectories arriving at site 1 every three hours during 9 and 10 July 2021. The air circulated over metropolitan Melbourne and southwest of metropolitan Melbourne for 24-48 hours, including Port Phillip Bay. Prior to this, the air also travelled over central northern Victoria. Based on the air back-trajectories, it is reasonable to assume that the source of ammonia could be somewhere in under these trajectory lines.

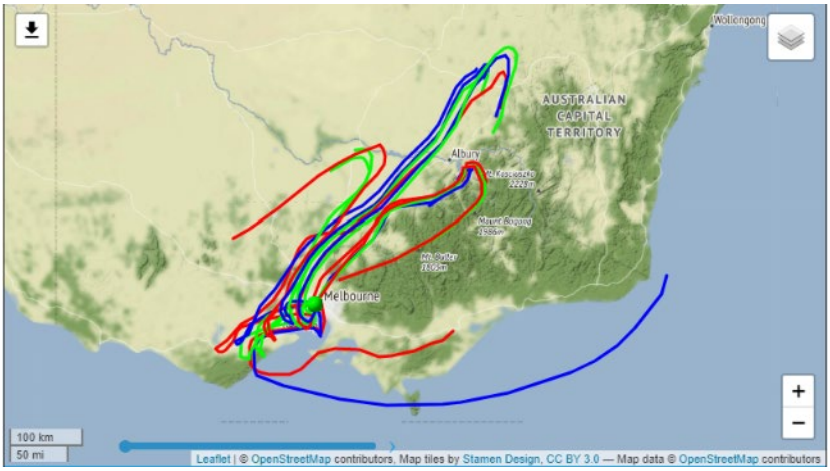

Figure 28. 96-hour air back-trajectories arriving at site 1 every three hours during 9 and 10 July 2021 (Stein, et al., 2015; Rolph, et al., 2017) at 10 m height. Location of site 1 is shown by green dot.

In 2020, there were 154 industries across Victoria that emitted ammonia vapours (Figure 29) (Department of Agriculture, Water and the Environment, 2020). The two largest ammonia emission sources were beef cattle feedlot sites (these were also the only beef cattle feedlot sites that reported ammonia emissions in Victoria in 2020). Emissions from these two sites combined accounted for over 50% of all the ammonia emissions in Victoria in 2020. One of these beef cattle feedlot sites is in northern Victoria and sits under the air back trajectory lines. This site emitted 1.36 million kg of ammonia in 2020. Using this source alone, on average this would produce approximately 3,700 kg of ammonia vapours per day.

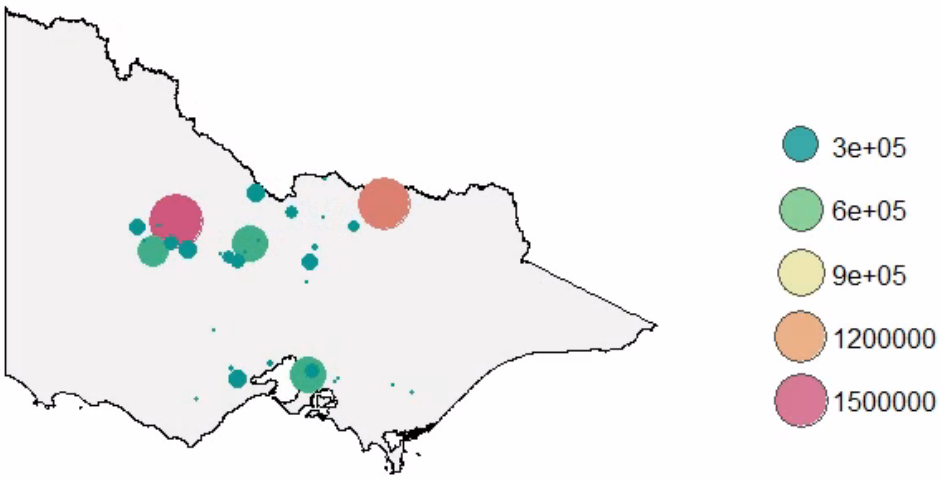

Figure 29. Industries with ammonia emissions in Victoria in 2020, the size and colour of the dots represent the amount of ammonia emissions (kg).

$PM_{2.5}$ concentrations were elevated at all EPA air monitoring stations in metropolitan Melbourne on 10 July 2021. Based on the meteorological conditions and the similar sources attributed to $PM_{2.5}$ at both sites 1 and 2 on 10 July 2021, it is also reasonable to assume that this was a widespread event across metropolitan Melbourne.

If we estimate that the area impacted across metropolitan Melbourne had a 15 km radius and 1,900 m mixing height (July maximum mixing height over several years) (Bi, et al., 2013), then the air volume of interest is approximately 1,300 km^3. This equals approximately 8,600 kg of ammonium nitrate aerosol in the Melbourne airshed on 10 July 2021 (based on a concentration of 6.4 µg m^{-3} ammonium nitrate aerosol at sites 1 and 2), or potentially 4,300 kg of ammonia. Based on these rough estimations, the beef cattle feedlot ammonia emissions (average approx. 3,700 kg per day) accounted for approximately 86 % of the ammonia particle mass in the Melbourne airshed on 10 July 2021.

It's possible that the ammonia could have come from agricultural sources like beef cattle feedlots.

Summary

The study examined $PM_{2.5}$ samples collected from 11 sites across inner west Melbourne between May 2021 to May 2022. Two of the 11 sites were generally representative of ambient air conditions. These were Site 1: Yarraville and Site 2: Spotswood.

The main chemical species identified were black carbon (BC) and organic carbon (OC), comprising ~ 60% of the average $PM_{2.5}$ concentrations at sites 1 and 2. Some BC and OC particles are harmful to human health, and some have a warming effect on the atmosphere.

Ten common sources of $PM_{2.5}$ were identified at the two ambient locations in inner west Melbourne (see Table 4), with two additional industry sources impacting site 1.

Some of the ten common sources were local, such as vehicles emissions, wood heating, industry and shipping. And other sources are regional or from afar, such as hazard reduction burning, marine aerosol and secondary sulphate aerosol.

Most sources of $PM_{2.5}$ in inner west Melbourne were from human activities, such as diesel vehicle emissions and biomass burning or smoke (from residential wood heater use in winter and hazard reduction burning in autumn). The sources that are related to human activities can be managed to reduce pollution.

Some $PM_{2.5}$ in the study formed when natural and human sources reacted. For example, the formation of secondary nitrate.

Other sources were natural, such as sea salts, and cannot be managed. Sea salts are not harmful to human health.

Bushfires and dust storms are also natural sources that can impact Melbourne. However, no bushfires or dust storms impacted metropolitan Melbourne during the study.

Table 4. Ten sources of $PM_{2.5}$ observed at both sites 1 and 2.

Source	Contribution	Origin	Locality	Description
Diesel vehicle emissions	Major contributor to $PM_{2.5}$	Human activities	Local	Most likely heavy vehicles/trucks
Fresh biomass burning	Major contributor to $PM_{2.5}$ in winter	Human activities	Local	Residential wood heating
Aged biomass burning	Major contributor to $PM_{2.5}$ in autumn and winter	Human activities	Mixed local and regional	Hazard reduction burns (autumn) Residential wood heating (winter)
Secondary sulphate	Major contributor to $PM_{2.5}$ in summer	Mixed natural and human activities	Regional	Undetermined source, could come from various sources of sulphur such as natural sources, burning of fossil fuels or wood burning
Marine aerosol	Major contributor to $PM_{2.5}$ in summer	Natural	Regional	Sea salt
Secondary nitrate	Major contributor to $PM_{2.5}$ in summer	Mixed natural and human activities	Mixed local and regional	Nitrous oxides from motor vehicles mixed with aged marine aerosol
Petrol vehicle emissions	Minor contributor to $PM_{2.5}$	Human activities	Local	Most likely passenger petrol vehicles
Crustal matter	Minor contributor to $PM_{2.5}$	Human activities	Local	Most likely windblown road dust
Shipping	Minor contributor to $PM_{2.5}$	Human activities	Local	Shipping exhaust
Ammonium nitrate	Major contributor to a single $PM_{2.5}$ pollution event in winter	Human activities	Mixed local and regional	Nitrous oxides from motor vehicles mixed with ammonia potentially from agricultural sources

$PM_{2.5}$ concentrations were highest in summer, autumn and winter. Source apportionment and receptor modelling of $PM_{2.5}$ showed marine aerosol, diesel vehicle emissions and secondary aerosol sources were the main contributing sources of $PM_{2.5}$ in **summer** at both sites. At site 1, industry emissions were also a contributing source in summer.

Biomass burning due to hazard reduction burns and diesel vehicle emissions were the main contributing sources of $PM_{2.5}$ in **autumn** at both sites. At site 2, marine aerosol was also a significant contributing source in autumn.

Biomass burning due to the use of wood heaters for domestic heating (in local and regional areas) and diesel vehicle emissions were the main contributing sources of $PM_{2.5}$ in **winter** at both sites.

Crustal matter, shipping and petrol vehicle emissions were minor contributors at both sites all year. However, shipping concentrations were so low at site 2 that receptor modelling analysis could not accurately attribute shipping as a factor at site 2. Industry emissions were also minor contributors at site 1. No industry emissions were identified at site 2.

The **highest recorded $PM_{2.5}$** daily average concentrations occurred on 10 July 2021 at both sites 1 and 2. On this day, $PM_{2.5}$ daily average concentrations were close to and in some cases were higher than the Environmental Reference Standard (ERS) for $PM_{2.5}$ across metropolitan Melbourne.

Three main sources contributed up to 93% and 90% of elevated levels of $PM_{2.5}$ on this day at sites 1 and 2 respectively:

1. biomass combustion from local and regional wood heaters
2. secondary sulphate
3. ammonium nitrate particles, which likely formed when motor vehicle exhausts from Melbourne reacted with ammonia possibly from agricultural sources.

Because this ammonium nitrate source occurred as an isolated event, receptor modelling did not attribute ammonium nitrate as a factor.

In summary, the most predominant sources of $PM_{2.5}$ in inner west Melbourne are from human activities and include:

- local and regional biomass burning (from residential wood heaters in winter and hazard reduction burning in autumn),
- diesel vehicle exhaust emissions
- secondary aerosols.

Reducing air pollution

Results show that more work needs to be done to control sources of air pollution that originate from human activities. For example, results from our study show that diesel vehicle emissions are lower during the weekends, when industrial and commercial traffic is reduced and truck curfews in inner west Melbourne are in place.

A major source of air pollution in winter was smoke from wood heaters. This was surprising as inner west Melbourne is not typically categorised as an area with a high density of wood heater use, such as in peri-urban suburbs of Melbourne or regional areas in Victoria.

Targeting interventions to human activities linked to major $PM_{2.5}$ sources, such as diesel vehicle emissions and wood heater smoke, will have the greatest impact on reducing $PM_{2.5}$ pollution and improve human health in inner west Melbourne.

While natural sources (e.g. marine aerosols) also contribute to $PM_{2.5}$, we cannot control these sources. However, marine aerosols are not a concern for human health.

The study has identified a range of human-related sources of $PM_{2.5}$ in the inner west. Polluters, community, EPA and other decision-makers can use this information to help target pollution-reduction efforts. These efforts may involve:

- cost-benefit analyses of activities that create air pollution to better understand the health impacts and the costs of air pollution

- assessing mitigation measures and policy options for specific sources of air pollution
- informing programs for improving public health outcomes for people impacted by air pollution,
- identifying contributors to climate warming
- understand the air pollution issues that may arise around new developments, such as the Fisherman's Bend urban renewal project.

This study supports the objectives of the Victorian Air Quality Strategy, which is working to reduce air pollution and tackle major pollution sources.

References

Adam, M. et al., 2021. Biomass burning events measured by lidars in EARLINET - Part 2: optical properties investigation. *Atmos. Chem. Phys. Discuss.*.

Agrawal, H. et al., 2008. In-use gaseous and particulate matter emissions from a modern ocean going container vessel. *Atmospheric Environment,* 42(21), pp. 5504-5510.

Agrawal, H., Welch, W. A., Miller, J. W. & Cocker, D. R., 2008. Emission measurements from a crude oil tanker at sea. *Environmental Science and Technology,* 42(19), pp. 7098-7103.

Agriculture Victoria, 2020. *Victoria's Climate.* [Online]
Available at: https://vro.agriculture.vic.gov.au/dpi/vro/vrosite.nsf/pages/climate_vic

Ancelet, T. et al., 2011. Carbonaceous aerosols in an urban tunnel. *Atmospheric Environment,* 45(26), pp. 4463-4469. Doi: 10.1016/j.atmosenv.2011.05.032.

ARA Instruments, 2023. *N-FRM Sampler.* [Online]
Available at: https://arainstruments.com/products/n-frm-sensor

AS 3580.14, 2014. *Methods for sampling and analysis of ambient air, Part 14: Meteorological monitoring for ambient air quality monitoring applications. Standards Australia,* s.l.: s.n.

AS 3580.5.1, 2011. *Methods for sampling and analysis of ambient air, Method 5.1: Determination of oxides of nitrogen - Direct reading instrumental method. Standards Australia,* s.l.: s.n.

AS 3580.9.10, 2017. *Methods for sampling and analysis of ambient air, Determination of suspended particulate matter - PM2.5 low volume sampler - Gravimetric method. Standards Australia.,* s.l.: s.n.

AS 3580.9.12, 2013. *Methods for sampling and analysis of ambient air, Method 9.12: Determination of suspended particulate matter - PM2.5 beta attenuation monitors. Standards Australia,* s.l.: s.n.

Australian Government, 2021. *National Environment Protection (Ambient Air Quality) Measure.* [Online]
Available at: https://www.legislation.gov.au/Details/F2021C00475

Bi, D. et al., 2013. The ACCESS Coupled Model: Description, Control Climate and Evaluation. *Australian Meteorological and Oceanographic Journal,* 63(1), pp. 41-64. Doi: 10.22499/2.6301.004.

Binskin, M. M., Bennett, A. & Macintosh, A., 2020. *The Royal Commission into National Natural Distaster Arrangements Report. Commonwealth of Australia.*. [Online]
Available at: https://naturaldisaster.royalcommission.gov.au/publications/royal-commission-national-natural-disaster-arrangements-report

Brown, S. G., Eberly, S., Paatero, P. & Norris, G. A., 2015. Methods for estimating uncertainty in PMF solutions: Examples with ambient air and water quality data and guidance on reporting PMF results. *Science of the Total Environment,* Volume 518-519, pp. 626-635. Doi: 10.1016/j.scitotenv.2015.01.022.

Cahill, T. A., Eldred, R. A., Motallebi, N. & Malm, W. C., 1989. Indirect measurement of hydrocarbon aerosols across the United States by nonsulfate hydrogen-remaining gravimetric mass correlations. *Aerosol Science and Technology,* 10(2), pp. 421-429. Doi: 10.1080/02786828959281.

Cahill, T. A. et al., 1990. *Sptial and temporal trends of fine particles at remote US sites. In proceedings: 83rd Air and Waste Management Association Annual Meeting.* Pittsburgh, Pennsylvania, Air and Waste Management Association.

Carslaw, D. C. & Ropkins, K., 2012. openair - An R package for air quality data analysis. *Environment Modelling and Software,* 0(27-28), pp. 52-61. Doi: 10.1016/j.envsoft.2011.09.008.

Chow, J. C. et al., 2007. The IMPROVE_A Temperature Protocol for Thermal/Optical Carbon Analysis: Maintaining Consistency with a Long-Term Database. *Journal of the Air and Waste Management Association,* 57(9), pp. 1014-1023. Doi: 10.3155/1047-3289.57.9.1014.

Cohen, D., 1999. Accelerator based ion beam techniques for trace element aerosol analysis.. In: S. Landsberger & M. Creatchman, eds. *Elemental analysis of airborne particles.* Amsterdam (NL): Gordon and Breach Science Publishers, pp. 139-196.

Cohen, D. D., Garton, D. & Stelcer, E., 2000. Multi-elemental methods for fine particle source apportionment at the global baseline station at Cape Grim, Tasmania. *Nuclear instruments and methods in physics research, Section B: Beam interactions with materials and atoms,* Volume 161-163, pp. 775-779. Doi: 10.1016/S0168-583X(99)00910-6.

Conkling, J. A., 2000. *Pyrotechnics.* s.l.:Kirk-Othmer Encyclopedia of Chemical Technology.

De Silva, S., Ball, A. S., Indrapala, D. V. & Reichman, S. M., 2021 and references therein. Review of the interactions between vehicular emitted potentially toxic elements, roadside soils and associated biota. *Chemosphere,* Volume 263, p. 128135. Doi: 10.1016/j.chemosphere.2020.128135.

Deniver van der Gon, H. A. C. et al., 2013. The policy relevance of wear emissions from road transport, now and in the future - An international workshop report consensus statement. *Journal of the Air and Waste Management Association,* Volume 63, pp. 136-149.

Department of Agriculture, Water and the Environment, 2020. *National Pollutant Inventory.* [Online] Available at: https://www.npi.gov.au/npi-data/search-npi-data

Department of Environment, Land, Water and Planning, 2019. *Victoria in future.* [Online] Available at: https://www.planning.vic.gov.au/land-use-and-population-research/victoria-in-future

Department of Transport Victoria, 2021. *Traffic Volumes for Freeways and Arterial Roads.* [Online] Available at: https://discover.data.vic.gov.au/dataset/traffic-volume

Dunne, E. et al., 2019. *Measurements of air quality at a hydraulic fracturing site in the Surat Basin, Queensland - Draft report. Task 3 report for project W.12 to the Gas Industry Social and Environmental Research Alliance (GISERA),* Canberra, Australia: CSIRO.

EPA Victoria, 2021. *Publication 2028: 2016 emissions inventory report.* [Online] Available at: https://www.epa.vic.gov.au/about-epa/publications/2028

EPA Victoria, 2022. *Publication 2052: Air Monitoring report 2021: Compliance with the Ambient Air Quality National Environment Protection Measure.* [Online] Available at: https://www.epa.vic.gov.au/about-epa/publications/2052-nepm-compliance-air-monitoring-report

Fitzgerald, J. W., 1991. Marine aerosols: A review. *Atmospheric Environment - Part A General Topics,* 25(3-4), pp. 533-545.

Fridell, E., Steen, E. & Peterson, K., 2008. Primary particles in ship emissions. *Atmospheric Environment,* 42(5), pp. 1160-1168.

Goldsworthy, L. & Goldsworthy, B., 2015. Modelling of ship engine exhaust emissions in ports and extensive coastal waters based on terrestrial AIS data - An Australian case study. *Environmental Modelling and Software,* Volume 63, pp. 45-60.

Healy, R. M. et al., 2009. Characterisation of single particles from in-port ship emissions. *Atmospheric Environment,* 43(40), pp. 6408-6414.

Horvath, H., 1993. Modelling of ship engine exhaust emissions in ports and extensive coastal waters based on terrestrial AIS data - An Australian case study. *Atmospheric Environment - Part A General Topics,* 27(3), pp. 45-60.

Horvath, H., 1997. Experimental calibration for aerosol light absorption measurements using the integrating plate method - summary of the data. *Journal of Aerosol Science,* 28(7), pp. 1149-1161. Doi: 10.1016/S0021-8502(97)00007-4.

Hyslop, N. P. et al., 2019. An inter-laboratory evaluation of new multi-element reference materials for atmospheric particulate matter measurements. *Aerosol Science and Technology,* 53(7), pp. 771-782. Doi: 10.1080/02786826.2019.1606413.

Iinuma, Y. et al., 2007. Source characterisation of biomass burning particles: The combustion of selected European conifers, African hardwood, savanna grass, and German and Indonesian peat. *Journal of Geophysical Research: Atmospheres,* 112(D8).

Inner West Air Quality Community Reference Group, 2020. *Report: Air pollution in Melbourne's inner west: taking direct action to reduce our community's exposure.* [Online]
Available at: https://www.environment.vic.gov.au/sustainability/inner-west-air-quality-reference-group

Kara, M. et al., 2015. Characterization of PM using multiple site data in a heavily industrialized region of Turkey. *Aerosol and Air Quality Research,* 15(1), pp. 11-27. Doi: 10.4209/aaqr.2014.02.0039.

Keywood, M. et al., 2019. Comprehensive aerosol and gas data set from the Sydney Particle Study. *Earth System Science Data,* 11(4), pp. 1883-1903. Doi: 10.5194/essd-11-1883-2019.

Lee, E., Chan, C. K. & Paatero, P., 1999. Application of positive matrix factorization in source apportionment of particulate pollutants in Hong Kong. *Atmospheric Environment,* 33(19), pp. 3201-3212.

Lide, D. R., 1992. *CRC Handbook of Chemistry and Physics.* s.l.:CRC Press Inc..

Li, Y. et al., 2021 and references therein. Impacts of chemical degradation on the global budget of atmospheric levoglucosan and its use as a biomass burning tracer. *Environmental Science and Technology,* 55(8), pp. 5525-5536. Doi: 10.1021/acs.0c07313.

Luben, T. J. et al., 2017 and references therein. A systematic review of cardiovascular emergency department visits, hospital admissions and mortality associated with ambient black carbon. *Environment International,* Volume 107, pp. 154-162. Doi 10.1016/j.envint.2017.07.005.

Malm, W. C. et al., 1994. Spatial and seasonal trends in particle concentration and optical extinction in the United States. *Journal of Geophysical Research: Atmospheres,* 99(D1), pp. 1347-1370. Doi: 10.1029/93jd02916.

Mohr, C. et al., 2013. Contribution of nitrated phenols to wood burning brown carbon light absorption in Detling, United Kingdom during winter time. *Environmental Science and Technology,* Volume 47, pp. 6316-6324.

Moldanova, J. et al., 2009. Characterisation of particulate matter and gaseous emissions from a large ship diesel engine. *Atmospheric Environment,* 43(16), pp. 2632-2641.

Paatero, P., Elberly, S., Brown, S. & Norris, G., 2014. Methods for estimating uncertainty in factor analytic solutions. *Atmospheric measurement techniques,* 3(7), pp. 781-797. Doi: 10.5194/amt-7-781-2014.

Paatero, P. & Hopke, P. K., 2003. Discarding or downweighting high-noise variables in factor analytic models. *Analytica Chimica Acta,* 490(1), pp. 277-289. Doi: 10.1016/S0003-2670(02)01643-4.

Pani, S. H. et al., 2020. Thepnuan black carbon over an urban atmosphere in northern peninsular Southeast Asia: characteristics, source apportionment, and associated health risks. *Environmental Pollution,* Volume 259, p. 113871. Doi: 10.1016/j.envpol.2019.113871.

Pant, P. & Harrison, R. M., 2013. Estimation of the contribution of road traffic emissions to particulate matter concentrations from field measurements: A review. *Atmospheric Environment,* Volume 77, pp. 78-97. Doi: 10.1016/j.atmosenv.2013.04.028.

Polissar, A. V., Hopke, P. K. & Harris, J. M., 2001. Source regions for atmospheric aerosol measured at Barrow, Alaska. *Environmental Science and Technology,* 35(21), pp. 4214-4226.

Polissar, A. V. et al., 1998. Atmospheric aerosol over Alaska: 2. Elemental composition and sources.. *Journal of Geophysical Research: Atmospheres,* 103(D15), pp. 19045-19057. Doi: 10.1029/98JD01212.

R Core Team, 2011. *R: A language and environment for statistical computing. R Foundation for Statistical Computing, Vienna, Austria.* [Online]
Available at: https://www.R-project.org

Rolph, G., Stein, A. & Stunder, B., 2017. Real-time Environmental Applications and Display sYstem: READY. *Environmental Modelling and Software,* Volume 95, pp. 210-228. Doi: 10.1016/j.envsoft.2017.06.025.

Satish, R. & Rastogi, N., 2019. On the use of brown carbon spectra as a tool to understand their broader composition and characteristics: a case study from crop residue burning samples. *ACS Omega,* Volume 4, pp. 1847-1853.

Seinfeld, J. H. & Pandis, S. N., 2006. *Atmospheric Chemistry and Physics: From Air Pollution to Climate Change.* New York: John Wiley and Sons, Inc.

Song, X. H., Polissar, A. V. & Hopke, P. K., 2001. Sources of fine particle composition in the northeast US. *Atmospheric Environment,* 35(31), pp. 5277-5286. Doi: 10.1016/S1352-2310(01)00338-7.

Stein, A. F. et al., 2015. NOAA's HYSPLIT atmospheric transport and dispersion modelling system. *Bulletin of the American Meteorological Society,* Volume 96, pp. 2059-2077. Doi: 10.1175/BAMS-D-14-00110.1.

USEPA IO-3.3, 1999. *USEPA Compendium Method OI-3.3, Determination of metals in ambient particulate matter using x-ray fluorescence (XRF) spectroscopy. US Environment Protection Authority.,* EPA-ORD, Cincinnati: s.n.

USEPA, 2009. *Integrated Science Assessment for Particulate Matter (Final report). Technical Report. US EPA Natoinal Centre for Environmental Assessment. Research Triangle Park.* [Online]
Available at: https://cfpub.epa.gov/ncea/cfm/recordisplay.cfm?deid=216546

Victorian Government, 2021. *Environmental reference standard.* [Online]
Available at: https://www.gazette.vic.gov.au/gazette/Gazettes2021/GG2021S245.pdf

Wang, M., Kong, W. & Marten, R., 2020. Rapid growth of new atmospheric particles by nitric acid and ammonia condensation. *Nature,* Volume 581, pp. 184-189. Doi: 10.1038/s41586-020-2270-4.

Wang, X. et al., 2022. Apportionment of vehicle fleet emissions by linear regression, positive matrix factorisation, and emission modelling. *Atmosphere,* Volume 13, p. 1066. Doi: 10.3390/atmos13071066.

Watson, J. G., Chow, J. C. & Frazier , C. A., 1999. X-ray fluorescence analysis of ambient air samples. In: S. Landsberger & M. Creatchman, eds. *Elemental analysis of airborne particles.* Amsterdam (NL): Gordon

and Breach Science Publishers, pp. 67-96. (Advances in environmental, industrial and process control technologies, 1).

Whitacre, S. D., Tsai, H. C. & Orban, J., 2002. *Lubricant basestock and additive effects on diesel engine emissions,* Washington, DC, USA: U.S. Department of Energy.

WHO Regional Office for Europe, 2013. *Review of evidence on health aspects of air pollution - REVIHAAP. Technical report. ,* Copenhagen: WHO Regional Office for Europe.

WHO, 2021. *WHO global air quality guidelines: Particulate matter (PM2.5 and PM10), ozone, nitrogen dioxide, sulfur dioxide and carbon monoxide*. [Online]
Available at: https://apps.who.int/iris/handle/10665/34532

Wickham, H., 2016. *ggplot2: Elegant Graphics for Data Analysis,* New York: Springer-Verlag.

Yatkin, S. et al., 2020. Comparison of a priori and interlaboratory-measurement-consesus approaches for value assignment of multi-element reference materials on PTFE filters. *Microchemical Journal,* Volume 158. Doi: 10.1016/j.microc.2020.105225.

Yuan, W. et al., 2020. Characterisation of the light-absorbing properties, chromosphere composition and sources of brown carbon aerosol in Xi'an, northwest China. *Atmospheric Chemistry and Physics,* Volume 20, pp. 5129-5144.

Zhang, Q. et al., 2007. Ubiquity and dominance of oxygenated species in organic aerosols in anthropogenically-influenced Northern Hemisphere midlatitudes. *Geophysical Research Letters,* 34(13).

Zhang, R. et al., 2015. Formation of urban fine particulate matter. *Chemical Reviews,* Volume 115, pp. 3803-3855. Doi: 10.1021/acs.chemrev.5b00067.

Appendix 1. Conceptual model for inner west Melbourne

This conceptual model is a representation of the inner west Melbourne airshed that describes emission sources and receptors. The model was developed to consider the study area, meteorology, receptors and source identification. The information was layered in a series of maps to build a spatial model of inner west Melbourne $PM_{2.5}$ pollution. This model informed the $PM_{2.5}$ source apportionment project.

Study area

The study area comprised approximately 63 square kilometres extending from Brooklyn in the west through to North Melbourne in the east; Newport in the south through to Footscray in the north. The following Local Government Areas (LGAs) are part of the study area:

- City of Brimbank
- City of Hobsons Bay
- City of Maribyrnong
- City of Melbourne
- City of Port Phillip

The study area is relatively flat, with elevations at or near sea level for land adjacent to Hobsons Bay, the Yarra River, the Maribyrnong River and the lower reaches of Kororoit Creek. The highest elevations are 20 to 30 m in Tottenham and parts of Brooklyn.

Receptors

Receptors are people or places within the environment that are impacted by $PM_{2.5}$ pollution in the air. There are numerous residential zones within the study area as well as public parks and recreational zones.

The greatest number of people in the study area are located immediately west of Melbourne, in locations near to major roads associated with the West Gate Freeway and industrial activities in Port Melbourne (Figure A1). Estimated Resident Population (ERP) predictions for 2035/2036 show that all suburbs within the study area will increase in ERP, with the greatest change predicted for industrial Port Melbourne (Department of Environment, Land, Water and Planning, 2019). This area currently has negligible ERP, however this is predicted to increase to 23,501 people in 2035/2036 with significant development in the Fishermans Bend Precinct.

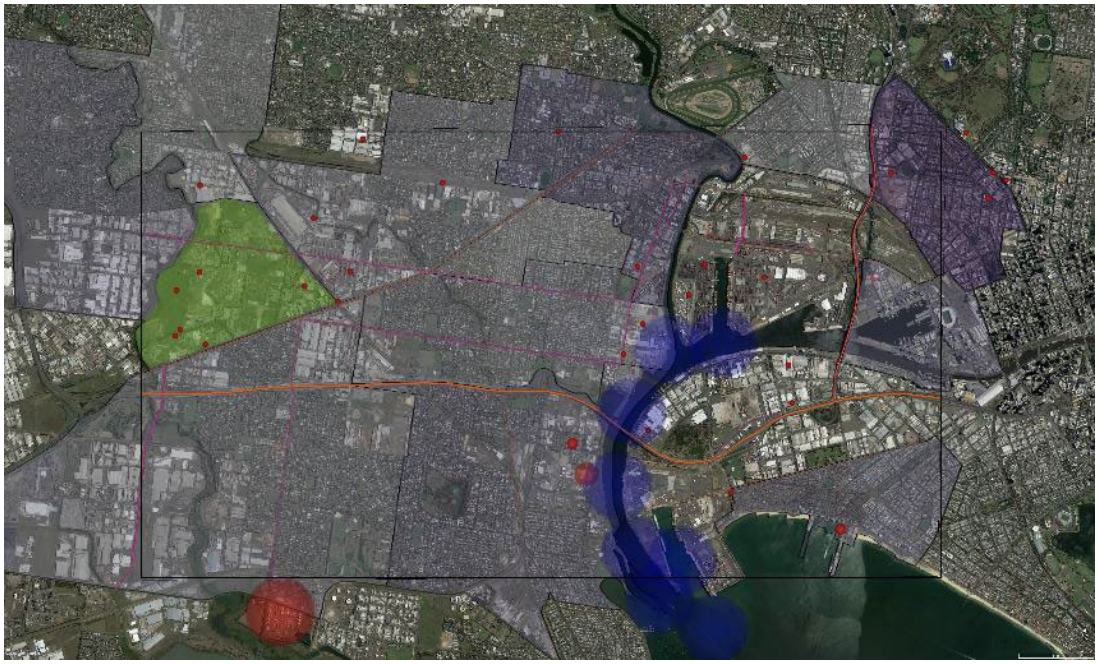

KEY

Traffic		**Industry**		**Population**	
	≤ 10% trucks		NPI reporting facility $PM_{2.5}$ emissions ≤6,000 kg/year	No colour	<2,500 ERP
	>10% ≤20% trucks		NPI reporting facility $PM_{2.5}$ emissions >6,000 ≤ 12,000 kg/year		2,500 – 7,500 ERP
	>20% ≤30% trucks		NPI reporting facility $PM_{2.5}$ emissions >12,000 ≤ 24,000 kg/year		7,500 – 12,500 ERP
	>30% ≤40% trucks		NPI reporting facility $PM_{2.5}$ emissions >24,000 ≤ 36,000 kg/year		12,500 – 17,500 ERP
	>40% ≤50% trucks		NPI reporting facility $PM_{2.5}$ emissions >36,000 ≤ 48,000 kg/year		17,500 – 22,500 ERP
	≤40,000 AADV		NPI reporting facility $PM_{2.5}$ emissions >48,000 <60,000 kg/year		22,500 – 27,500 ERP
	>40,000 ≤80,0000 AADV		Shipping emission ≅ 55,000 kg/year		27,500 – 32,500 ERP
	>80,000 ≤120,000 AADV		Brooklyn Industrial Estate, potential windblown dust sources		
	>120000 ≤160,000 AADV				
	>160,000 ≤200,000 AADV				

Figure A1. Conceptual model of emission sources and receptors (image: Google Earth, accessed on 5 November 2020).

Meteorology

Victoria's climate is a function of its proximity to the Southern Ocean and the east-west topographical features of the Great Dividing Range. Weather generally moves from west to east, influenced by seasonal Southern Ocean weather patterns and the El Nino Southern Oscillation (Agriculture Victoria, 2020).

EPA's long term monitoring at the Footscray ambient air monitoring station (AAMS) has recorded meteorological trends in the inner west over time, so that data was used in the study.

Footscray AAMS temperature, wind speed and wind direction data showed seasonal variation, with the warmest months being November to February and the coolest minimum recorded in August. The wind patterns also displayed seasonal variation, with the summer months recording frequent southerlies, changing to northerly and north-north westerly in the winter. Spring and autumn recorded variable wind regimens. Easterlies were rarely observed in any season.

Source identification

$PM_{2.5}$ in ambient air is a result of polluting activities within the airshed, and secondary formation processes associated with atmospheric chemistry. Activities contributing to $PM_{2.5}$ in Victoria are:

- industry and commercial activity
- wood heaters
- windblown dust
- bushfires and hazard-reduction burning
- transport.

$PM_{2.5}$ can also occur from atmospheric mixing, when chemicals such as oxides of sulphur (SOx), oxides of nitrogen (NOx), ammonia (NH_3) and volatile organic compounds mix with particles downwind of the emission source, generating more $PM_{2.5}$ particles.

Sea salt can also be a source of $PM_{2.5}$, with sea salt forming over water surfaces and creating particles that travel inland and contribute to total $PM_{2.5}$ in the air. Sea salt can also interact with other species to form new particles or change their chemical composition – these are called secondary aerosols.

The sources of $PM_{2.5}$ relating to these broad categories in Melbourne's inner west is presented in the following sections.

Industrial and commercial activity

The National Pollutant Inventory (NPI) is an inventory of 93 pollutants emitted from industrial sources across Australia. In the reporting period of 2018/2019, the NPI listed 34 pollutants within, or immediately adjacent to, the study area. The study area includes a wide range of NPI reporting activities, including oil refining (48%), fossil fuel electricity generation (22%) and glass and glass product manufacturing (7%) (Department of Agriculture, Water and the Environment, 2020).

The NPI does not require reporting of $PM_{2.5}$ emissions from diffuse mobile sources such as shipping. Shipping emissions for Melbourne were estimated by researchers at the Australian Maritime College/University of Tasmania as 440,000 kg per year, for the year 2010/2011 (Goldsworthy & Goldsworthy, 2015). In comparison with the other industrial sources, $PM_{2.5}$ emissions from shipping are approximately 8 times greater than the largest facility emission reported to NPI.

The NPI reported emissions and estimated shipping emissions are presented in their geographical context in Figure A1. The results show a group of small emission sources in north west of the study

domain, centred on the Brooklyn Industrial Estate. In the south west corner, on the edge of the study area, Mobil Refining is the only emission source. However its contribution is significant, comprising approximately half NPI-reported $PM_{2.5}$.

Mobil is transitioning its Altona plant from refining to an import terminal, and emissions are expected to decrease in future years as oil production ceases at the facility. Although Altona isn't in the study area, under certain weather conditions, emissions from Altona could impact the study area.

The remaining cluster of industrial sources are near to the Port of Melbourne in adjoining suburbs Yarraville, West Melbourne, industrial Port Melbourne and Spotswood. The Port itself contributes emissions from stevedoring and a significant contribution from shipping.

Wood heaters

In addition to the NPI, EPA has compiled an emissions inventory, which lists $PM_{2.5}$ sources by emission type and LGA (EPA Victoria, 2021). The EPA emissions inventory includes $PM_{2.5}$ estimates from wood heater use in the five LGAs intersecting with the study area. The estimates are reproduced in Table A1 and Figure A2.

The City of Brimbank is predicted to have the highest $PM_{2.5}$ emissions from solid fuel burning, followed by the City of Port Phillip. Despite these differences, the results are within the same order of magnitude, and $PM_{2.5}$ wood heater emissions are likely to be a consistent component of $PM_{2.5}$ pollution during the winter months across the study area.

Table A1. $PM_{2.5}$ emissions (kg/year) by LGA in 2016 (EPA Victoria, 2021).

LGA	Industry	Commercial	Shipping	Wood heaters	Rail transport	Road transport
City of Brimbank	4,107	5,489	0	40,010	433	160,914
City Hobsons Bay	73,079	3,126	0	19,641	784	95,263
City of Maribyrnong	3,773	2,488	0	19,474	595	39,922
City of Melbourne	34,942	20,350	450,000	25,774	470	96,182
City of Port Phillip	8,097	3,158	0	31,138	0	49,522

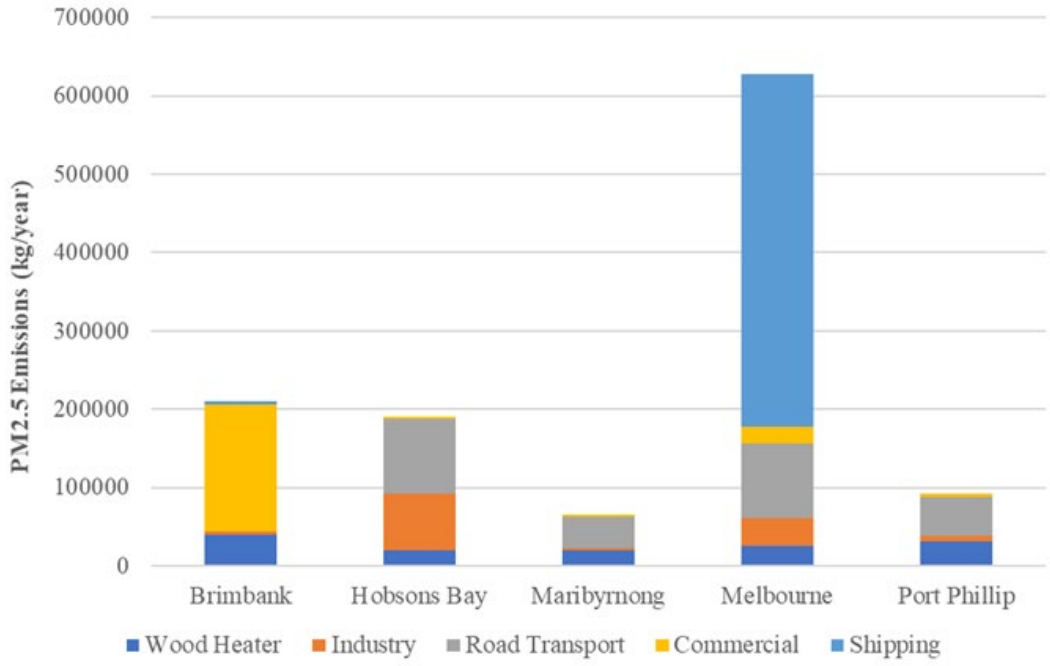

Figure A2. $PM_{2.5}$ emissions (kg/year) by LGA in 2016 (EPA Victoria, 2021).

Crustal material/windblown dust

Airborne crustal particulate matter is mostly coarse particulate matter (larger than $PM_{2.5}$), but also includes a $PM_{2.5}$ component. Meteorological conditions contribute to dust generation, with warm, windy days conducive to higher concentrations of airborne dust.

The Inner West Air Quality Community Reference Group identified the following windblown dust sources in their report on air pollution (Inner West Air Quality Community Reference Group, 2020):

- Material crushing facilities
- Demolition and material handling and processing sites
- Landfills
- Shipping container storage areas and container parks
- Open, unsealed land in industrial facilities
- Undeveloped and vacant sites
- Unsealed roads and verges
- Major construction and development sites.

Bushfires and hazard reduction burns

Smoke from bushfires and hazard reduction burns has the potential to impact the airshed and significantly contribute to the $PM_{2.5}$ fraction. In the extreme example of the 2019/2020 bushfires, smoke travelled hundreds of kilometres from its source, and blanketed large parts of Australia (Binskin, et al., 2020). The impact of smoke from bushfires and hazard reduction burns is seasonal, typically occurring in summer and autumn.

Transport

Transport emissions are a broad category that includes rail and road transport. $PM_{2.5}$ emissions from rail transport are primarily emissions from diesel fuelled locomotives and railcars. Road transport $PM_{2.5}$ emissions are the product of combustion in light vehicles and heavy vehicles as well as non-exhaust emissions from road, brake and tyre wear.

EPA's emissions inventory estimates $PM_{2.5}$ emissions from roads and rail at the LGA resolution (Table A1). The majority of transport emissions are road based.

The Department of Transport data for 2020 (Department of Transport Victoria, 2021) was used to identify freeways and arterial roads with the highest vehicle and truck volumes in the study area. Annual Average Daily Vehicle (AADV) and Annual Average Daily Truck (AADT) measures were used to identify the top ten roads by traffic volume and top ten roads by percentage of trucks within the study area (Table A2).

Table A2. Top ten roads within the study area by AADV and AADT (Department of Transport Victoria, 2021). Note: the maximum AADV or AADT for all segments is reported for each road.

Top ten roads by traffic volume				Top ten roads by percentage trucks			
Road Name	**Annual Average Daily Vehicles**	**Annual Average Daily Trucks**	**% Trucks**	**Road Name**	**Annual Average Daily Vehicles**	**Annual Average Daily Trucks**	**% Trucks**
West Gate Freeway	200,000	25, 000	14%	Dock Link Road	2,400	1,100	46%
Western Link Tollway	148,000	18,000	15%	Grieve Parade	29,000	6,800	29%
Geelong Road	53,000	6,600	13%	Somerville Road	14,000	3,400	24%
Docklands Highway	39,000	7,400	19%	Whitehall Street	18,000	2,800	22%
Williamstown Road	39,000	4,300	13%	Francis Street	16,000	3,200	20%
Dynon Road	38,000	3,300	10%	Docklands HWY	39,000	7,400	19%
Smithfield Road	37,000	1,300	4%	Moreland Street	19,000	3,500	18%
Footscray Road	35,000	2,000	6%	Millers Road	30,000	4,000	16%
Melbourne Road	32,000	2,800	9%	Cook Street	19,000	2,600	15%
Hopkins Street	30,000	1,700	12%	Western Link Tollway	148,000	18,000	15%

This coarse analysis assumed the AADT and AADV for the segment with the highest values were consistent for the entire road. The results of the traffic volume analysis indicate that the West Gate Freeway, Western Link Tollway and Geelong Road have the highest traffic volumes in the study area, which includes a significant component of heavy vehicle transport. However additional corridors such as Dock Link Road, Grieve Parade, Somerville Road, Whitehall Street and Francis Street have a significant proportion of trucks (>20%) included in the daily traffic averages.

Traffic volumes at various locations within a 1 km radius of each site were also investigated (Table A3). This analysis showed that vehicle volumes were almost 4 times higher at site 2 compared with site 1. With truck volumes approximately 4.4 times higher at site 2 than site 1.

Table A3. Number of vehicles per day at various locations within a 1 km radius of sites 1 and 2 in 2020 (Department of Transport Victoria, 2021).

Site	Vehicle type	Average	Median	Std Dev	Min	Max	Vehicle count locations
1	All vehicles	7726	6000	4226	1800	20000	34
	Trucks	872	393	910	0	3800	34
2	All vehicles	30813	16000	33963	2300	88000	30
	Trucks	4002	1400	5011	143	13000	30

Appendix 2. Source specific sampling

Source specific sampling is most successful when the sample is comprised, as far as practical, of emissions from the target source. The sample location must be positioned to maximise capture of the plume without unnecessary dilution or influence from extraneous sources. This is best achieved through locating the sampling equipment close to the emission point, and sampling during calm to light wind conditions or when the sampler is downwind.

Two types of sample positions meet these objectives:

- **Short term, unattended** monitoring station, enclosed by temporary fencing.
- **Agile monitoring station**, operated for a short duration whilst attended by EPA staff.

Table A4 outlines the details of each type of installation. Table A5 is a summary of all source specific samples collected.

Table A4. Source specific sampling methodology: station type.

Component	Short term, unattended	Agile
Sample duration	Minimum of 3 hours, up to 24 hours dependent on the source activity	Minimum of 3 hours, dependent on the source activity
Wind conditions	As far as practical for the duration of the sample, the wind conditions should be Beaufort scale 0 – 3: 0: Calm: <0.3 m/s 1: Light air: 0.3 – 1.5 m/s 2: Light breeze: 1.6 – 3.3 m/s 3: Gentle breeze: 3.4 – 5.4 m/s	
Security	Temporary fencing	EPA staff remain with the equipment
Power	Solar panel powered installation	Battery powered installation

Table A5. Source specific samples.

Site	Sample start time	Sample end time	$PM_{2.5}$ ($\mu g\ m^{-3}$)	Observations
3	29/09/21 4:30	29/09/21 8:30	12.2	Six ship arrivals
3	3/10/21 1:00	3/10/21 8:00	1.5	Two ship arrivals and two ship departures
3	12/10/21 13:30	12/10/21 23:00	7.1	One ship arrival and seven ship departures. COVID lockdown 6.0
3	21/10/21 2:00	21/10/21 8:00	0.6	Four ship arrivals. Covid lockdown 6.0
3	21/10/21 23:00	22/10/21 8:00	6.0	Six ship arrivals and three ship departures. COVID lockdown 6.0
3	27/10/21 0:00	27/10/21 8:00	13.9	Five ship arrivals and one ship departure
3	3/11/21 1:30	3/11/21 4:00	14.5	No ship movements
3	16/11/21 20:00	17/11/21 5:00	2.7	Six ship arrivals and two ship departures
3	2/12/21 5:00	2/12/21 10:00	2.9	Ship movements not available
3	6/12/21 2:00	6/12/21 6:00	12.2	Two ship arrivals
3	15/12/21 4:00	15/12/21 8:00	10.6	Five ship arrivals and two ship departures
3	20/12/21 20:00	21/12/21 6:30	14.5	Two ship arrivals and two ship departures
3	18/01/22 20:00	18/01/22 23:59	3.5	Two ship arrivals and four ship departures
3	31/01/22 23:00	1/02/22 5:00	6.11	One ship arrival, fireworks
3	6/02/22 2:00	6/02/22 14:00	6.1	Four ship arrivals and two ship departures
3	8/02/22 22:00	9/02/22 7:00	6.5	Five ship arrivals and three ship departures
3	23/02/22 0:00	23/02/22 12:30	13.4	Seven ship arrivals and four ship departures
3	3/03/22 23:00	4/03/22 11:00	11.1	Nine ship arrivals and six ship departures
3	10/03/22 20:00	11/03/22 14:00	2.3	Ship movements not available
3	28/03/22 13:40	4/04/22 16:40	4.3	99-hour sample. Ship movements not available
4	30/11/21 11:15	30/11/21 14:15	18.8	Heavy vehicles
4	14/02/22 8:12	14/06/22 11:12	4.8	Heavy vehicles queuing
4	22/02/22 7:57	22/02/22 10:57	2.4	Heavy vehicles queuing
5	24/01/22 10:10	24/01/22 12:10	13.7	Heavy vehicles
5	8/02/22 8:06	8/02/22 11:06	14.4	Heavy vehicles
5	28/03/22 8:15	28/03/22 11:15	16.8	Heavy vehicles
6	22/03/22 9:00	23/03/22 15:00	5.8	Ship stationary in Holden dock and sampling occurred at the same time as unloading of diesel from ship
7	5/04/22 9:10	5/04/22 12:10	4.7	Light and heavy vehicles

7	21/05/22 8:30	21/05/22 11:30	14.7	Light and heavy vehicles Heavy vehicles avg. count = 6 per minute
7	23/05/22 10:30	23/05/22 13:30	16.2	Light and heavy vehicles and windblown dust Heavy vehicles avg. count = 12 per minute
7	24/05/22 9:40	24/05/22 12:40	16.3	Light and heavy vehicles Heavy vehicle avg. count = 15 per minute
8	6/04/22 0:00	7/04/22 0:00	8.1	Stevedoring, heavy vehicles and shipping. Ship movements not available
8	3/05/22 0:00	4/05/22 0:00	5.4	Earthworks, stevedoring and heavy vehicles
8	21/05/22 6:00	21/05/22 10:00	22.6	Earthworks, stevedoring and heavy vehicles
8	22/05/22 6:00	22/05/22 10:00	11.0	Stevedoring, shipping and heavy vehicles
8	23/05/22 10:30	23/05/22 13:30	15.1	
8	24/05/22 4:00	24/05/22 10:00	24.7	Earthworks, stevedoring and heavy vehicles
8	25/05/22 0:00	26/05/22 0:00	9.2	
8	18/06/22 4:00	18/06/22 8:00	7.7	Earthworks, stevedoring and heavy vehicles
8	19/06/22 4:00	19/06/22 8:00	11.8	Earthworks, stevedoring and heavy vehicles
8	20/06/22 3:00	20/06/22 9:00	2.9	Earthworks, stevedoring and heavy vehicles
10	18/06/22 9:00	18/06/22 12:00	17.3	Light vehicles avg. count = 10 per minute Heavy vehicles avg. count = 3 per minute
10	19/06/22 9:00	19/06/22 12:00	6.9	Light vehicles avg. count = 8 per minute Heavy vehicles avg. count = 1 per minute
10	20/06/22 10:15	20/06/22 13:15	7.0	Light vehicles avg. count = 8 per minute Heavy vehicles avg. count = 7 per minute
11	18/06/22 13:00	18/06/22 16:00	0	Light vehicles avg. count = 44 per minute
11	19/06/22 13:00	19/06/22 16:00	10.4	Light vehicles avg. count = 38 per minute
11	22/06/22 13:30	22/06/22 16:30	4.7	Light vehicles avg. count = 44 per minute
12	22/06/22 9:15	22/06/22 12:15	4.6	Light vehicles avg. count = 27 per minute Heavy vehicles avg. count = 11 per minute
12	23/06/22 8:35	23/06/22 11:35	1.2	Light vehicles avg. count = 43 per minute Heavy vehicles avg. count = 9 per minute
12	25/06/22 8:10	25/06/22 11:10	6.9	Light vehicles avg. count = 60 per minute Heavy vehicles avg. count = 4 per minute

Appendix 3. Chemical analysis and data quality assurance

Black carbon (BC) analysis by light reflection/transmission

Black carbon (soot) collected on filters was **analysed by light reflection/transmission** to provide the BC concentration. The way the particles absorb or reflect visible light depends on the particle concentration, density, refractive index and size. In the atmosphere, BC is the most effective particle at absorbing light in the visible spectrum, with negligible contributions from soils, sulphates and nitrate (Horvath, 1993; Horvath, 1997). So, for this study, we assumed that all the absorption on the filters is due to BC.

When measuring BC by light reflection/transmission, light from a light source is transmitted through a filter onto a photocell. The amount of light absorption is proportional to the amount of BC present and provides a value that is a measure of the BC on the filter. Conversion of the absorbance value to an atmospheric concentration value of BC requires an empirically derived equation (Cohen, et al., 2000):

$$BC\ (\mu g\ cm^{-2}) = (100/2(F\varepsilon))\ \ln[R_0/R]$$

Where:

- ε is the mass absorbent coefficient for BC ($m^2\ g^{-1}$) at a given wavelength
- F is a correction factor to account for other absorbing factors, such as sulphates, nitrates, shadowing and filter loading. These effects are generally assumed to be negligible and F is set at 1.00.
- R_0, R are the pre- and post-reflection intensity measurements, respectively.

BC was measured at GNS Science using the M43D Digital Smoke Stain Reflectometer. The following equation (from Willy Maenhaut, Institute for Nuclear Sciences, University of Gent, Proeftuinstraat 86, B-9000 GENT, Belgium) was used for obtaining BC from reflectance measurements on Nucleopore polycarbonate filters or Pall Life Sciences Teflon filters:

$$BC\ (\mu g\ cm^{-2}) = [1000\ ´\ LOG(R_{blank}/R_{sample}) + 2.39] / 45.8$$

Where:

- R_{blank} is the average reflectance for a series of blank filters; R_{blank} is close, but not identical, to 100 (GNS Science always uses the same blank filter for adjusting to 100)
- R_{sample} is the reflectance for a filter sample (normally lower than 100)
- 2.39 and 45.8 constants are derived using a series of 100 Nuclepore polycarbonate filter samples, which served as secondary standards.
- BC loading (in $\mu g\ cm^{-2}$) for these samples had been determined by Prof. Dr. MO Andreae (Max Planck Institute of Chemistry, Mainz, Germany) relative to standards that were prepared by collecting burning acetylene soot on filters and determining the mass concentration gravimetrically (Ancelet, et al., 2011).

Elemental concentrations by X-ray fluorescence spectroscopy

X-ray fluorescence spectroscopy (XRF) was used to measure elemental concentrations in $PM_{2.5}$ samples collected on Teflon filters. XRF measurements in this study were performed at the GNS Science XRF

facility. The spectrometer used was a PANalytical Epsilon 5 (PANalytical, the Netherlands). XRF is a nondestructive and relatively rapid method to analyse elements in particulate matter samples.

XRF is based on the measurement of characteristic X-rays produced by the ejection of an inner shell electron from an atom in the sample. This creates a vacancy in the inner atomic shell. A higher-energy electron then drops into the lower-energy orbital and releases a fluorescent X-ray to remove excess energy (Watson, et al., 1999). The energy of the released X-ray is particular to the emitting element, and the area of the fluorescent X-ray peak (intensity of the peak) is proportional to the number of emitting atoms in the sample. From the intensity, it is possible to calculate a specific element's concentration by direct comparison with standards.

To eject inner shell electrons from atoms in a sample, the XRF spectrometer at GNS Science uses a 100 kV Sc/W X-ray tube. The 100 kV X-rays produced by this tube are able to provide elemental information for elements from Na–U. Unlike ion beam analysis techniques, which are similar to XRF, the PANalytical Epsilon 5 is able to use characteristic K-lines produced by each element for quantification. This is crucial for optimising LOD, because K-lines have higher intensities and are located in less-crowded regions of the X-ray spectrum. The X-rays emitted by the sample are detected using a high-performance Ge detector, which further improves the detection limits. Figure A3 presents a sample X-ray spectrum.

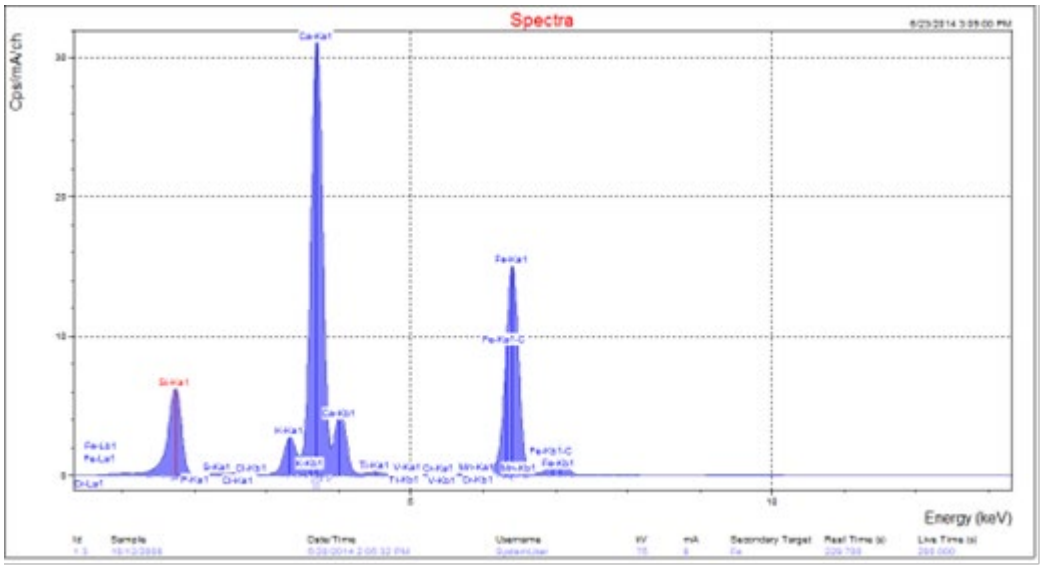

Figure A3. Example x-ray spectrum from a PM_{10} sample.

At GNS Science, calibration standards for each of the elements of interest were analysed prior to the samples being run. Once the calibration standards were analysed, spectral deconvolutions were performed using PANalytical software to correct for line overlaps and ensure that the spectra were accurately fit. Calibration curves for each element of interest were produced and used to determine the elemental concentrations from particulate matter samples. A National Institute of Standards and Technology reference sample (SRM 2783) and multi-elemental reference standards from Crocker National Laboratory (University of California, Davis) were also analysed to ensure that the results obtained were robust and accurate (Hyslop, et al., 2019; Yatkin, et al., 2020).

X-ray fluorescence spectroscopy data reporting

Most filters used to collect particulate matter samples for XRF analysis are sufficiently thin enough that the X-rays penetrate the entire depth, producing a quantitative analysis of elements present. Because

of the thinness of the air particulate matter filters, the concentrations reported from the analyses are therefore in aerial density units (ng cm^{-2}), and the total concentration of each element on the filters is calculated by multiplying with the exposed area of the filter. Typically, the exposed area is approximately 12.5 cm^2 for the sample deposit on the standard 46.2 mm PTFE filters used at the Melbourne sites. To convert from Cl (ng cm^{-2}) into Cl (ng m^{-3}) for filter samples, the equation is

$$\text{Cl (ng m}^{-3}\text{)} = 12.5\ (\text{cm}^2) * \text{Cl (ng cm}^{-2}\text{) / sample volume (m}^3\text{)}$$

Limits of detection (LOD) and uncertainty reporting for elements

The exact LOD and associated analytical uncertainties for the concentration of each element depends on a number of factors such as:

- the method of detection
- filter composition
- sample composition
- the detector resolution
- spectral interference from other elements.

Also, where an individual elemental concentration is reported as zero (0), this means that the measurement value (as derived from the spectral deconvolution) was zero but does not necessarily mean it was not present; rather, it was below the method LOD and indeterminate. Where this is the case, then the corresponding uncertainty value (±) can be regarded as 5/6 LOD (Kara, et al., 2015).

An overview of this process for XRF is presented next.

For XRF elemental data, the detection limits are defined in terms of the uncertainty in the blank (1σ) of 10 repeat measurements (USEPA IO-3.3, 1999). This ignores the effect of other elements, which is generally small due to the use of multiple excitation frequencies, except for the light elements (potassium and lower), where overlapping spectral lines will increase the detection limit.

Uncertainties for the XRF elemental data were calculated using the following equations (Kara, et al., 2015):

$\sigma ij = xij + 2/3(DLj)$ for samples below LOD

$\sigma ij = 0.2xij + 2/3(DLj);\ DLj < xij < 3DLj$ and $\sigma ij = 0.1xij + 2/3(DLj);\ xij > 3DLj$ for detected values

Where xij is the determined concentration for species j in sample i and DLj is the detection limit for species j.

Ion chromatography analysis

The 47 mm Whatman PTFE filters were analysed for major water-soluble ions by capillary high pressure ion chromatography; and anhydrous sugars, including levoglucosan, by capillary high-performance ion-exchange chromatography with electrical detection (ED).

The filters underwent initial wetting with 100 µl of methanol prior to extraction in a 10 ml volume of 18.2 mΩ de-ionized water. The extract solution was then preserved using 1% chloroform. Anion and cation concentrations were determined with a Thermo Fisher Dionex ICS-6000 reagent free ion chromatograph (RFIC).

Anions were separated using a Dionex IonPac AS17-C analytical column (2 x 250 mm), an ADRS-600 suppressor and a gradient eluent of 0.75 mM to 35 mM potassium hydroxide.

Cations were separated using a Thermo Fisher Dionex CS12A column (2 x 250 mm), a CDRS-600 suppressor and an isocratic eluent of 20 mM methanesulfonic acid.

A net ionic balance of anion and cation results was completed to ensure the reliability of the analysis and ensure that all major ion concentrations have been measured.

Anhydrous sugar concentrations, including the woodsmoke tracer levoglucosan, were determined by high-pH anion-exchange chromatography (HPAEC) with pulsed amperometric detection (PAD) using the Thermo Fisher Dionex ICS-6000 chromatograph. The electrochemical detector uses disposable gold electrodes and is operated in the integrating (pulsed) amperometric mode using the carbohydrate (standard quad) waveform. Carbohydrates were separated using a Dionex CarboPac MA1 analytical column (4 x 250 mm) with a gradient eluent of 300 mM to 550 mM sodium hydroxide.

Method detection limit (MDL) and uncertainty reporting for ions and sugars

The average concentration of all the field blanks (n = 28) was subtracted from each ambient measurement. The blanks were also used to calculate the method detection limit (MDL) using a standard volume of 23 m^3. We followed the Standards Australia procedures which are those of the International Standard ISO 6879:1995 Air quality – Performance characteristics and related concepts for air quality measuring methods. Section 5.2.7 of the Standard states that a zero sample has a 5% probability of causing a measured concentration above the detection limit, so that:

$$Sc(0) * t0.95$$

Where:

- Sc(0) is the standard deviation of the blanks
- t0.95 is value of the 1-tailed t distribution for P<0.05 (i.e. the 95 % confidence limit).

The MDL is for an uncertainty of 95% with a one-sided t-stat (n=28).

Calculated MDL from variation in field blanks using cumulative probability of 0.95 and a one-tail distribution at 28 degrees of freedom = 1.701.

$$MDL = stdev * 1.701 * stdev\ field\ blanks$$

There were no field blank detections for mannosan, galactosan and glucose so MDL values derived from previous measurements of sugars in aerosols were used (Dunne, et al., 2019).

Elemental and organic carbon analysis

Elemental and organic carbon analysis was performed using a DRI Model 2001A Thermal-Optical Carbon Analyzer following the IMPROVE-A temperature protocol (Chow, et al., 2007). Laser reflectance was used to correct for charring, since reflectance has been shown to be less sensitive to the composition and extent of primary organic carbon. Prior to analysis of filter samples, the sample was baked in an oven to 910°C for 10 minutes to remove residual carbon. System blank levels were then tested until < 0.20 mg C cm^{-2} was reported (with repeat oven baking if necessary). Twice-daily calibration checks were performed to monitor possible catalyst degeneration. The analyser is reported to effectively measure carbon concentrations between 0.05 – 750 mg C cm^{-2}, with uncertainties in organic carbon (OC) and elemental carbon (EC) of ± 10%.

A hole punch sample (0.507 cm^2) of the exposed filter was taken and used for analysis. The IMPROVE-A carbon method measures four OC fractions at four non-oxidizing heat ramps (OC1 at 140°C, OC2 at 280°C, OC3 at 480°C, OC4 at 580°C) and three EC fractions at three oxidizing heat ramps (EC1 at 580°C,

EC2 at 740°C, EC3 at 840°C). The quartz filter sample is held at the target temperature until all carbon is desorbed at that fraction. During the non-oxidizing heat ramps some of the OC can be pyrolyzed and will not combust until the oxidized stages.

The quantity of OC that was pyrolyzed (Ocpyro) during the non-oxidizing heat ramps is determined based on the time the reflectance of the filter rises back up to its initial value. We consider all pyrolyzed OC to have been removed and all of the remaining carbon is associated with EC. As a result, the carbon evolved before the split point is assigned to OC and the carbon evolved after the split point is assigned to EC. Total OC is then calculated from the addition of all the OC fractions plus Ocpyro. Total EC is calculated from the addition of all the EC fractions minus Ocpyro. The optical reflectance is used to adjust:

1. charring of OC that could be mistaken for EC
2. oxidation of EC in the He atmosphere that could be mistaken for OC.

Elemental and organic carbon data reporting

The concentrations reported from the analyses are in aerial density units (ng m^{-3}), and the total concentration of OC, EC and TC on the filters is calculated by first multiplying with the area of the hole-punched sample of the exposed filter that is used for analysis (0.507 cm^2):

OC (μg cm^2) = ((O1TC + O2TC + O3TC + O4TC + OP635TRC) * (Cal Slope / Cal Peak Area)) / punch area (cm^2)

EC (μg m^2) = ((E1TC + E2TC + E3TC – OP635TC) * Cal Slope / Cal Peak Area)) / punch area (cm^2)

TC (μg m^2) = (OC (μg m^2) + EC (μg m^2))

Where:

- O1TC, O2TC, O3TC, O4TC are the four OC fractions at three oxidizing heat ramps
- E1TC, E2TC, E3TC are the three EC fractions at three oxidizing heat ramps
- OP635TRC is pyrolyzed OC
- The punch area is the hole punch sample (0.507 cm^2) of the exposed filter.

Then, the concentration of OC, EC and TC on the hole punched sample is multiplied with the sample area (12.566 cm^2). For example, to convert from OC (μg cm^{-2}) into OC (ng m^{-3}) the equation is:

OC(ng m^{-3}) = (OC (μg cm^{-2}) * sampled filter area (cm^2) * 1000) / sample volume (m^3)

Method detection limit (MDL) and uncertainty reporting for elemental and organic carbon

The average concentration of all the field blanks (n = 28) was subtracted from each ambient measurement. The blanks were also used to calculate the method detection limit (MDL) using a standard sample volume of 23 m^3. For example, to calculate the MDL for OC the concentration of OC (μg cm^{-2}) is determined in each of the field blank samples, then the standard deviation of all field blanks is determined used to calculate the MDL using the following equation

MDL (ng m^{-3}) = 3 * stdev for OC blanks (μg cm^{-2}) * 1000 / standard sample volume (m^3)

Dataset quality assurance

Quality assurance of sample identified datasets is vital so that any dubious samples, measurements and outliers are removed, as these will invariably affect the results of receptor modelling. In general, the larger the dataset used for receptor modelling, the more robust the analysis. The following sections describe the methodology used to check data integrity and provide a quality assurance process that ensured that the data being used in subsequent factor analysis were as robust as possible.

Mass reconstruction and mass closure

Once the sample analysis for the range of analytes is complete, it is important to check that total measured mass does not exceed gravimetric mass (Cohen, 1999). Ideally, when elemental analysis and organic compound analysis has been undertaken on the same sample, one can reconstruct the mass using the following general equation for ambient samples as a first approximation (Cahill, et al., 1990; Cohen, 1999; Malm, et al., 1994):

$$\text{Reconstructed mass} = [\text{Soil}] + [\text{OC}] + [\text{BC}] + [\text{Smoke}] + [\text{Sulphate}] + [\text{Sea salt}]$$

Where:

- [Soil] = 2.20[Al] + 2.49[Si] + 1.63[Ca] + 2.42[Fe] + 1.94[Ti]
- [OC] = Σ[Concentrations of organic compounds]
- [BC] = Concentration of black carbon (soot)
- [Smoke] = [K] – 0.6[Fe]
- [Sea salt] = 2.54[Na]
- [Sulphate] = 4.125[S]

The reconstructed mass (RCM) is based on the fact that the six composite variables, or 'pseudo' sources, given in the above equation, are generally the major contributors to fine and coarse particle mass, and are based on geochemical principles and constraints.

The [Soil] factor contains elements predominantly found crustal matter (Al, Si, Ca, Fe, Ti) and includes a multiplier to correct for oxygen content, and an additional multiplier of 1.16 to correct for the fact that three major oxide contributors (MgO, K_2O, Na_2O), carbonate, and bound water are excluded from the equation.

[BC] is the concentration of black carbon, measured in this case by light reflectance/absorbance.

[Smoke] represents K not included as part of crustal matter and tends to be an indicator of biomass burning.

[Sea-salt] represents the marine aerosol contribution and assumes that the NaCl weight is 2.54 times the Na concentration. Na is used as it is well known that Cl can be volatilised from aerosol or from filters in the presence of acidic aerosol, particularly in the fine fraction via the following reactions (Lee, et al., 1999):

$$NaCl(p) + HNO_3(ag) \rightarrow NaNO_3(p) + HCl(g)$$

$$2NaCl(p) + H_2SO_4(ag) \rightarrow Na_2SO_4(p) + 2HCl(g)$$

Alternatively, where Cl loss is likely to be minimal, such as in the coarse fraction or for both size fractions near coastal locations and relatively clean air in the absence of acid aerosol, then the reciprocal calculation of [Sea-salt] = 1.65[Cl] can be substituted, particularly where Na concentrations are uncertain.

Most fine sulphate particles are the result of oxidation of SO_2 gas to sulphate particles in the atmosphere (Malm, et al., 1994). It is assumed that sulphate is present in a fully neutralised form – as

ammonium sulphate. [Sulphate] therefore represents the ammonium sulphate contribution to aerosol mass with the multiplicative factor of 4.125[S] to account for ammonium ion and oxygen mass (i.e. $(NH_4)_2SO_4$ = ((14 + 4)2 + 32 + (16x4)/32)).

Additionally, the sulphate component not associated with sea-salt can be calculated by Cohen (1999):

Non-sea-salt sulphate (NSS-Sulphate) = 4.125 ([Stot] – 0.0543[Cl])

The sulphur concentrations contributed by sea-salt are inferred from the chlorine concentrations, i.e. [S/Cl] sea-salt = 0.0543, and the factor of 4.125 assumes that the sulphate has been fully neutralised and is generally present as $(NH_4)_2SO_4$ (Cahill, et al., 1989; Malm, et al., 1994; Cohen, 1999).

The RCM and mass closure calculations using the pseudo-source and pseudo-element approach are a useful way to examine initial relationships in the data and how the measured mass of species in samples compares to gravimetric mass. Note that some scatter is possible because not all aerosols are necessarily measured and accounted for; such as all OC, ammonium species, nitrates and unbound water. CSIRO is doing further analysis of the samples that include these species, at Aspendale, Melbourne. It is expected that the combined datasets will provide a more complete picture.

Dataset mass reconstruction summary for inner west Melbourne $PM_{2.5}$ ambient sites

Using the methodology outlined above, the following figures present the mass reconstruction results for $PM_{2.5}$ collected at all sites. The large scatter in Figure A4 could be due to larger uncertainty associated with shorter sample times (at least 3 hours) for these samples.

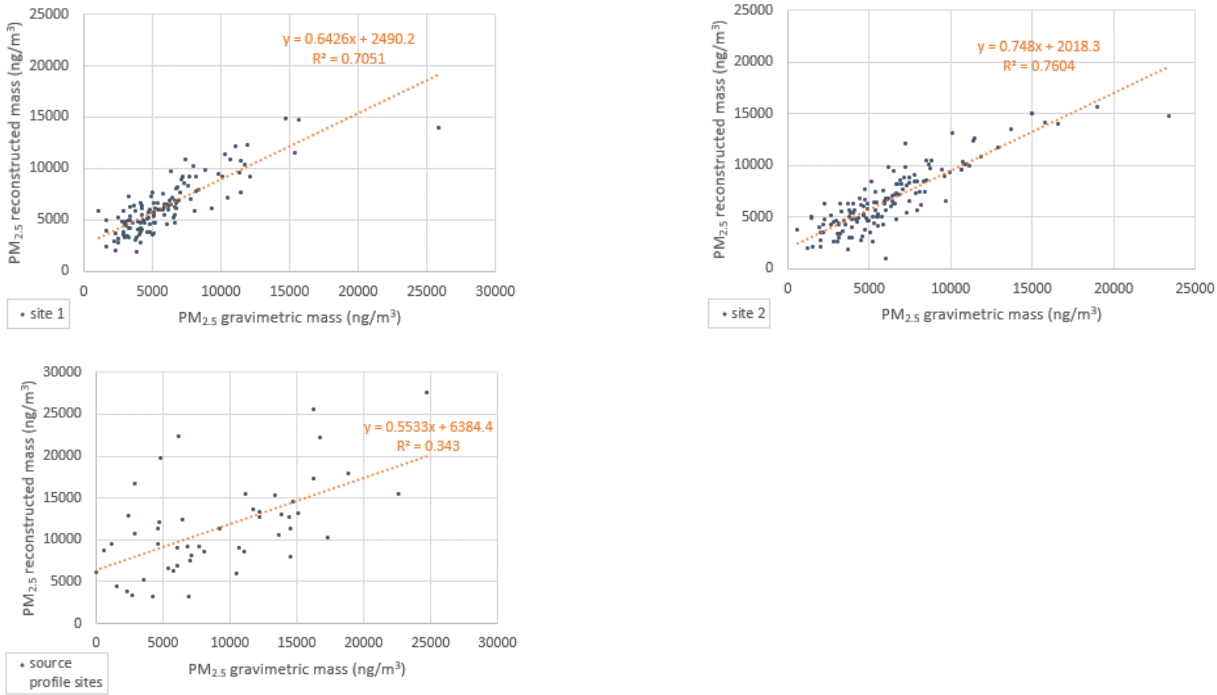

Figure A4. Mass reconstruction versus gravimetric mass for $PM_{2.5}$ at site 1 (top left), site 2 (top right and all source specific sites (bottom).

Appendix 4. $PM_{2.5}$ annual average concentrations using different sampling regimes

Here we compare two methods for measuring $PM_{2.5}$ mass concentrations based on sample collection days selected at 4 locations in metropolitan Melbourne (project sites 1 and 2, and EPA air monitoring stations Alphington and Footscray) (Table A6, Figure A5 and Figure A6). At each location, $PM_{2.5}$ was measured by manually collecting gravimetric mass samples (24-hour average samples) on filters every 3 days. $PM_{2.5}$ was also measured with a Beta Attenuation Monitor (BAM) at the same time at or near each location, semi-continuously (5-minute average samples) every day.

Annual summary statistics (Table A6) for samples collected on a 1-in-3-day schedule sometimes underestimated or overestimate $PM_{2.5}$ concentrations compared to sampling every day. We note that these results may be different for different years, or even if the samples collected on a 1-in-3-day sampling schedule were collected on different days.

Table A6. Comparison of $PM_{2.5}$ concentrations ($\mu g\ m^{-3}$) collected on a 1-in-3-day sample schedule and collected every day at 4 sites from 5 May 2021 to 12 May 2022.

Site	Sample schedule	$PM_{2.5}$ Median	$PM_{2.5}$ Average	$PM_{2.5}$ 90th percentile	$PM_{2.5}$ Max.	$PM_{2.5}$ Std Dev.	# days data collected	Method
Project site 1 and WGTP station 1	Everyday	5.8	6.7	11.0	23.9	3.7	337	WGTP BAM (AS 3580.9.12, 2013)
	1 in 3 days	5.1	5.9	10.4	25.9	3.4	122	EPA gravimetric mass (AS 3580.9.10, 2017)
Project site 2 and WGTP station 5	Everyday	6.1	7.0	11.4	22.3	3.7	311	WGTP BAM (AS 3580.9.12, 2013)
	1 in 3 days	5.3	5.9	9.6	23.4	3.3	123	EPA gravimetric mass (AS 3580.9.10, 2017)
EPA Footscray air monitoring station	Everyday	4.6	5.4	9.7	21.5	3.3	321	EPA BAM (AS 3580.9.12, 2013)
	1 in 3 days	5.1	5.7	8.6	24.9	2.9	117	EPA gravimetric mass (AS 3580.9.10, 2017)
EPA Alphington air monitoring station	Everyday	5.7	6.5	10.2	34.3	3.8	356	EPA BAM (AS 3580.9.12, 2013)
	1 in 3 days	5.4	6.3	10.6	33.4	4.1	123	EPA gravimetric mass (AS 3580.9.10, 2017)

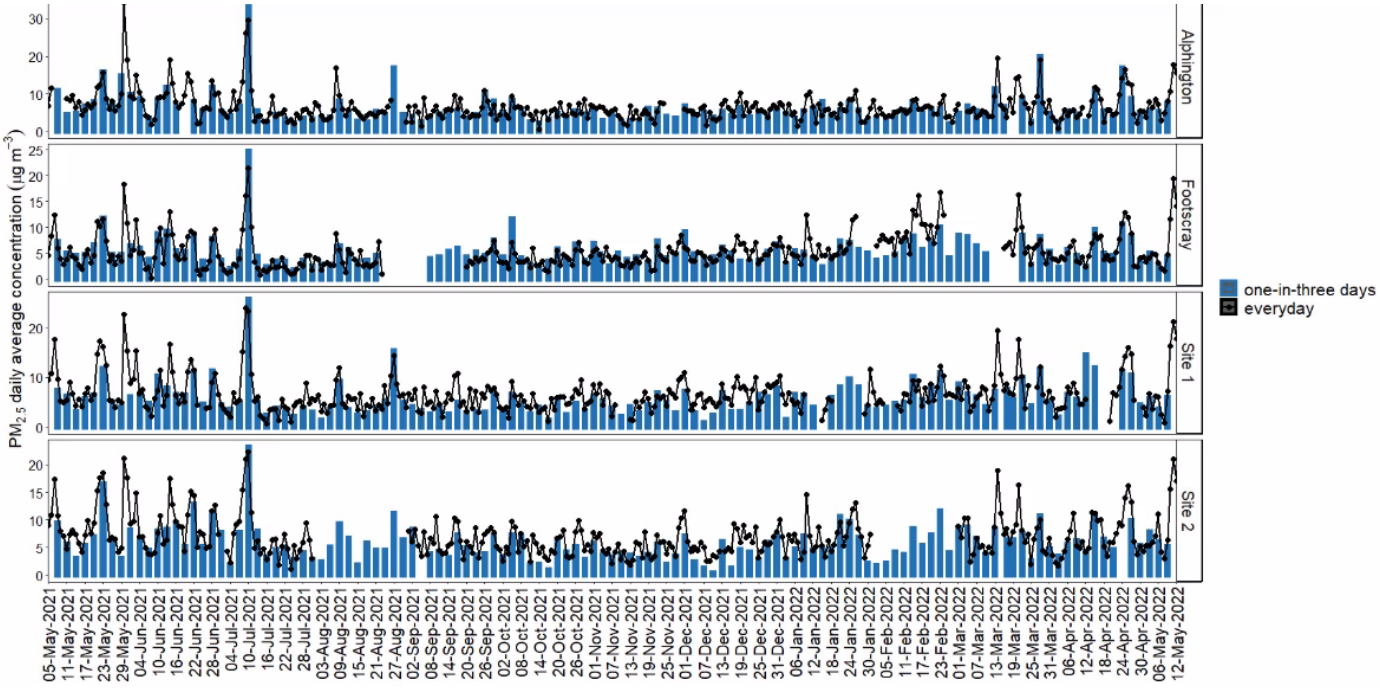

Figure A5. Timeseries plot comparing $PM_{2.5}$ gravimetric mass measurements collected on a 1-in-3-day sample schedule (blue bars) and collected everyday (black lines) at 4 sites.

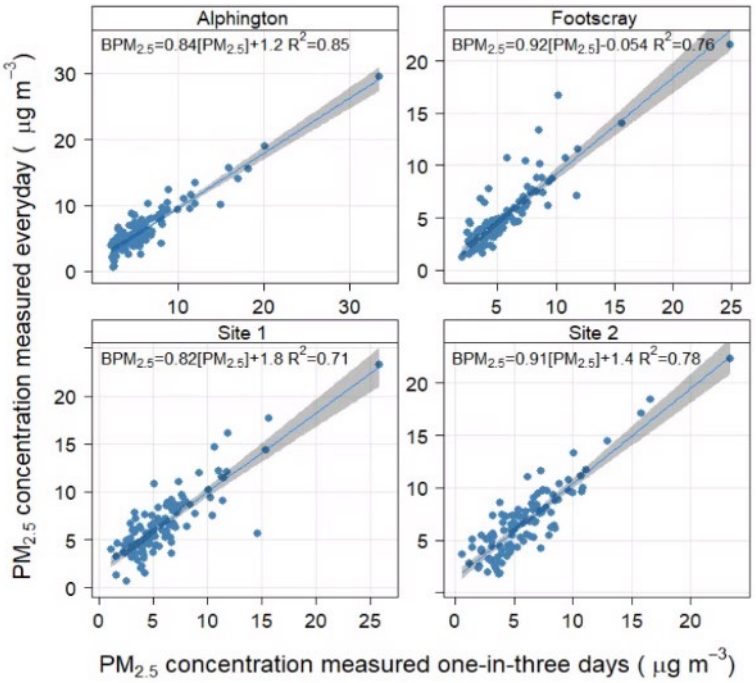

Figure A6. Comparison of $PM_{2.5}$ concentrations collected on a 1-in-3-day sample schedule ($PM_{2.5}$) and collected every day ($BPM_{2.5}$) at 4 sites from 5 May 2021 to 12 May 2022.

Appendix 5. Particle chemistry results for sites 1 and 2

Summary statistics for all chemical compounds analysed are shown in Table A7 and Table A8, except for sorbitol and mannitol. Sorbitol and mannitol have not been included as they had large uncertainties associated with their measurements.

Correlation plots, time variation and CPF polar plots of the key chemical species are also presented in this Appendix.

Table A7. Summary of $PM_{2.5}$ chemistry results at site 1 from 5 May 2021 to 12 May 2022 (124 samples). $PM_{2.5}$ concentrations are μg m^{-3}; concentrations for all other species are ng m^{-3}.

Species	Median	Average	90th percentile	Max.	Std Dev.	Average LOD	#>LOD
$PM_{2.5}$	**5**	**6**	**10**	**26**	**3**		
BC	1311	1592	3176	5424	1078	110	122
Na	415	530	1158	2296	413	5	122
Mg	47	53	99	204	37	6	117
Al	41	46	78	135	25	7	120
Si	73	90	193	360	65	5	122
P	0	0	0	3	0	1	1
S	191	228	411	843	155	2	122
Cl	270	480	1236	3002	553	1	114
K	41	50	83	200	29	1	122
Ca	37	48	102	218	39	0	121
Ti	3	5	8	55	5	1	108
V	0.2	0.7	1.8	10.1	1.4	0.4	54
Cr	0	0	1	27	2	1	12
Mn	2	3	5	14	3	1	75
Fe	68	79	136	381	54	1	122
Co	0	0	0	1	0	0	18
Ni	0.8	1.2	2.2	14.6	1.6	0.5	85
Cu	2	2	5	7	2	1	92
Zn	6	8	15	33	6	0	122
Ga	0	1	1	2	1	1	33
As	0	0	1	3	1	1	23

Se	0	1	4	8	2	1	39
Br	1	2	4	11	2	1	87
Sr	1	1	2	4	1	1	43
Mo	0	1	2	14	2	2	22
Cd	2	5	15	27	7	5	44
Sn	4	5	12	30	5	5	50
Sb	1	4	10	19	5	4	46
Te	3	5	13	28	6	6	41
Cs	1	5	15	23	6	11	22
Ba	5	7	22	27	9	12	36
La	7	10	25	42	11	9	57
Ce	0	26	88	214	47	126	7
Sm	0	30	94	246	51	106	11
Pb	2	3	6	14	3	3	49
Hg	0	1	2	4	1	1	20
In	0	1	3	8	2	4	11
W	0	48	154	298	73	41	45
Na^+	330	417	846	1673	330	14	122
NH_4^+	104	155	284	1974	202	1	122
K^+	33	40	69	172	27	6	121
Mg^{2+}	32	41	85	182	34	3	120
Ca^{2+}	46	52	101	191	36	9	117
Cl^-	230	426	1060	2614	498	36	85
Br^-	1	2	7	11	3	2	42
NO_3^-	168	266	472	4640	439	4	122
SO_4^{2-}	517	638	1155	2346	452	4	122
$C_2O_4^{2-}$	40	53	117	191	43	3	122
PO_4^{3-}	5	8	18	63	11	1	102
F^-	0	1	1	13	2	0	18
Acetate	0	5	18	34	8	17	13
Formate	10	14	33	81	14	17	30

MSA^-	30	38	79	138	28	16	92
Levoglucosan	21	88	245	811	156	3	87
Arabitol	0	8	9	129	25	4	46
Mannosan	0	14	47	75	20	0	44
Galactosan	0	4	0	158	21	0	9
Glucose	0	8	18	157	18	1	48
OC	1703	1975	3605	11224	1482	540	113
EC	741	921	2087	4026	682	391	95

Table A8. Summary of $PM_{2.5}$ chemistry results at site 2 from 28 February 2021 to 12 May 2022 (140 samples). $PM_{2.5}$ concentrations are μg m^{-3}; concentrations for all other species are ng m^{-3}.

Species	Median	Average	90th percentile	Max.	Std Dev.	Average LOD	#>LOD
$PM_{2.5}$	**6**	**6**	**11**	**23**	**4**		
BC	1658	1955	4199	6315	1551	110	138
Na	446	539	1117	2334	408	5	138
Mg	49	57	103	181	36	6	136
Al	45	50	90	174	29	7	136
Si	79	97	198	349	73	5	139
P	0	0	0	1	0	1	0
S	173	225	405	1247	183	2	139
Cl	302	513	1243	3076	578	1	132
K	43	53	89	217	33	1	139
Ca	28	33	66	95	22	0	139
Ti	4	5	10	15	4	1	113
V	0.2	0.4	1.2	4.9	0.6	0.4	51
Cr	0	0	1	7	1	1	13
Mn	2	2	4	13	2	1	79
Fe	75	85	173	286	66	1	139
Co	0	0	1	1	0	0	26
Ni	0.6	0.7	1.5	3.9	0.7	0.5	83
Cu	3	3	7	14	3	1	109

Zn	8	10	22	55	9	0	131
Ga	0	1	2	3	1	1	43
As	0	0	1	4	1	1	31
Se	0	1	2	6	1	1	24
Br	1	2	4	45	4	1	92
Sr	1	1	2	4	1	1	48
Mo	0	1	2	4	1	2	23
Cd	4	8	22	36	10	5	62
Sn	2	4	11	26	5	5	51
Sb	3	4	12	18	5	4	55
Te	4	6	14	29	6	6	56
Cs	3	7	22	39	9	11	42
Ba	5	9	24	42	10	12	42
La	8	11	28	46	12	9	65
Ce	0	42	145	283	65	126	20
Sm	0	30	99	196	46	107	13
Pb	2	2	6	12	2	3	48
Hg	0	1	2	7	1	1	26
In	0	1	4	11	2	4	13
W	6	91	275	517	124	41	60
Na^+	328	419	817	1678	310	14	139
NH_4^+	100	160	304	1848	206	1	139
K^+	32	41	69	189	29	6	138
Mg^{2+}	32	44	87	192	35	3	138
Ca^{2+}	33	37	64	95	19	9	135
Cl^-	295	467	1154	2696	526	36	98
Br^-	1	2	7	33	4	2	47
NO_3^-	184	262	462	3998	370	4	139
SO_4^{2-}	491	623	1097	3305	499	4	139
$C_2O_4^{2-}$	39	56	136	305	51	3	139
PO_4^{3-}	3	4	9	28	4	1	104

F^-	0	1	1	13	2	0	21
Acetate	0	9	20	201	28	17	18
Formate	11	18	39	180	23	17	48
MSA^-	31	38	80	133	27	16	106
Levoglucosan	8	90	272	964	172	3	95
Arabitol	0	7	8	129	24	4	54
Mannosan	0	14	48	72	20	0	49
Galactosan	0	2	0	62	9	0	8
Glucose	0	5	14	125	14	1	43
OC	1765	1952	3647	6540	1289	548	127
EC	958	1183	2602	4647	941	397	111

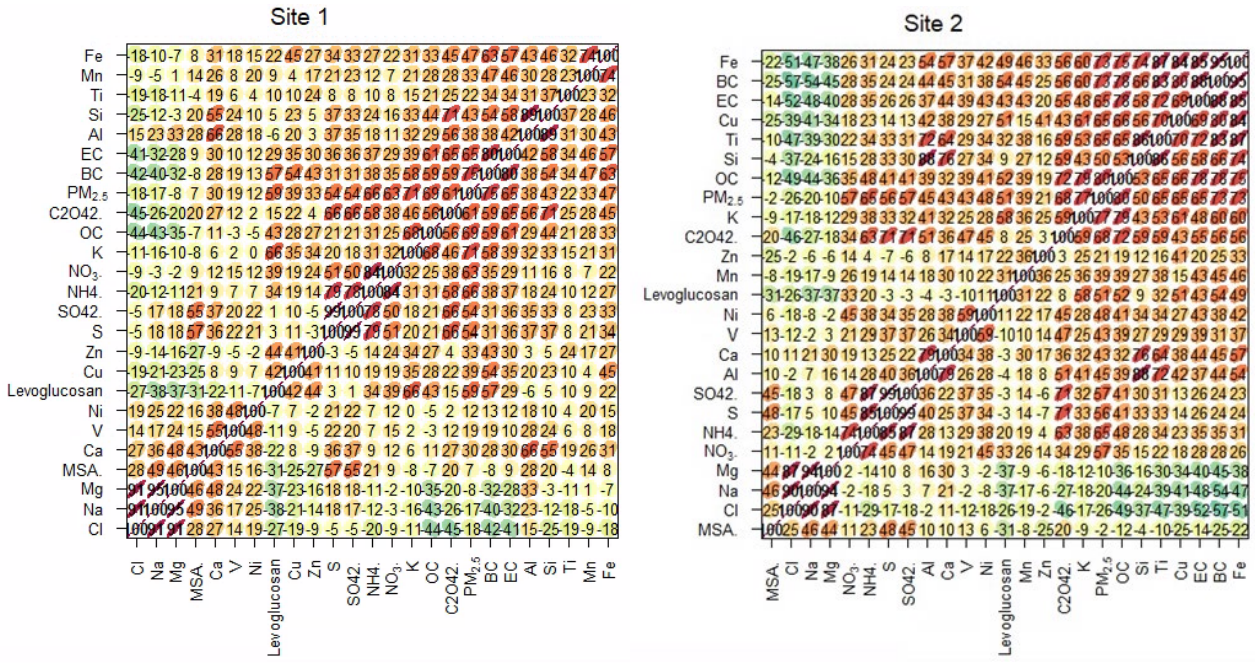

Figure A7. Correlation plots for key chemical species in $PM_{2.5}$ at site 1 (left) from 5 May 2021 to 12 May 2022 (124 samples) and at site 2 (right) from 28 February 2021 to 12 May 2022 (140 samples).

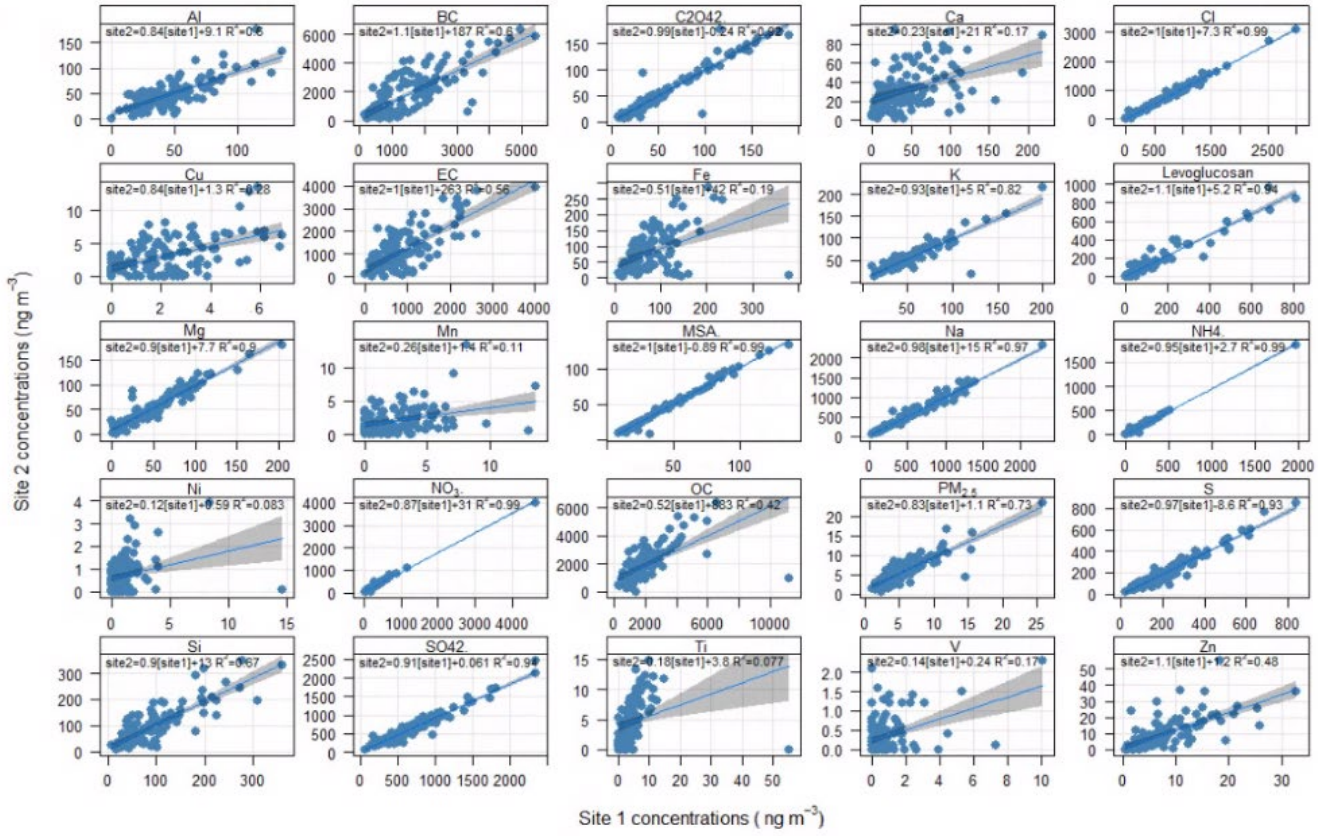

Figure A8. Correlation plots for key chemical species in $PM_{2.5}$ at sites 1 and 2 from 5 May 2021 to 12 May 2022. Note: concentrations are ng m^{-3} for all chemical species except $PM_{2.5}$. $PM_{2.5}$ concentrations are $\mu g\ m^{-3}$.

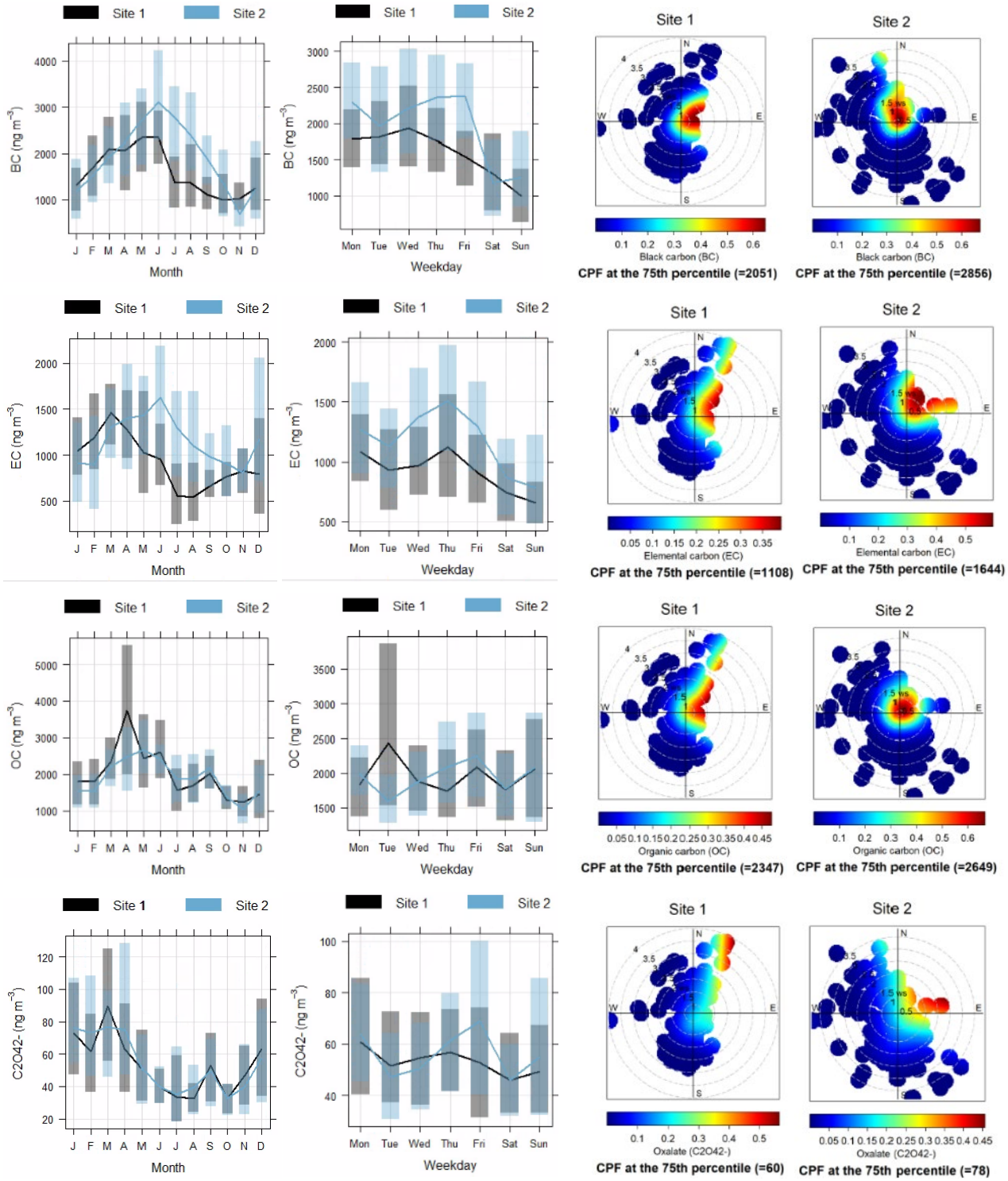

Figure A9. Timeseries and CPF polar plots for black carbon (BC), elemental carbon (EC), organic carbon (OC) and oxalate ($C_2O_4^{2-}$) daily average concentrations (ng m^{-1}) at site 1 from May 2021 to May 2022 and at site 2 from March 2021 to May 2022. Wind speeds are meters per second (m s^{-1}).

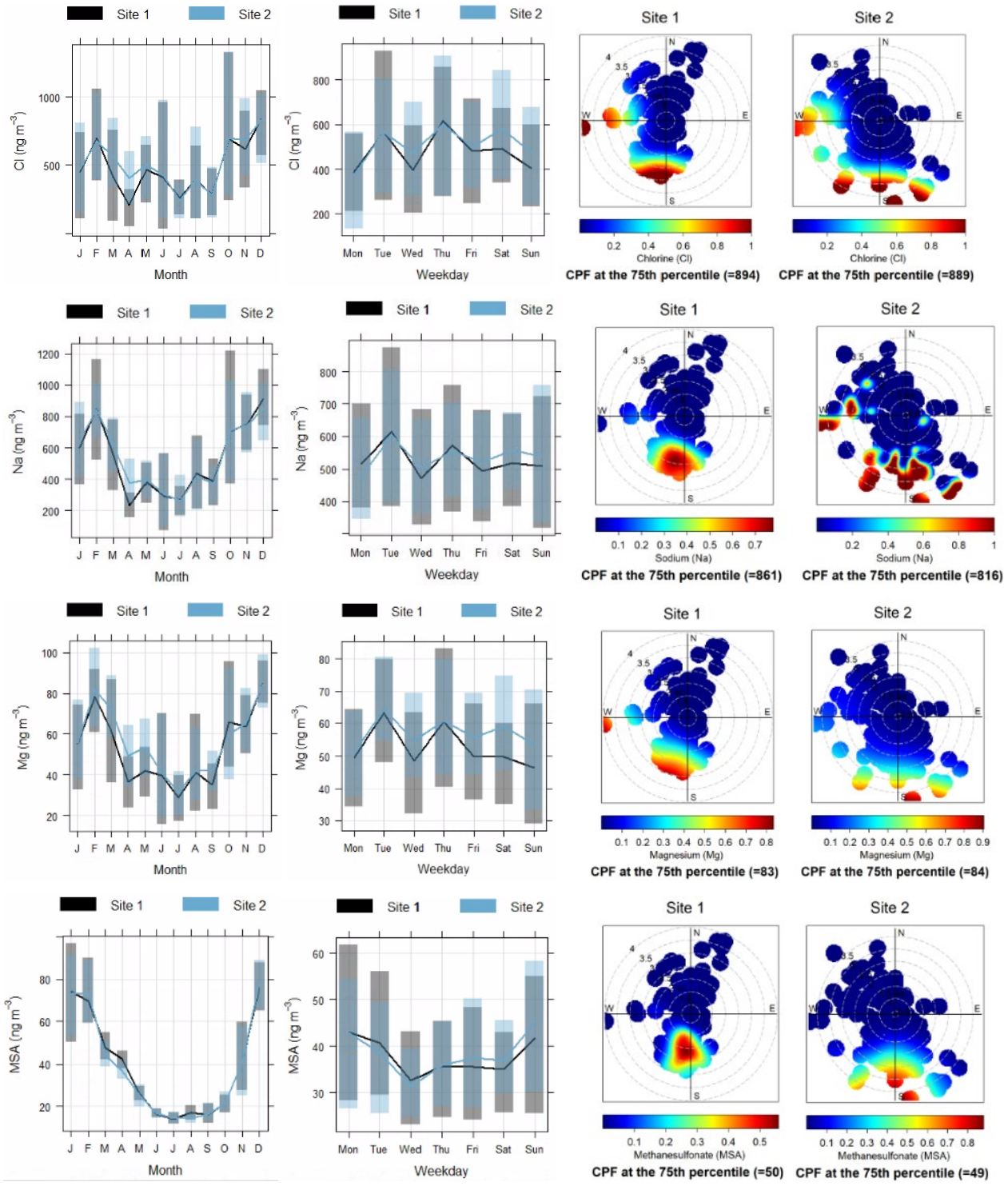

Figure A10. Timeseries and CPF polar plots for chlorine (Cl), sodium (Na), magnesium (Mg) and methanesulfonate (MSA^-) daily average concentrations (ng m^{-1}) at site 1 from May 2021 to May 2022 and at site 2 from March 2021 to May 2022. Wind speeds are meters per second (m s^{-1}).

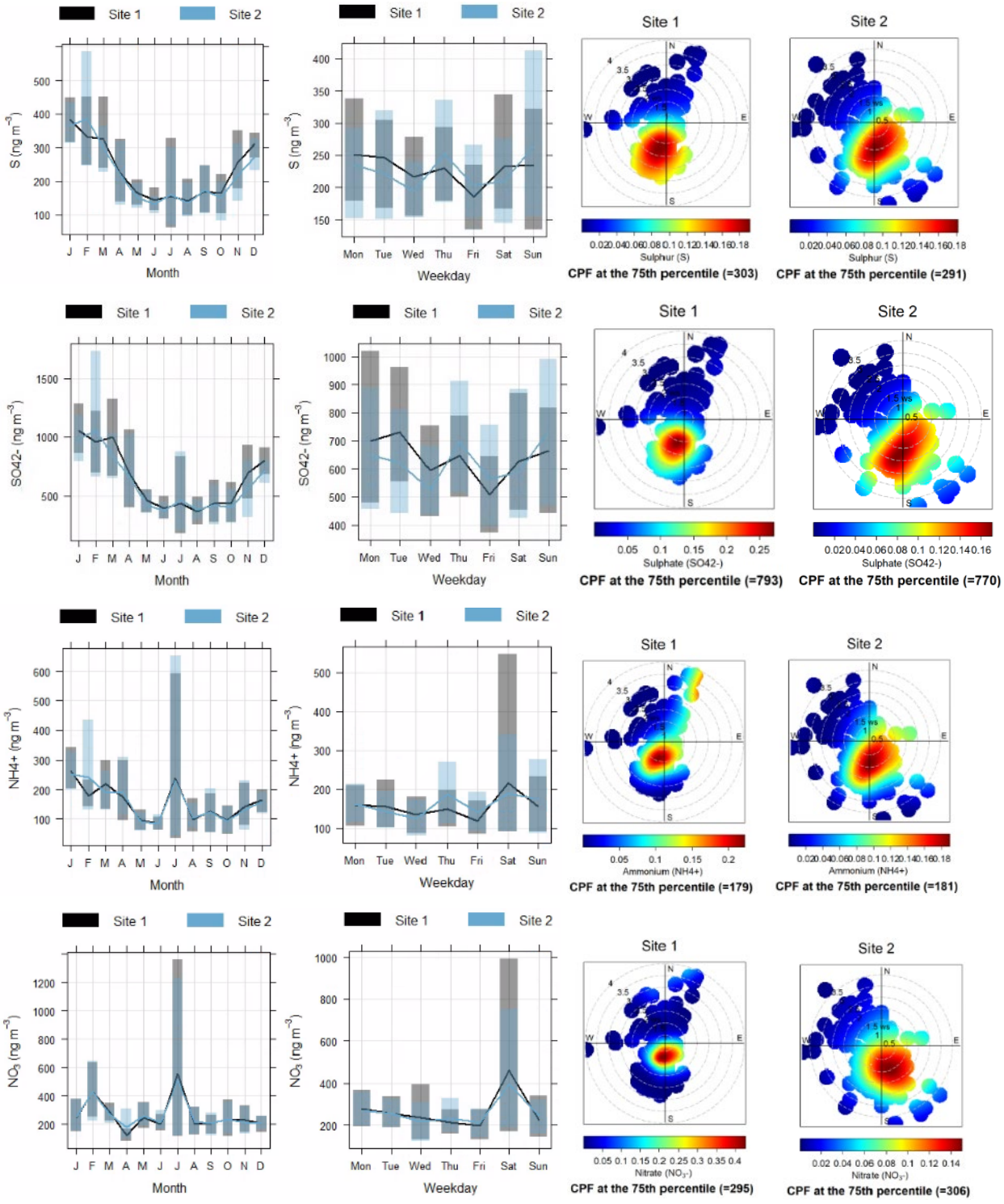

Figure A11. Timeseries and CPF polar plots for sulfur (S), sulphate (SO_4^{2-}), ammonium (NH_4^+) and nitrate (NO_3^-) daily average concentrations (ng m^{-1}) at site 1 from May 2021 to May 2022 and at site 2 from March 2021 to May 2022. Wind speeds are meters per second (m s^{-1}).

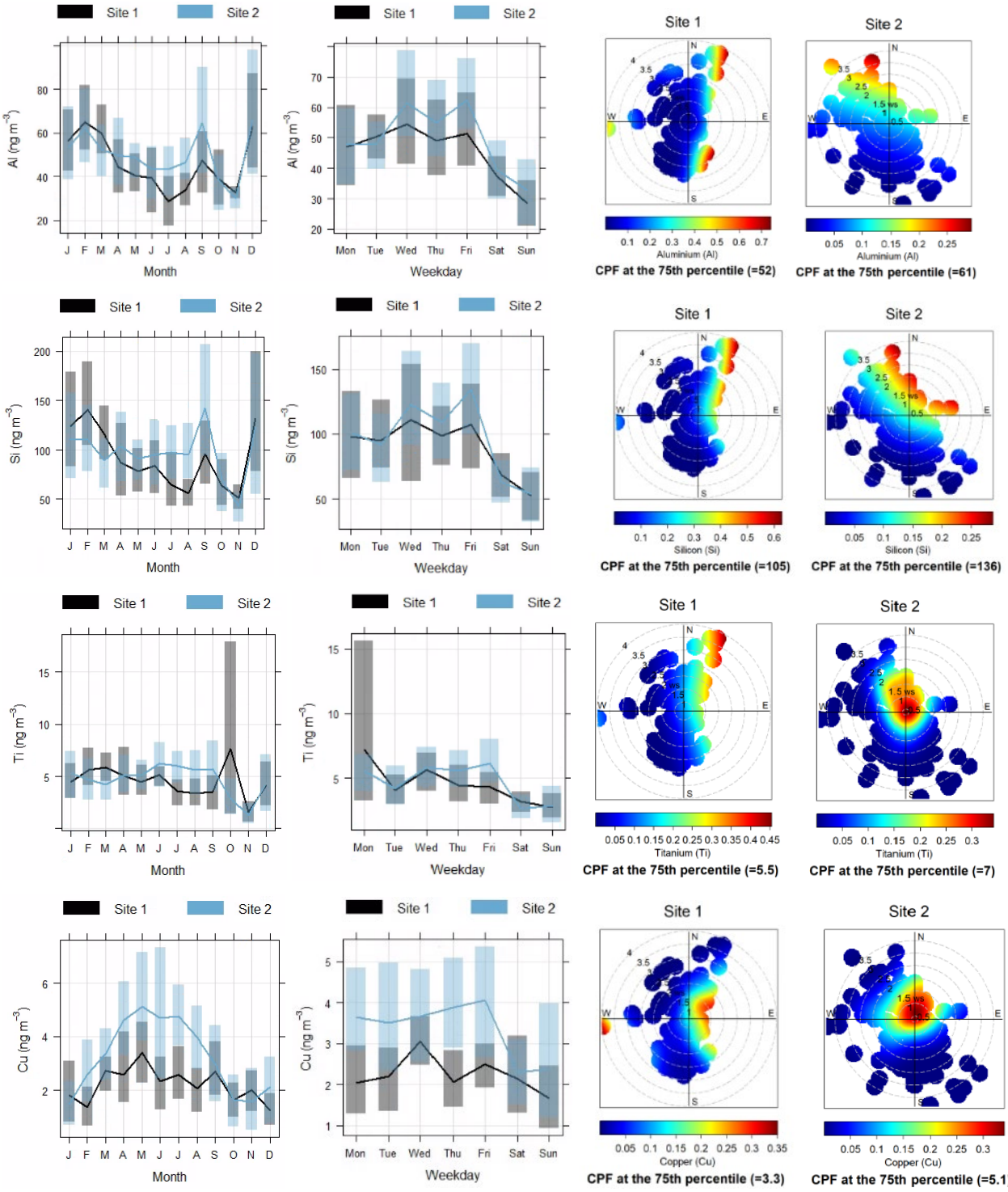

Figure A12. Timeseries and CPF polar plots for aluminium (Al), silicon (Si), titanium (Ti) and copper (Cu) daily average concentrations (ng m^{-1}) at site 1 from May 2021 to May 2022 and at site 2 from March 2021 to May 2022. Wind speeds are meters per second (m s^{-1}).

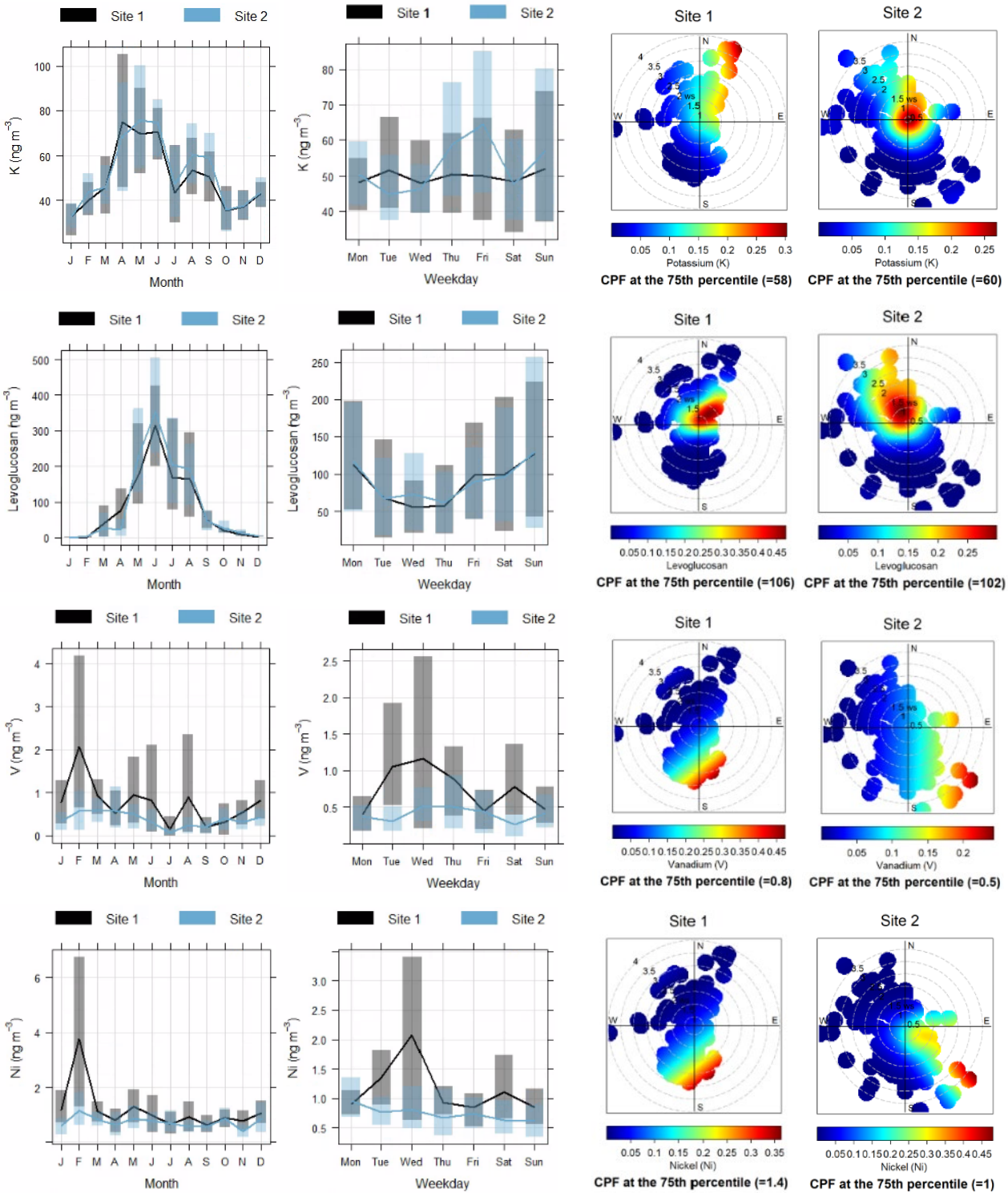

Figure A13. Timeseries and CPF polar plots for potassium (K), levoglucosan, vanadium (V) and nickel (Ni) daily average concentrations (ng m^{-1}) at site 1 from May 2021 to May 2022 and at site 2 from March 2021 to May 2022. Wind speeds are meters per second (m s^{-1}).

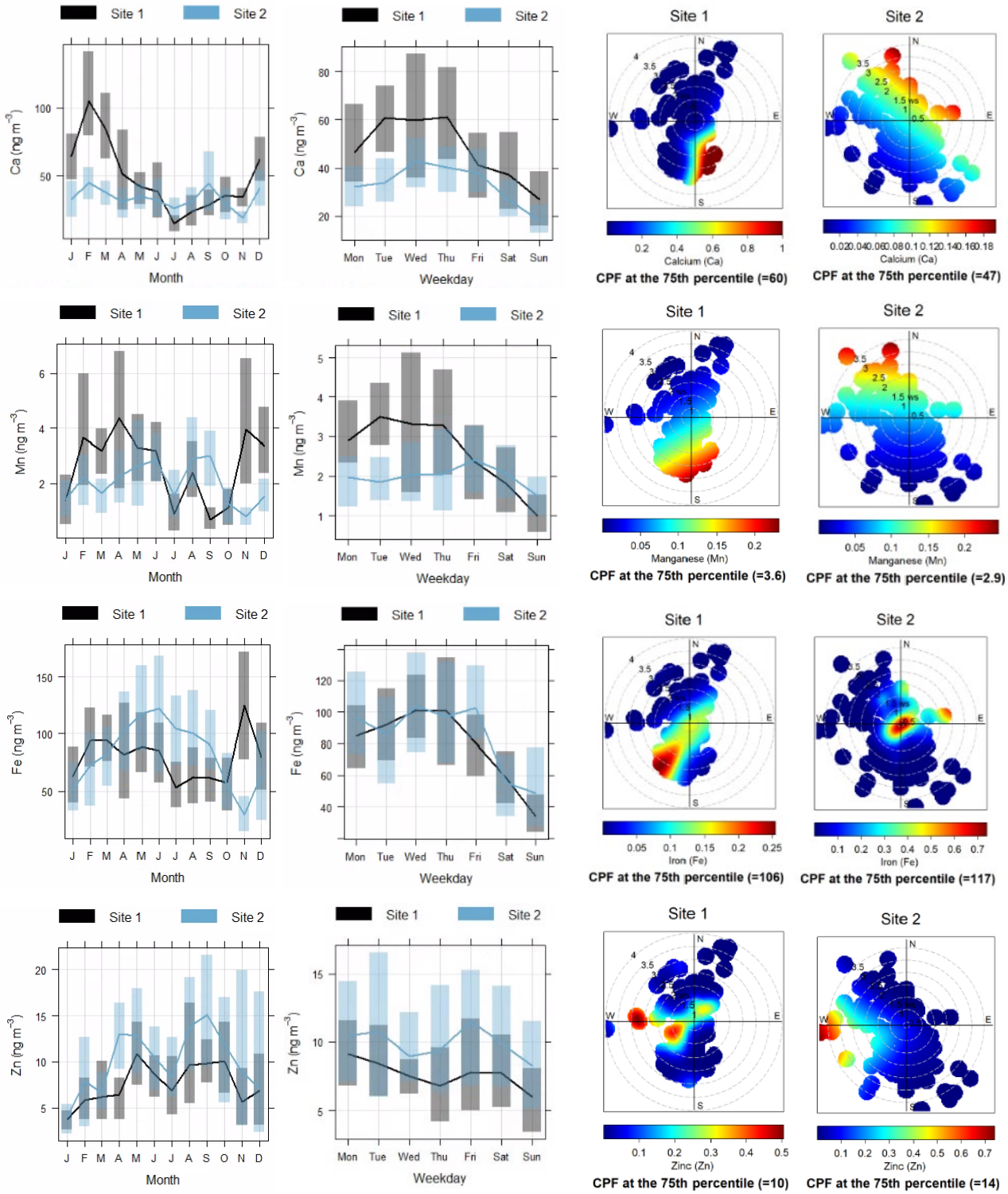

Figure A 14. Timeseries and CPF polar plots for calcium (Ca), manganese (Mn), iron (Fe) and zinc (Zn) daily average concentrations (ng m^{-1}) at site 1 from May 2021 to May 2022 and at site 2 from March 2021 to May 2022. Wind speeds are meters per second (m s^{-1}).

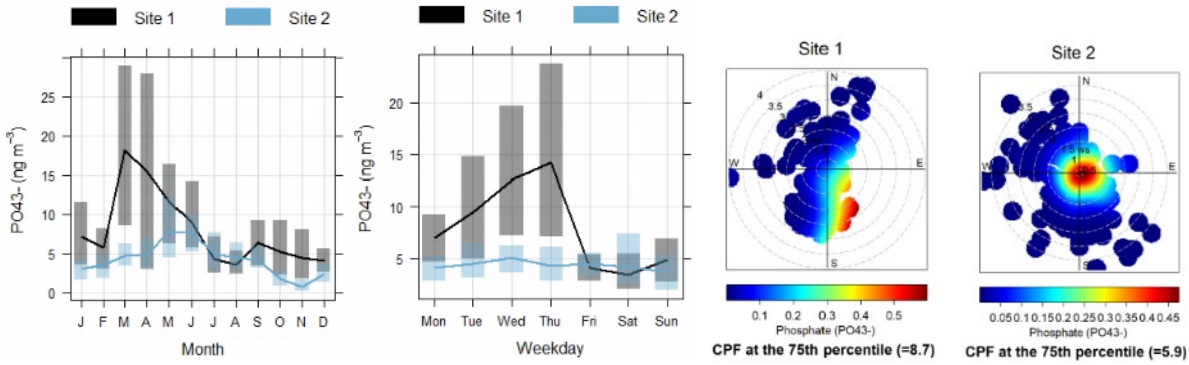

Figure A15. Timeseries and CPF polar plots for phosphate (PO_4^{3-}) daily average concentrations (ng m^{-1}) at Site 1 from May 2021 to May 2022 and at Site 2 from March 2021 to May 2022. Wind speeds are meters per second (m s^{-1}).

Appendix 6. Source apportionment and receptor modelling using Positive Matrix Factorisation (PMF)

Receptor modelling and source apportionment of PM mass by positive matrix factorisation (PMF) was performed using EPAPMF software version 5.0.14 in accordance with the user guide:

https://www.epa.gov/airreseach/epa-positive-matrix-factorization-50-fundamentalsand-user-guide

With PMF, sources are constrained to have non-negative species concentrations. This is because no sample can have a negative source contribution. Error estimates for each observed point are used as point-by-point weights. This is a distinct advantage of PMF, since it can accommodate missing or below detection limit data that is a common feature of environmental monitoring (Song, et al., 2001).

Another advantage of PMF is that PM mass concentrations can be included in the model as another variable and the results are directly interpretable as the covariant PM mass contributions associated with each factor (source). Prior to PMF analyses, data and uncertainty matrices were prepared as described in Appendix 2. If the concentration was less than or equal to the MDL provided, the uncertainty was calculated using a fixed fraction of the MDL as recommended by the EPAPMF user guide (Equation 5-1 (Polissar, et al., 1998)).

Uncertainty = 5/6 * MDL

Data screening and the source apportionment were performed in accordance with the protocols and recommendations set out by Paatero, et al. (2014) and Brown, et al. (2015). Due to the effect that random analytical noise can have on the receptor modelling process, variables with a low signal-to-noise ratio (less than 0.5), and/or where at least 50% of the data was below detection or missing, were examined by alternate inclusion and exclusion in a modelling run. Only those variables that could be explained in association with source emissions were included in the final results (Paatero & Hopke, 2003).

The following species were excluded from PMF analysis due to their signal-to-noise ratios being less than 0.5 and/or at least 50% of the data was below detection or missing: P, Cr, Co, Ga, As, Se, Br, Sr, Mo, Cd, Sn, Sb, Te, Cs, Ba, La, Ce, Sm, Pb, Hg, In, W, PO_4^{3-}, F-, acetate, formate, arabitol, sorbitol, mannosan, mannitol, galactosan and glucose. However, an industrial source of PO_4^{3-} was identified near site 1, and so this species was added back in for site 1 PMF analyses.

Some duplicate measurements were included in the PMF analysis, for example, BC and EC, Na and Na^+, Cl and Cl^-, Mg and Mg^{2+} K and K^+, Ca and Ca^{2+}, and S and SO_4^{2-}. However, TC was excluded as it is the sum of OC and EC and not an independent species.

An extra modelling uncertainty of 10% was used. Each scenario was also assessed against a bootstrap analysis using 200 bootstrap runs.

There were two cases where concentrations of key chemical species were missing. To continue to use these samples in the PMF analysis, median concentrations were used in place of missing concentrations that were calculated from all samples collected at that site. Also, much higher uncertainties were used (at least 90% uncertainty for the given sample). These two cases were for concentrations:

- OC and EC that were missing on the 28 November 2021 sample collected at site 1
- levoglucosan at site 2 on 17 February 2022 (where a high levoglucosan concentration measured was flagged as an outlier).

The sample collected at site 3 on 31 January 2022 (impacted by fireworks) was excluded from all PMF analysis runs.

PMF analyses split the data into factors that can be attributed to sources. This is a reiterative process, and examples of some of the modelling scenarios tested are summarised in Table A9, Table A10 and Table A11.

The final PMF solutions for site 1 and site 2 are highlighted in bold in Table A9, Table A10 and Table A11. The final solution for site 1 includes 11 factors or sources that were found, on average, to explain 100% of the $PM_{2.5}$ gravimetric mass (chemical species associated with each source can be seen in the source profiles extracted from the PMF analysis in Figure A16).

The final solution for site 2 includes 8 factors or sources that were found (all present at site 1), on average, to explain 93 % of the $PM_{2.5}$ gravimetric mass. The chemical species associated with each source can be seen in the source profiles extracted from the PMF analysis in Figure A17. A discussion on each factor or source is included in the results and discussion section of this report above.

Table A9. Example of various PMF scenarios tested.

PMF ID	Site	Exclusions	Factors	Comments
1	2	PO_4^{3-}	8	No shipping factor or industry factor. V and Ni are not well defined by the PMF model for this site, when V and Ni were excluded to reduce noise, a similar result was obtained. **Final solution for site 2.**
2	2	PO_4^{3-}	9	This solution was not accepted because secondary nitrate was split between two factors (one with MSA and one with shipping) and this doesn't make sense.
3	1 and 2	PO_4^{3-}	9	This solution was not accepted because shipping and industry were combined in one factor. We don't really want this, as we want to define the shipping contribution on its own. Note: when levoglucosan was excluded, K was all accounted for in one biomass burning factor and an unexplained factor appeared as the 9th factor. Boot Strapping showed that 25% of this unexplained factor is split between diesel and crustal.
4	1, 2 and source specific samples	PO_4^{3-}	10	Addition of the source specific samples meant that the shipping and industry factors were able to be separated by the PMF model. However, this solution was not accepted because: • The industry factor (unassigned Ca) looked wrong at site 2. It was concluded that there is likely no impact at site 2 from this industry. • A PO_4^{3-} industrial site was identified near site 1. The model needs to include PO_4^{3-} for site 1 analyses.
5	1 and source specific samples	PO_4^{3-}	10	Similar result to PMF ID 4. This solution was not accepted because a PO_4^{3-} industrial site was identified near site 1.

6	1 and source specific samples	10	This solution was not accepted because aged biomass burning, crustal, shipping and industry (Ca and PO_4^{3-}) factors were unable to be completely resolved. They appeared across several factors as demonstrated by Boot Strapping results.
7	1 and source specific samples	11	All the same factors are present as PMF ID 4 and 5 and the 11th factor is a phosphate factor. The model has confirmed that there are two industry sources of Ca and PO_4^{3-} at site 1. **Final solution for site 1.**

Table A10. Average factor source contributions (μg m^{-3} (%)) at site 1 for various PMF modelling scenarios. $PM_{2.5}$ average concentration at site 1 was 5.9 μg m^{-3}.

PMF ID	Site	Exclusions	Factor 1	Factor 2	Factor 3	Factor 4	Factor 5	Factor 6	Factor 7	Factor 8	Factor 9	Factor 10	Factor 11
3	1 and 2	PO_4^{3-}	0.03 (0%) V1	0.9 (14%) V2	0.8 (13%) S1	0.5 (9%) S2 and I1	0.9 (15%) S3	0.8 (13%) S4	1.0 (16%) B1	0.9 (16%) B2	0.2 (4%) S5		
4	1, 2 and source specific samples	PO_4^{3-}	0.02 (0%) V1	0.7 (13%) V2	0.7 (13%) S1	0.1 (2%) S2	0.9 (15%) S3	0.8 (14%) S4	1.0 (15%) B1	0.9 (16%) B2	0.2 (3%) S5	0.6 (10%) I1	
5	1 and source specific samples	PO_4^{3-}	0.06 (1%) V1	0.9 (15%) V2	0.9 (14%) S1	0.2 (3%) S2	0.7 (11%) S3	0.6 (10%) S4	0.9 (16%) B1	1.1 (18%) B2	0.2 (3%) S5	0.6 (10%) I1	
6	1 and source specific samples		0.1 (2%) V1	0.8 (13%) V2	0.9 (15%) S1	0.2 (3%) S2	0.9 (14%) S3	0.7 (11%) S4	1.2 (20%) B1	0.8 (13%) B2 and S5	0.2 (3%) I1 and S5	0.4 (6%) I1 and I2	
7	**1 and source specific samples**		**0.1 (1%) V1**	**0.8 (13%) V2**	**0.8 (13%) S1**	**0.2 (3%) S2**	**0.7 (11%) S3**	**0.7 (12%) S4**	**0.7 (12%) B1**	**1.3 (22%) B2**	**0.5 (8%) I1 and S5**	**0.1 (2%) S5**	**0.2 (3%) I2**

V1 = petrol vehicle exhaust (Zn)
V2 = diesel vehicle exhaust (BC, Ti, Fe, Cu)
S1 = secondary sulphate (SO42-, S, NH4+)
S2 = shipping (V, Ni)
S3 = seasalt or marine (Na, Cl, Mg, MSA) S:Cl = 0.053
S4 = secondary nitrate (NO3, Na, Mg, MSA)
S5 = soil/crustal (Al, Si)
I1 = industry (Ca)
I2 = industry (PO_4^{3-})
B1 = fresh biomass burning/smoke (levoglucosan)
B2 = aged biomass burning/smoke (K, C2O42-, OC)
X1 = unassigned source (various)

Table A11. Average factor source contributions (μg m^{-3} (%)) at site 2 for various PMF modelling scenarios. $PM_{2.5}$ average concentration at site 2 was 6.3 μg m^{-3}.

PMF ID	Site	Exclusions	Factor 1	Factor 2	Factor 3	Factor 4	Factor 5	Factor 6	Factor 7	Factor 8	Factor 9	Factor 10
1	**2**	**PO_4^{3-}**	**0.2 (3%) V1**	**1.5 (24%) V2**	**0.6 (10%) S1**	**0.04 (1%) S5**	**1.1 (17%) S3**	**0.9 (14%) S4**	**0.9 (15%) B1**	**1 (16%) B2**		
2	2	PO_4^{3-}	0.3 (5%) V1	1.3 (21%) V2	1.3 (20%) S1	0.1 (1%) S5	0.9 (15%)	1.1 (17%) S4 and S2	0.8 (13%) B1	0.5 (7%) B2	0 (0%) X1	
3	1 and 2	PO_4^{3-}	0.04 (1%) V1	1.4 (22%) V2	0.8 (13%) S1	0.2 (3%) S2 and I1	0.9 (15%) S3	0.7 (12%) S4	0.9 (15%) B1	1.0 (16%) B2	0.2 (3%) S5	
4	1, 2 and source specific samples	PO_4^{3-}	0.03 (1%) V1	1.2 (19%) V2	0.7 (10%) S1	0.06 (1%) S2	0.9 (14%) S3	0.8 (13%) S4	1.1 (18%) B1	0.8 (13%) B2	0.2 (3%) S5	0.2 (4%) X1

V1 = petrol vehicle exhaust (Zn)
V2 = diesel vehicle exhaust (BC, Ti, Fe, Cu)
S1 = secondary sulphate (SO42-, S, NH4+)
S2 = shipping (V, Ni)
S3 = seasalt or marine (Na, Cl, Mg, MSA) S:Cl = 0.053
S4 = secondary nitrate (NO3, Na, Mg, MSA)
S5 = soil/crustal (Al, Si)
I1 = industry (Ca)
B1 = fresh biomass burning/smoke (levoglucosan)
B2 = aged biomass burning/smoke (K, C2O42-, OC)
X1 = unassigned source (various)

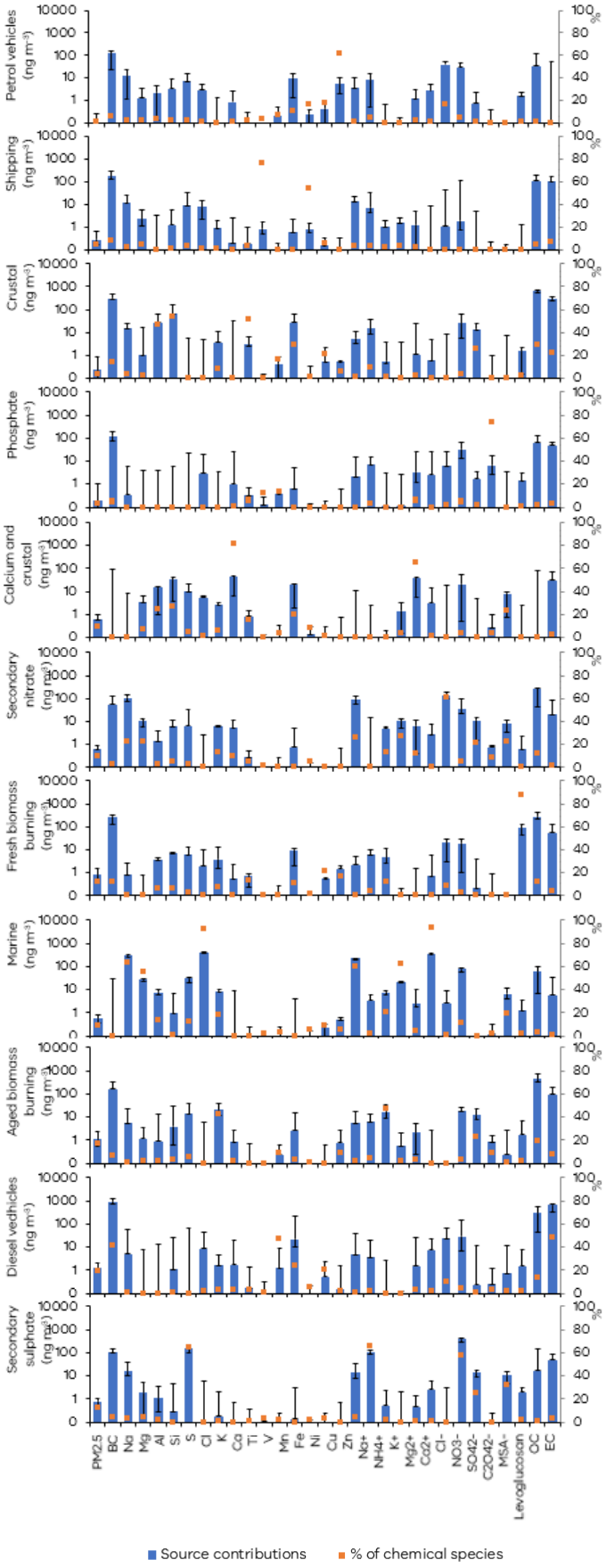

Figure A16. Chemical species associated with each source at site 1 (from PMF ID 7).

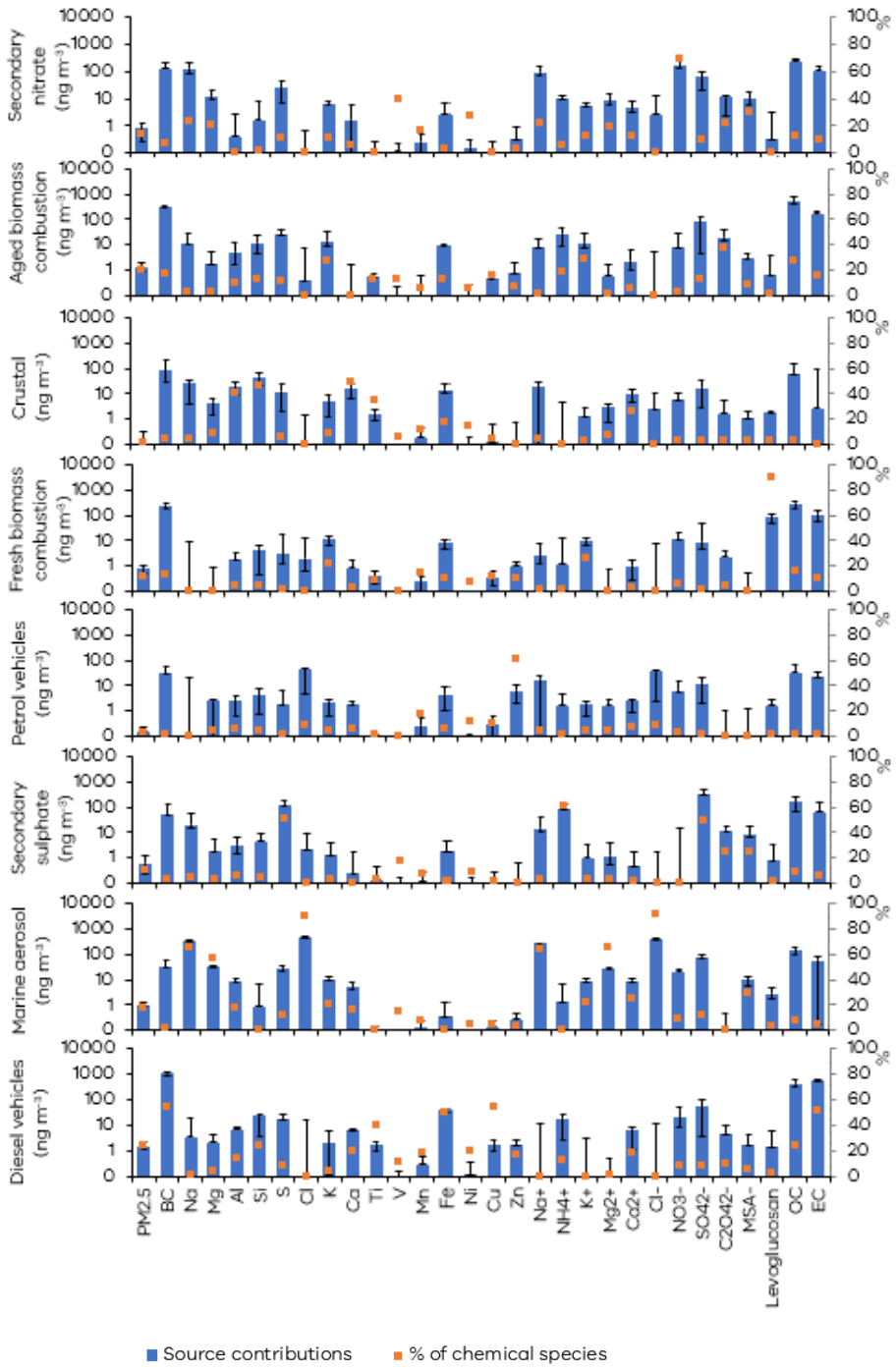

Figure A17. Chemical species associated with each source at site 2 (from PMF ID 1).

Unassigned sources occur when a PMF factor cannot be realistically explained. This usually happens when too many factors are used in the PMF model and the PMF model forces the data into an additional factor. For example, when looking at the results for the 10 factor PMF analysis using all sites (PMF ID 4 in Table A9, Table A10 Table A11), an industry factor appears that is mostly attributed to a calcium source.

An industry located approximately 550 m south of site 1 was identified, which uses large quantities of gyprock – a source of calcium. Analysis of the wind direction and highest concentrations of calcium at

site 1 confirmed the direction of a calcium source was from the south (Figure A18). The highest concentrations of the industry factor also came from the south. This provided sufficient evidence to confirm that the calcium industry factor was real at site 1.

However, when looking at site 2, this was not the case. If we assume, like the PMF model does, that the industry factor is the same source at sites 1 and 2, then we would expect the industry factor to be coming from the east at site 2. However, both the calcium concentrations and the industry factor are not coming from the east at site 2 (Figure A18). This is compelling evidence to suggest that this factor is unrealistically assigned at site 2 or is not the same source as assumed by the PMF model at sites 1 and 2. Also, site 2 is approximately 1.9 km away from the calcium industry site. This is much further away than site 1 and it is likely that site 1 is more impacted by this calcium industry source than site 2.

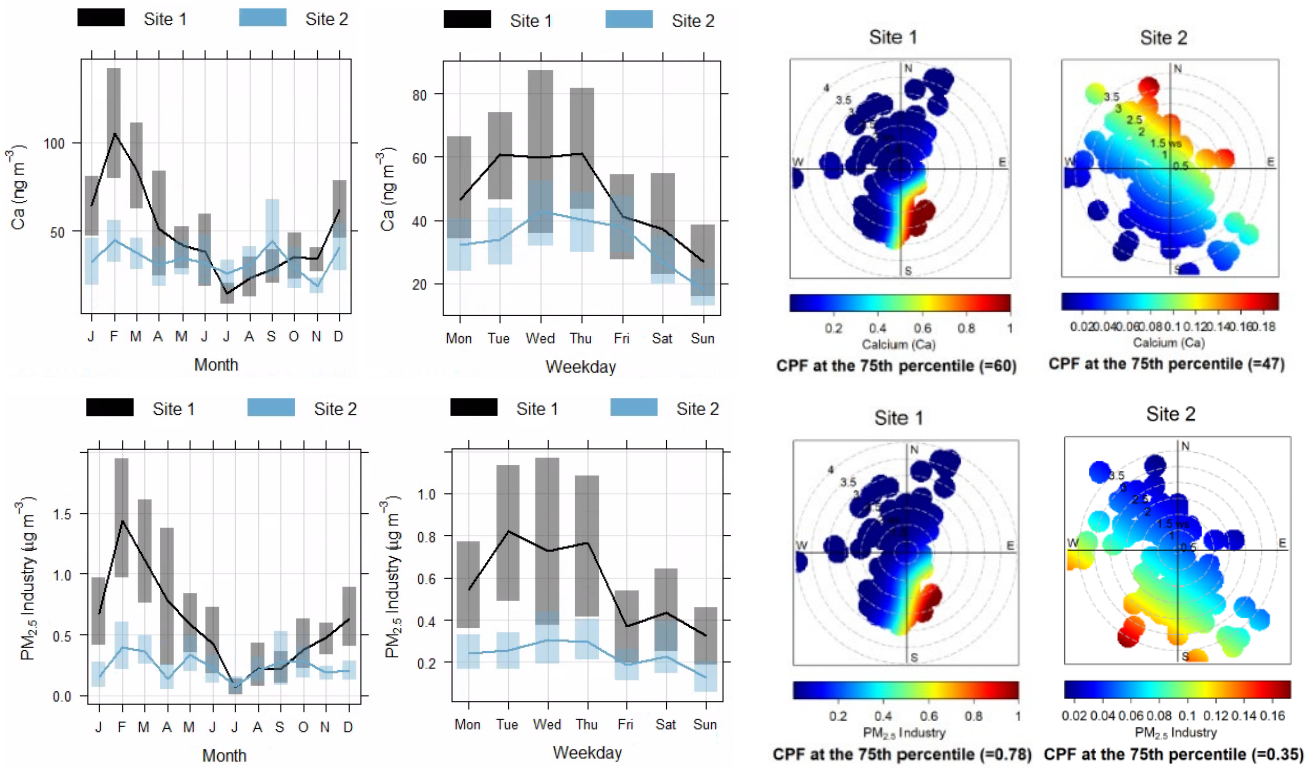

Figure A18. Timeseries and CPF polar plots for calcium (Ca) daily average concentrations (top plots) and $PM_{2.5}$ daily average industry source contributions (bottom plots) derived from PMF ID 4. Data for Site 1 is from May 2021 to May 2022 and for Site 2 from March 2021 to May 2022. Wind directions are meters per second (m s^{-1}). Note: Industry source at site 2 is not real and an artefact of the PMF model.

The concentrations of each chemical species predicted by the PMF model can be compared to the observed concentrations at each site to give an indication of the performance of the PMF model. That is, the concentrations that are highly correlated indicate good prediction of that chemical species by the PMF model, such as chlorine (Cl), sodium (Na) and magnesium (Mg) concentrations at sites 1 and 2 (Figure A19 and Figure A20). Whereas the increased scatter observed for manganese (Mn) and methanesulfonate (MSA^-) at sites 1 and 2 and vanadium (V) and nickel (Ni) at site 2 suggest that the PMF model is not representing these chemical species well.

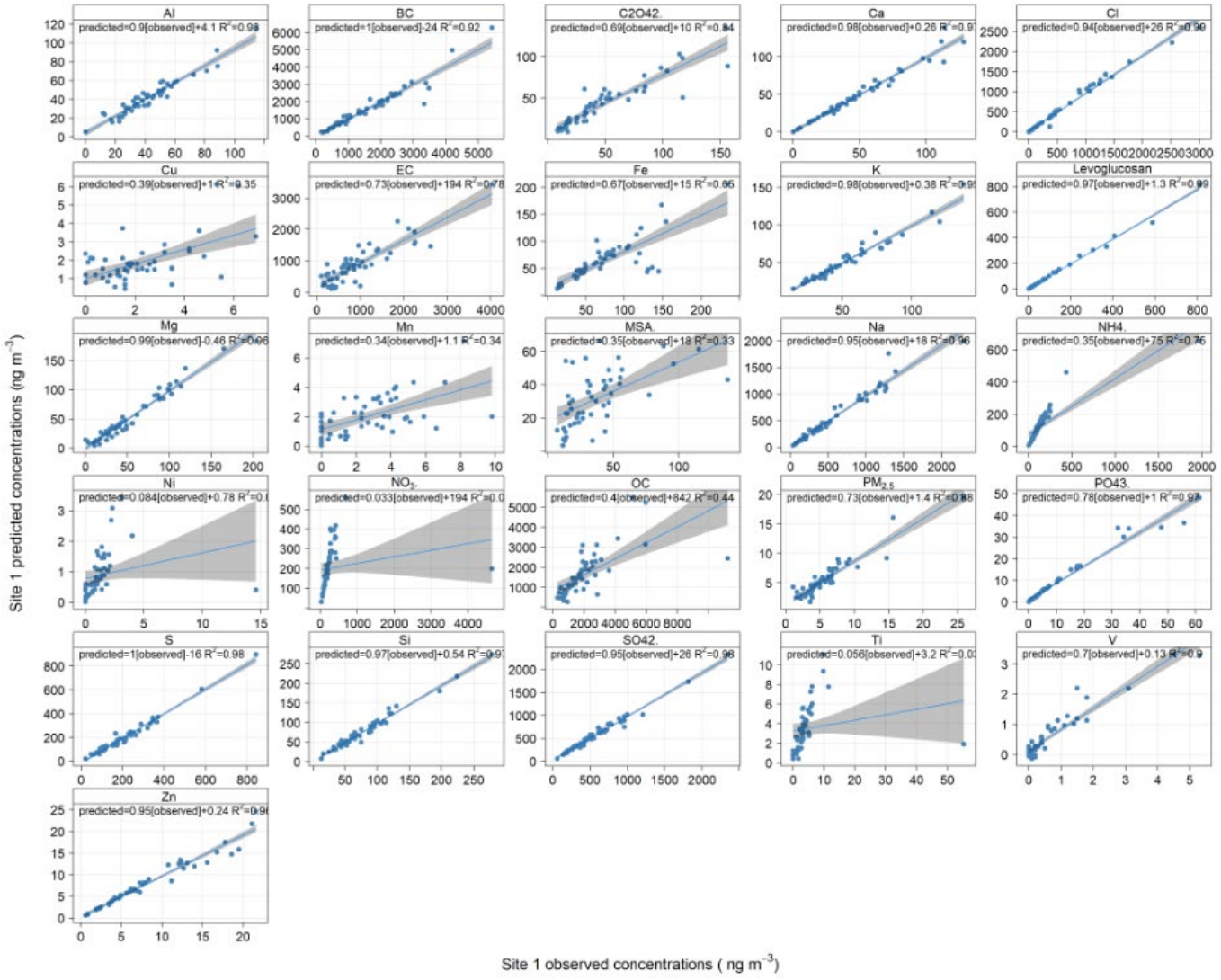

Figure A19. Correlation plots for observed versus predicted chemical species for site 1 (from PMF ID 7). Note: concentrations are ng m^{-3} for all chemical species except $PM_{2.5}$. $PM_{2.5}$ concentrations are μg m^{-3}.

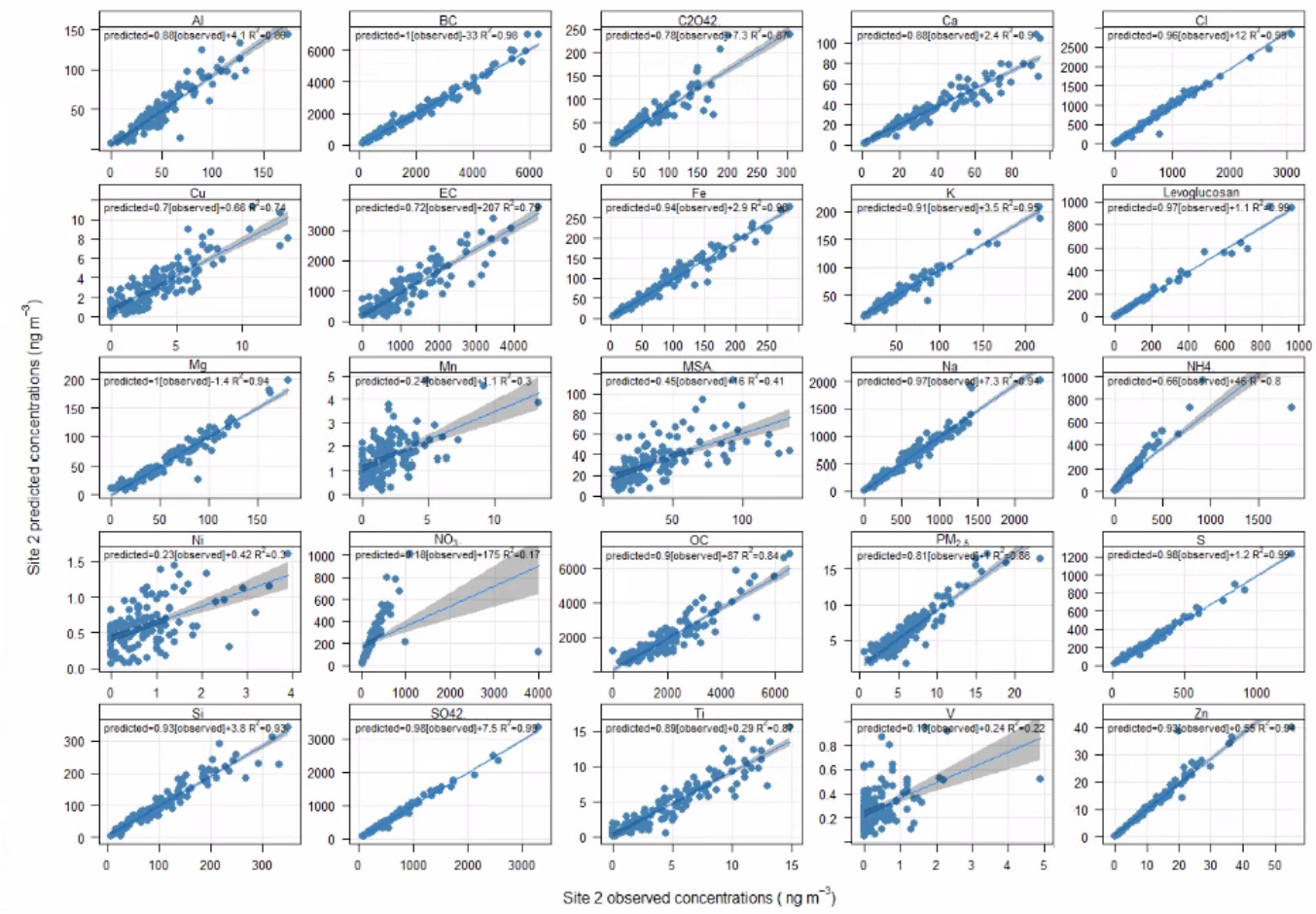

Figure A20. Correlation plots for observed versus predicted chemical species for site 2 (from PMF ID 1). Note: concentrations are ng m^{-3} for all chemical species except $PM_{2.5}$. $PM_{2.5}$ concentrations are µg m^{-3}.

Understanding why the model is not representing certain species is important. For example, vanadium (V) and nickel (Ni) are two key tracer species associated with shipping exhaust emissions. A shipping factor was identified by the PMF model at site 1 with 80% V and 54% Ni mass attributed to this factor (Figure A16). A trace shipping signal was observed at site 2 based on the concentrations of these two key tracer species during some PMF scenarios. However, the concentrations of V and Ni are much lower at site 2 compared to site 1.

At the lower concentrations, in all modelled scenarios, the PMF model was unable to accurately predict patterns in these two chemical species for site 2, results all showed large scatter. A timeseries of V and Ni at both sites 1 and 2 in Figure A21 shows a comparison of the fairly good prediction at site 1 versus poor prediction at site 2. As a result of the low concentrations of V and Ni at site 2, no factors were able to be attributed to shipping at this site by the PMF model, even though we know that a trace shipping signal is present.

Also, understanding why an outlier has occurred is important, for example, see nitrate (NO_3^-) concentrations at both sites 1 and 2 in Figure A19 and Figure A20. In this case, an exceptional event was identified. Exceptional events are events that occur that do not follow typical pollution patterns. While PMF is very good at identifying typical pollution patterns, it can also help identify exceptional events.

However, these events are typically not well represented by the PMF model. For more information about this exceptional event concerning nitrate, see Appendix 7.

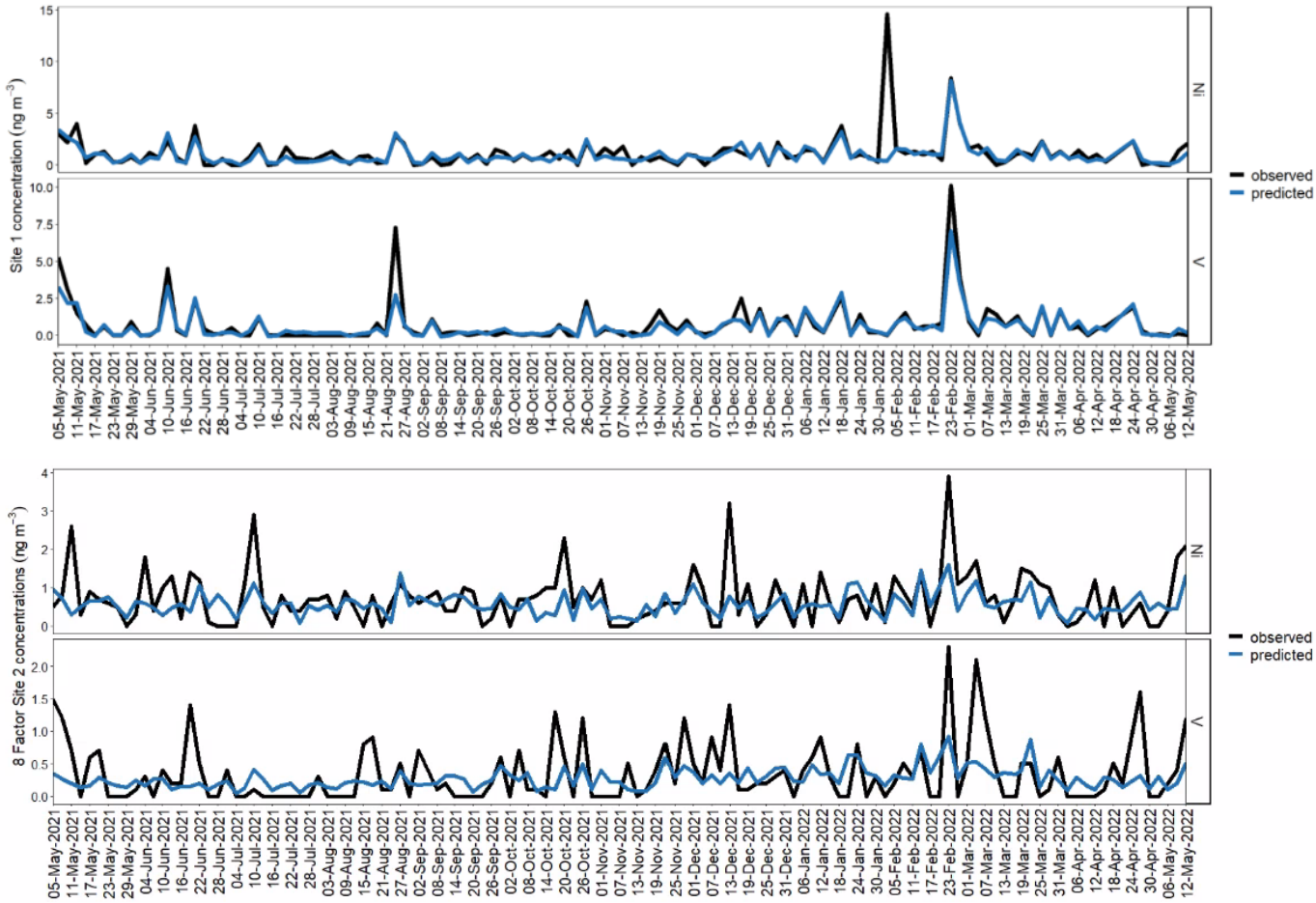

Figure A21. Observed versus predicted vanadium (V) and nickel (Ni) concentrations for: Top plot – fairly good predictions at site 1 (from PMF ID 7). Bottom plot – poor predictions at site 2 (from PMF ID 1).

Appendix 7. Exceptional events

Exceptional events are events that do not follow typical pollution patterns. While PMF is very good at identifying typical pollution patterns, it also helps to identify exceptional events. However, these events are typically not well represented by the PMF model.

This section discusses the 4 exceptional events that were identified during the project.

Ammonium nitrate on 10 July 2021 at sites 1 and 2

On 10 July 2021, PMF analysis underpredicted elevated ammonium (NH_4^+) and nitrate (NO_3^-) concentrations at both sites 1 and 2 (Figure A22 and Table A12). The differences between observed versus predicted NH_4^+ and NO_3^- concentrations on 10 July 2021 were 5.7 $\pm$ 0.7 and 5.1 $\pm$ 0.6 µg m^{-3} for sites 1 and 2 respectively. This was approximately 90% and 80% of the remaining $PM_{2.5}$ mass concentration not predicted by the PMF model on 10 July 2021 for sites 1 and 2 respectively (6.2 µg m^{-3} and 6.4 µg m^{-3}). Therefore, most of the remaining $PM_{2.5}$ mass concentration on 10 July 2021 not predicted by the PMF model was attributed to an ammonium nitrate exceptional event.

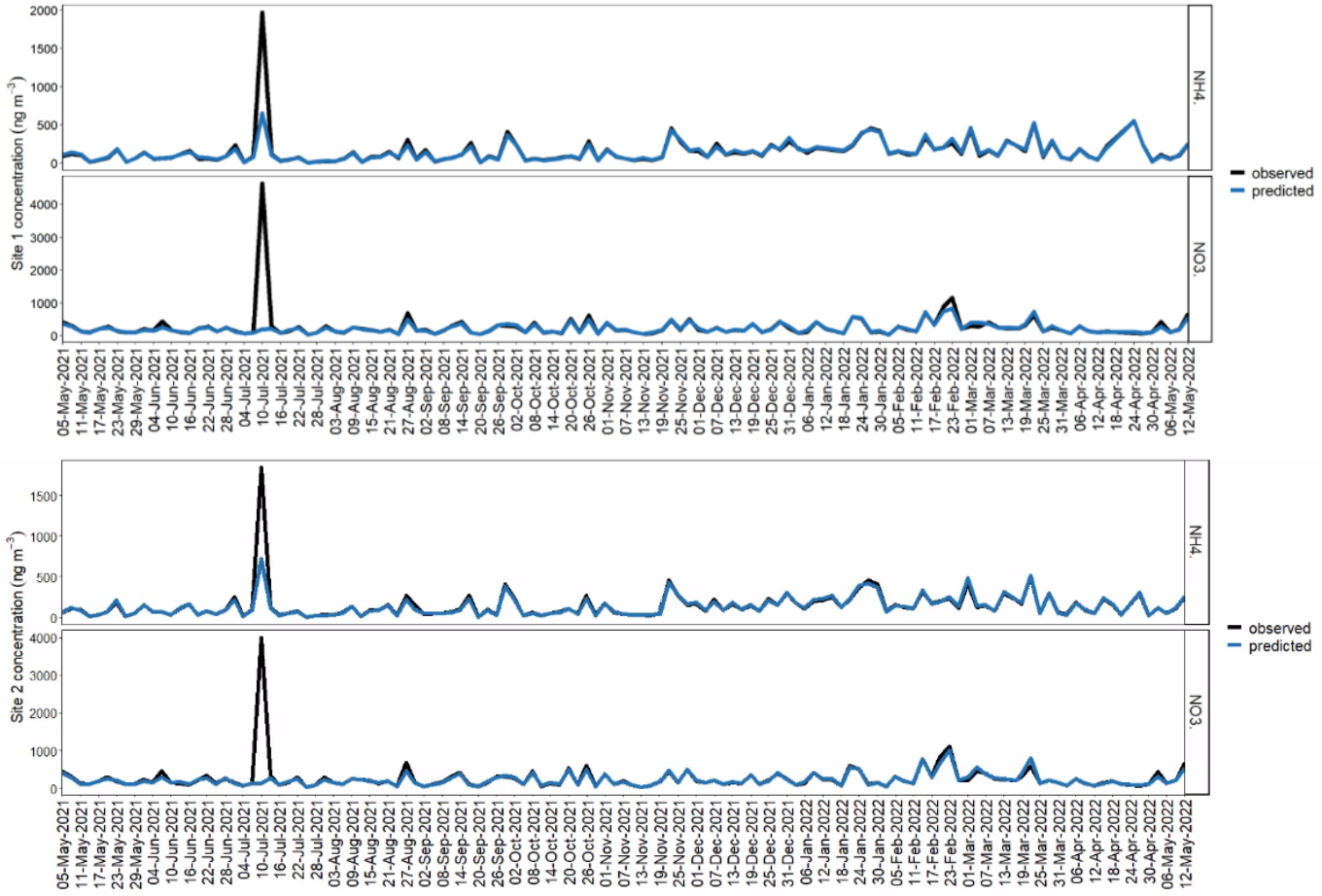

Figure A22. Timeseries of ammonium (NH_4^+) and nitrate (NO_3^-) observed and predicted concentrations at sites 1 and 2.

Table A12. Comparison between NH_4^+ and NO_3^- observed and predicted concentrations on 10 July 2021. Concentrations are μg m^{-3}.

Site	Species	Observed concentration	Predicted concentration	Difference between observed and predicted concentrations
1	NH_4^+	2.0 ± 0.2	0.7	1.3 ± 0.2
	NO_3^-	4.6 ± 0.5	0.2	4.4 ± 0.5
	$NH_4^+ + NO_3^-$	6.6 ± 0.7	0.9	5.7 ± 0.7
2	NH_4^+	1.9 ± 0.2	0.7	1.2 ± 0.2
	NO_3^-	4.0 ± 0.4	0.1	3.9 ± 0.4
	$NH_4^+ + NO_3^-$	5.9 ± 0.6	0.8	5.1 ± 0.6

Fireworks overnight on 31 January – 1 February 2022 at site 3

A six-hour source specific sample was collected from 23:00 on 31 January 2022 to 5:00 on 1 February 2022. The sample was collected to represent general port and nearby industry emissions. However, this sample was excluded from the PMF analysis due to elevated concentrations of several chemical species associated with fireworks.

During this sample, several chemical species (V, Ni, Zn, K, S, SO_4^{2-}, Sr and Cu) measured their highest recorded concentrations throughout the project.

Vanadium (V) and nickel (Ni) are typically associated with shipping emissions, and accounted for less than 1% of the 6-hour average $PM_{2.5}$ mass recorded during this sample.

Potassium (K) is a primary chemical constituent of fireworks, while sulphate (SO_4^{2-}) compounds are formed during firework explosions and are found in firework smoke. K and SO_4^{2-} accounted for approximately 77% of the 6-hour average $PM_{2.5}$ mass recorded during this sample. Other chemical species found in fireworks depend on the colours of the pyrotechnic display. For example, strontium (Sr) and copper (Cu) are red and blue respectively (Conkling, 2000).

Coupled with the carbonaceous content associated with fireworks smoke, the evidence indicates that a pyrotechnics event was the primary contributor to $PM_{2.5}$ at site 3 during this sample.

Elevated iron concentrations from 4 to 25 November 2021 at site 1

PMF model underpredicted iron (Fe) concentrations during 4 to 25 November 2021 at site 1 (Figure A23). Including the highest concentration of iron recorded at site 1 on 25 November 2021. Iron is typically associated with crustal material like wind-blown dust, but in this case, iron was not associated with crustal elements. Instead, iron was strongly associated with manganese over this period, suggesting that this could be a nearby industrial source involving grinding/cutting of steel.

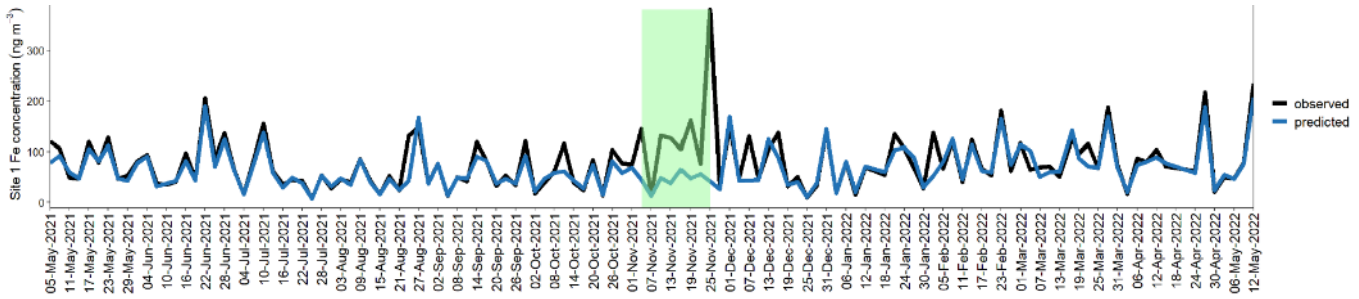

Figure A23. Timeseries of iron (Fe) observed and predicted concentrations at site 1.

Elevated summertime methanesulfonate (MSA^-) concentrations at sites 1 and 2

MSA is a natural source of $PM_{2.5}$ that is formed in the atmosphere by oxidised reactions with the organic sulphur gas, dimethyl sulphide (DMS), emitted from oceans. DMS is a by-product of an organic sulphur compound produced by marine bacteria and phytoplankton.

MSA has a distinct seasonal cycle with maximum concentrations observed over summer and minimum concentrations observed over winter (Figure A10). MSA concentrations at both sites were correlated (Figure A8) and this is expected as MSA has a regional source.

The PMF model poorly predicted MSA, and underpredicted MSA in summer (Figure A24). This is likely because MSA was carried over in the same air mass as secondary sulphate and marine aerosol, and the PMF model is unable to separate these sources.

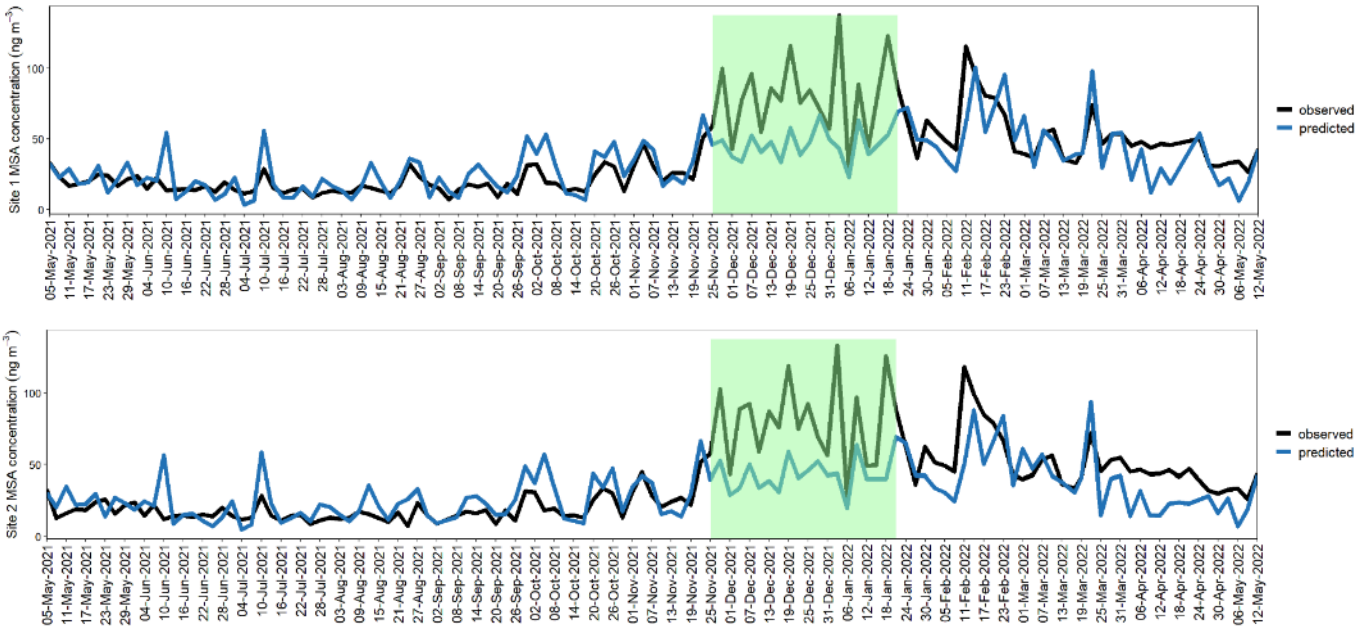

Figure A24. Timeseries of methanesulfonate (MSA^-) observed and predicted concentrations at sites 1 and 2. Green highlighted area shows underpredicted MSA^- during summer.

For languages other than English, please call **131 450**.
Visit **epa.vic.gov.au/language-help** for next steps.
If you need assistance because of a hearing or speech impairment, please visit **relayservice.gov.au**

epa.vic.gov.au

Environment Protection Authority Victoria

GPO BOX 4395 Melbourne VIC 3001

1300 372 842

VICTORIA State Government

Authorised and published by the Victorian Government, 1 Treasury Place, Melbourne